Formulations of the Pavement Performance Prediction Models in the Mechanistic-Empirical Asphalt Pavement Analysis (MEAPA) Web Application

Updated:
August 20, 2021

M. Emin Kutay, PhD, PE
&
Mike Lanotte, PhD

Table of Contents

1. INTRODUCTION

This document provides a description of the pavement performance prediction models implemented in MEAPA. The types of pavements that can currently be modeled are described below:

- AC-GB = Asphalt Concrete over Gravel Base
- AC-CSM = Asphalt Concrete over Chemically Stabilized Material
- AC-E-AC-GB = Asphalt Concrete over Existing Asphalt Concrete over Gravel Base
- AC-E-AC-CSM = Asphalt Concrete over Existing Asphalt Concrete over Chemically Stabilized Material
- AC-GB-E-AC-GB = Asphalt Concrete over Gravel Base over Existing Asphalt Concrete over Gravel Base
- AC-GB-E-AC-CSM = Asphalt Concrete over Gravel Base over Existing Asphalt Concrete over Chemically Stabilized Material

Table 1 shows the different distresses computed for each of the pavements considered in MEAPA. There are five general analysis steps in MEAPA models:

1. Traffic data processing.
2. Climate data processing and running the mechanistic climatic model (MCLIM) to compute temperature with depth.
3. Perform structural analysis to compute critical strains and stresses a mechanistic procedure.
4. Use phenomenological Material Damage Models (MDMs) to compute theoretical failure condition corresponding to an analysis period for a given critical stress or strain.
5. Compute accumulation of damage.
6. Compute actual distresses using empirical transfer functions.

Steps 1 and 2 are generally common to all of the pavement types. Steps 3 through 6 are implemented in different ways for different types of the pavements. Subsequent sections include the implementation details and the basic models used for each pavement type.

Table 1. MEAPA distress outputs for different types of pavements

Distress output \ Pavement type:	AC-GB	AC-CSM	AC-E-AC-GB	AC-E-AC-CSM	AC-GB-E-AC-GB	AC-GB-E-AC-CSM
AC top-down fatigue cracking (ft/mile)	✓	✓	✓	✓	✓	✓
AC bottom-up fatigue cracking (%)	✓	✓	✓	✓	✓	✓
AC thermal cracking (ft/mile)	✓	✓	✓	✓	✓	✓
Rutting – AC, base subbase and subgrade (in)	✓	✓	✓	✓	✓	✓
Reflective cracking (% lane area)	-	✓	✓	✓(1)	-	-
Chemically stabilized layer - fatigue fracture damage (% lane area)	-	✓	-	✓	-	-
Existing AC layer - fatigue fracture damage (% lane area)	-	-	✓	✓	-	-
International Roughness Index (IRI) (in/mile)	✓	✓	✓	✓	✓	✓

Notes: (1) Reflective cracking is due to the existing asphalt layer, not CSM.

2. TRAFFIC DATA PROCESSING

The main traffic inputs needed by the models are listed in Table 2. As shown, there are 19 different scalar inputs and 11 vectors or matrices (e.g., axle load spectra). These inputs are essentially the same inputs in the NCHRP 1-37A Mechanistic Empirical Pavement Design Guide (MEPDG). One of the most important steps in traffic data processing is the computation of the actual number of single, tandem, tridem and quad axles per analysis period, per weight category. In other words, all the traffic inputs, such as axle load spectra, axles per truck, class distribution, growth…etc. are all converted into the following:

- $\boldsymbol{N_{i,t,w_k}^{single}}$ =Number of single axles in month i, year t, corresponding to axle weight $\boldsymbol{w_k}$ where $k = 1 \dots 39$ and $\boldsymbol{w_k} = 3000, 4000, \dots 41000$ (lb).
- $\boldsymbol{N_{i,t,w_k}^{tandem}}$ =Number of tandem axles in month i, year t, corresponding to axle weight $\boldsymbol{w_k}$ where $k = 1 \dots 39$ and $\boldsymbol{w_k} = 6000, 8000, \dots 82000$ (lb).
- $\boldsymbol{N_{i,t,w_k}^{tridem}}$ =Number of tridem axles in month i, year t, corresponding to axle weight $\boldsymbol{w_k}$ where $k = 1 \dots 31$ and $\boldsymbol{w_k} = 12000, 15000, \dots 102000$ (lb).
- $\boldsymbol{N_{i,t,w_k}^{quad}}$ =Number of quad axles in month i, year t, corresponding to axle weight $\boldsymbol{w_k}$ where $k = 1 \dots 31$ and $\boldsymbol{w_k} = 12000, 15000, \dots 102000$ (lb).

The parameters listed above are used in damage accumulation models in different pavement types. The $\boldsymbol{N_{i,t,w_k}^{single}}$, $\boldsymbol{N_{i,t,w_k}^{tandem}}$, $\boldsymbol{N_{i,t,w_k}^{tridem}}$ and $\boldsymbol{N_{i,t,w_k}^{quad}}$ are three-dimensional matrices that includes the number of single, tandem, tridem and quad axle applications in month i, year t, corresponding to axle weight $\boldsymbol{w_k}$ in the k'th weight category. Computation of these matrices are described below. *It is noted that the bolded variables are either vectors or matrices, whereas un-bolded parameters are scalars.*

1. First, the number of trucks for each month for each class is calculated for year 1:

$$\boldsymbol{NT_{i,j,t=1}} = AADTT * P^D * P^L * \boldsymbol{MDF_{i,j}} * \boldsymbol{N_i^d} * \boldsymbol{P_j^T} \quad [1]$$

where ;

$\boldsymbol{NT_{i,j,t=1}}$=Number of trucks for each month i ($i = 1 \dots 12$), for each FHWA class j ($j = 1 \dots 10$) for year 1
$AADTT$ =Annual average daily truck traffic
P^D =Percentage of trucks in design direction
P^L =Percentage of trucks in design lane
$\boldsymbol{MDF_{i,j}}$ =Monthly distribution factor for each month i ($i = 1 \dots 12$), for each FHWA class j ($j = 1 \dots 10$)
$\boldsymbol{N_i^d}$ =Number of days in a given month. $\boldsymbol{N_i^d} = [31,28,31,30,31,30,31, 31, 30, 31, 30, 31]$ for January through December, respectively.
$\boldsymbol{P_j^T}$ =Percentage of trucks for a given class FHWA class j ($j = 1 \dots 10$). It is noted that $\sum_{j=1}^{10} \boldsymbol{P_j^T} = 100\%$

Table 2. MEAPA raw traffic inputs

Input Category	Variable[1]	Description
General	AADTT	Annual average daily truck traffic
	P^L	Percentage of trucks in design direction
	P^D	Percentage of trucks in design lane
	V	Operational speed
	t_o	Traffic opening year
	m_o	Traffic opening month
	t_a	Analysis duration
	S_d	Wheel wander standard deviation
Axle configuration	w_x	Average axle width[2]
	S_{xt}	Tandem axle spacing
	S_{xr}	Tridem axle spacing
	S_{xq}	Quad axle spacing
	S_{dt}	Dual tire spacing
	P_{tr}	Tire pressure
Wheelbase[2]	S_{sx}	Average spacing of short axles
	S_{mx}	Average spacing of medium axles
	S_{lx}	Average spacing of long axles
	P_{sx}	Percent trucks with short axles
	P_{mx}	Percent trucks with medium axles
	P_{lx}	Percent trucks with long axles
Vehicle Class, Growth & Monthly Distribution	$\boldsymbol{P_j^T}$	Percentage of vehicles in a given FHWA class *j*
	$\boldsymbol{G_j^T}$	Compound growth rate for a given FHWA class *j*
	$\boldsymbol{MDF_{ij}}$	Monthly distribution factor for each month *i* for each FHWA class *j*
Number of axles per FHWA class	$\boldsymbol{NA_j^{single}}$	Number of single axles per FHWA class *j*
	$\boldsymbol{NA_j^{tandem}}$	Number of tandem axles per FHWA class *j*
	$\boldsymbol{NA_j^{tridem}}$	Number of tridem axles per FHWA class *j*
	$\boldsymbol{NA_j^{quad}}$	Number of quad axles per FHWA class *j*
Axle Load Spectra	$\boldsymbol{P_{i,j,w_k}^{single}}$	Percentage of single axles in i^{th} month per FHWA class *j*, corresponding to axle weight $\boldsymbol{w_k}$ where $k = 1 \dots 39$ and $\boldsymbol{w_k} = 3000, 4000, \dots 41000$ (lb). Note that $\sum_{k=1}^{39} P_{i,j,w_k}^{single} = 100\%$
	$\boldsymbol{P_{i,j,w_k}^{tandem}}$	Percentage of tandem axles in i^{th} month per FHWA class *j*, corresponding to axle weight $\boldsymbol{w_k}$ where $k = 1 \dots 39$ and $\boldsymbol{w_k} = 6000, 8000, \dots 82000$ (lb). Note that $\sum_{k=1}^{39} P_{i,j,w_k}^{tandem} = 100\%$
	$\boldsymbol{P_{i,j,w_k}^{tridem}}$	Percentage of tridem axles in i^{th} month per FHWA class *j*, corresponding to axle weight $\boldsymbol{w_k}$ where $k = 1 \dots 31$ and $\boldsymbol{w_k} = 12000, 15000, \dots 102000$ (lb). Note that $\sum_{k=1}^{31} P_{i,j,w_k}^{tridem} = 100\%$
	$\boldsymbol{P_{i,j,w_k}^{quad}}$	Percentage of quad axles in i^{th} month per FHWA class *j*, corresponding to axle weight $\boldsymbol{w_k}$ where $k = 1 \dots 31$ and $\boldsymbol{w_k} = 12000, 15000, \dots 102000$ (lb). Note that $\sum_{k=1}^{31} P_{i,j,w_k}^{quad} = 100\%$

Notes: [1] Subscript i represents each month, i.e., $(i = 1 \dots 12)$. Subscript j represents each FHWA class, i.e., $(j = 1 \dots 10)$. [2] Only used in rigid pavement analysis.

Next, the number of single, tandem, tridem and quad axles are calculated for year 1, for each class for each month:

$$\boldsymbol{NA}_{\boldsymbol{i,j,t=1}}^{\boldsymbol{single}} = \boldsymbol{NT}_{\boldsymbol{i,j,t=1}} * \boldsymbol{NA}_{\boldsymbol{j}}^{\boldsymbol{single}} \quad [2]$$

$$\boldsymbol{NA}_{\boldsymbol{i,j,t=1}}^{\boldsymbol{tandem}} = \boldsymbol{NT}_{\boldsymbol{i,j,t=1}} * \boldsymbol{NA}_{\boldsymbol{j}}^{\boldsymbol{tandem}} \quad [3]$$

$$\boldsymbol{NA}_{\boldsymbol{i,j,t=1}}^{\boldsymbol{tridem}} = \boldsymbol{NT}_{\boldsymbol{i,j,t=1}} * \boldsymbol{NA}_{\boldsymbol{j}}^{\boldsymbol{tridem}} \quad [4]$$

$$\boldsymbol{NA}_{\boldsymbol{i,j,t=1}}^{\boldsymbol{quad}} = \boldsymbol{NT}_{\boldsymbol{i,j,t=1}} * \boldsymbol{NA}_{\boldsymbol{j}}^{\boldsymbol{quad}} \quad [5]$$

where;

$\boldsymbol{NT}_{\boldsymbol{i,j,t=1}}$ =Number of trucks for each FHWA class j ($j = 1 \dots 10$), for each month i ($i = 1 \dots 12$), for year 1

$\boldsymbol{NA}_{\boldsymbol{i,j,t=1}}^{\boldsymbol{single}}$ =Number of single axles in an FHWA class j ($j = 1 \dots 10$), for each month i ($i = 1 \dots 12$), for year 1

$\boldsymbol{NA}_{\boldsymbol{i,j,t=1}}^{\boldsymbol{tandem}}$ =Number of tandem axles in an FHWA class j ($j = 1 \dots 10$), for each month i ($i = 1 \dots 12$), for year 1

$\boldsymbol{NA}_{\boldsymbol{i,j,t=1}}^{\boldsymbol{tridem}}$ =Number of tridem axles in an FHWA class j ($j = 1 \dots 10$), for each month i ($i = 1 \dots 12$), for year 1

$\boldsymbol{NA}_{\boldsymbol{i,j,t=1}}^{\boldsymbol{quad}}$ =Number of quad axles in an FHWA class j ($j = 1 \dots 10$), for each month i ($i = 1 \dots 12$), for year 1

$\boldsymbol{NA}_{\boldsymbol{j}}^{\boldsymbol{single}}$ =Number of single axles per FHWA class j ($j = 1 \dots 10$)

$\boldsymbol{NA}_{\boldsymbol{j}}^{\boldsymbol{tandem}}$ =Number of tandem axles per FHWA class j ($j = 1 \dots 10$)

$\boldsymbol{NA}_{\boldsymbol{j}}^{\boldsymbol{tridem}}$ =Number of tridem axles per FHWA class j ($j = 1 \dots 10$)

$\boldsymbol{NA}_{\boldsymbol{j}}^{\boldsymbol{quad}}$ =Number of quad axles per FHWA class j ($j = 1 \dots 10$)

Next, the growth factor is computed for each year t. There are two options for growth of traffic; (i) compound and (ii) linear. If compound growth is assumed for a given truck class, the following equation is used to compute the growth factor:

$$\mathbf{GF}_{\mathbf{j,t}} = (\mathbf{1} + \boldsymbol{G}_{\boldsymbol{j}}^{\boldsymbol{T}})^{(t-1)} \quad [6]$$

where;

$\mathbf{GF}_{\mathbf{j,t}}$=Growth factor at time t (years) for an FHWA class j ($j = 1 \dots 10$)

$\boldsymbol{G}_{\boldsymbol{j}}^{\boldsymbol{T}}$ =Compound growth rate for an FHWA class j ($j = 1 \dots 10$), in terms of fractions, i.e., for 10% enter 0.1

t =Time in years, $t = 1 \dots t_a$ where t_a is analysis duration

If linear growth is selected for a given class, the following equation is used to compute the growth factor:

$$\mathbf{GF}_{\mathbf{j,t}} = (\mathbf{1} + (t-1)\boldsymbol{G}_{\boldsymbol{j}}^{\boldsymbol{T}}) \quad [7]$$

Then, the number of single, tandem, tridem and quad axles are calculated for each year t, for each month i, for each class j:

$$\boldsymbol{NA}_{\boldsymbol{i,j,t}}^{\boldsymbol{single}} = \boldsymbol{NA}_{\boldsymbol{i,j,t=1}}^{\boldsymbol{single}} * \mathbf{GF}_{\mathbf{j,t}} \quad [8]$$

$$\boldsymbol{NA}_{\boldsymbol{i,j,t}}^{\boldsymbol{tandem}} = \boldsymbol{NA}_{\boldsymbol{i,j,t=1}}^{\boldsymbol{tandem}} * \mathbf{GF}_{\mathbf{j,t}} \quad [9]$$

$$\boldsymbol{NA}_{\boldsymbol{i,j,t}}^{\boldsymbol{tridem}} = \boldsymbol{NA}_{\boldsymbol{i,j,t=1}}^{\boldsymbol{tridem}} * \mathbf{GF}_{\mathbf{j,t}} \quad [10]$$

$$\boldsymbol{NA}_{\boldsymbol{i,j,t}}^{\boldsymbol{quad}} = \boldsymbol{NA}_{\boldsymbol{i,j,t=1}}^{\boldsymbol{quad}} * \mathbf{GF}_{\mathbf{j,t}} \quad [11]$$

where;

$NA_{i,j,t}^{single}$ =Number of single axles in an FHWA class j ($j = 1 \dots 10$), for each month i ($i = 1 \dots 12$), for year t ($t = 1 \dots t_a$ where t_a is analysis duration)

$NA_{i,j,t}^{tandem}$ =Number of tandem axles in an FHWA class j ($j = 1 \dots 10$), for each month i ($i = 1 \dots 12$), for year t ($t = 1 \dots t_a$ where t_a is analysis duration)

$NA_{i,j,t}^{tridem}$ =Number of tridem axles in an FHWA class j ($j = 1 \dots 10$), for each month i ($i = 1 \dots 12$), for year t ($t = 1 \dots t_a$ where t_a is analysis duration)

$NA_{i,j,t}^{quad}$ =Number of quad axles in an FHWA class j ($j = 1 \dots 10$), for each month i ($i = 1 \dots 12$), for year t ($t = 1 \dots t_a$ where t_a is analysis duration)

Next, the number of axles corresponding to each axle weight category is computed:

$$NA_{i,j,t,w_k}^{single} = NA_{i,j,t}^{single} * P_{i,j,w_k}^{single} \quad [12]$$

$$NA_{i,j,t,w_k}^{tandem} = NA_{i,j,t}^{tandem} * P_{i,j,w_k}^{tandem} \quad [13]$$

$$NA_{i,j,t,w_k}^{tridem} = NA_{i,j,t}^{tridem} * P_{i,j,w_k}^{tridem} \quad [14]$$

$$NA_{i,j,t,w_k}^{quad} = NA_{i,j,t}^{quad} * P_{i,j,w_k}^{quad} \quad [15]$$

where;

NA_{i,j,t,w_k}^{single} = Number of single axles in an FHWA class j ($j = 1 \dots 10$), for each month i ($i = 1 \dots 12$), for year t ($t = 1 \dots t_a$, where t_a Is analysis duration), corresponding to axle weight $\boldsymbol{w_k}$ Where $k = 1 \dots 39$ and $\boldsymbol{w_k} = 3000, 4000, \dots 41000$ (lb).

NA_{i,j,t,w_k}^{tandem}= Number of tandem axles in an FHWA class j ($j = 1 \dots 10$), for each month i ($i = 1 \dots 12$), for year t ($t = 1 \dots t_a$, where t_a Is analysis duration), corresponding to axle weight $\boldsymbol{w_k}$ Where $k = 1 \dots 39$ and $\boldsymbol{w_k} = 6000, 8000, \dots 82000$ (lb).

NA_{i,j,t,w_k}^{tridem}= Number of tridem axles in an FHWA class j ($j = 1 \dots 10$), for each month i ($i = 1 \dots 12$), for year t ($t = 1 \dots t_a$, where t_a Is analysis duration), corresponding to axle weight $\boldsymbol{w_k}$ Where $k = 1 \dots 31$ and $\boldsymbol{w_k} = 12000, 15000, \dots 102000$ (lb).

NA_{i,j,t,w_k}^{quad} = Number of quad axles in an FHWA class j ($j = 1 \dots 10$), for each month i ($i = 1 \dots 12$), for year t ($t = 1 \dots t_a$, where t_a Is analysis duration), corresponding to axle weight $\boldsymbol{w_k}$ Where $k = 1 \dots 31$ and $\boldsymbol{w_k} = 12000, 15000, \dots 102000$ (lb).

P_{i,j,w_k}^{single} = Percentage of single axles in i^{th} month per fhwa class j, corresponding to axle weight $\boldsymbol{w_k}$ where $k = 1 \dots 39$ and $\boldsymbol{w_k} = 3000, 4000, \dots 41000$ (lb). Note that $\sum_{k=1}^{39} P_{i,j,w_k}^{single} = 100\%$

P_{i,j,w_k}^{tandem} = Percentage of tandem axles in i^{th} month per fhwa class j, corresponding to axle weight $\boldsymbol{w_k}$ where $k = 1 \dots 39$ and $\boldsymbol{w_k} = 6000, 8000, \dots 82000$ (lb). Note that $\sum_{k=1}^{39} P_{i,j,w_k}^{tandem} = 100\%$

P_{i,j,w_k}^{tridem} = Percentage of tridem axles in i^{th} month per FHWA class j, corresponding to axle weight $\boldsymbol{w_k}$ where $k = 1 \dots 31$ and $\boldsymbol{w_k} = 12000, 15000, \dots 102000$ (lb). Note that $\sum_{k=1}^{31} P_{i,j,w_k}^{tridem} = 100\%$

P_{i,j,w_k}^{quad} = Percentage of quad axles in i^{th} month per FHWA class j, corresponding to axle weight $\boldsymbol{w_k}$ where $k = 1 \dots 31$ and $\boldsymbol{w_k} = 12000, 15000, \dots 102000$ (lb). Note that $\sum_{k=1}^{31} P_{i,j,w_k}^{quad} = 100\%$

Finally, the number of axles are summed over j (i.e., classes) to compute the total number of applications of single, tandem, tridem and quad axles, *regardless of the class:*

$$N_{i,t,w_k}^{single} = \sum_{j=1}^{10} NA_{i,j,t,w_k}^{single} \quad [16]$$

$$N_{i,t,w_k}^{tandem} = \sum_{j=1}^{10} NA_{i,j,t,w_k}^{tandem} \quad [17]$$

$$N_{i,t,w_k}^{tridem} = \sum_{j=1}^{10} NA_{i,j,t,w_k}^{tridem} \quad [18]$$

$$N_{i,t,w_k}^{quad} = \sum_{j=1}^{10} NA_{i,j,t,w_k}^{quad} \quad [19]$$

where;

NA_{i,t,w_k}^{single} = Number of single axles for each month i ($i = 1 \dots 12$), for year t ($t = 1 \dots t_a$, where t_a is analysis duration), corresponding to axle weight $\boldsymbol{w_k}$ Where $k = 1 \dots 39$ and $\boldsymbol{w_k} = 3000, 4000, \dots 41000$ (lb).

NA_{i,t,w_k}^{tandem} = Number of tandem axles for each month i ($i = 1 \dots 12$), for year t ($t = 1 \dots t_a$, where t_a is analysis duration), corresponding to axle weight $\boldsymbol{w_k}$ Where $k = 1 \dots 39$ and $\boldsymbol{w_k} = 6000, 8000, \dots 82000$ (lb).

NA_{i,t,w_k}^{tridem} = Number of tridem axles, for each month i ($i = 1 \dots 12$), for year t ($t = 1 \dots t_a$, where t_a is analysis duration), corresponding to axle weight $\boldsymbol{w_k}$, where $k = 1 \dots 31$ and $\boldsymbol{w_k} = 12000, 15000, \dots 102000$ (lb).

NA_{i,t,w_k}^{quad} = Number of quad axles i, for each month i ($i = 1 \dots 12$), for year t ($t = 1 \dots t_a$, where t_a is analysis duration), corresponding to axle weight $\boldsymbol{w_k}$ Where $k = 1 \dots 31$ and $\boldsymbol{w_k} = 12000, 15000, \dots 102000$ (lb).

3. CLIMATIC MODEL

The climatic model in MEAPA is very similar to the Enhanced Integrated Climatic Model (EICM) in the MEPDG. The EICM in the MEPDG includes the following three major components:

- Prediction of temperature with depth is based on the model:
  - The Climatic-Materials-Structural Model (CMS Model) developed at the University of Illinois (Dempsey, 1969)
- Prediction of moisture with depth is based on the model:
  - The Infiltration and Drainage Model (ID Model) developed at the Texas A&M University(R L Lytton et al., 1993)
- Prediction of frost heave:
  - The CRREL Frost Heave and Thaw Settlement Model (CRREL Model) developed at the United States Anny Cold Regions Research and Engineering Laboratory (CRREL).

MEAPA climatic model is essentially the same as the CMS model implemented within the Enhanced Integrated Climatic Model (EICM) to predict pavement temperatures with depth. The main references cited for the EICM temperature prediction models in the MEPDG documentation are (Larson & Dempsey, 1997)(Dempsey & Thompson, 1970). Unfortunately, none of these references provided sufficient detail to implement the climatic model. The project team obtained the hard copy of the original PhD dissertation by Barry Dempsey (Dempsey, 1969), which included most of the details, but not entirely. Further literature review revealed that the information in Dempsey's dissertation (Dempsey, 1969) coupled with detailed formulations for daily solar radiation in (Diefenderfer & Al-Qadi, IL, 2003) provides most of the steps required. Further reading into the Fortran codes in Dempsey's dissertation, and using new algorithms for sunrise and sunset times in different days of the year at different geographic locations completed the steps.

Two major components of the MEAPA climatic model include:

- Energy balance at the surface, where convection and radiation are dominant
- Progression of temperature within the pavement, where conduction is dominant

Figure 1 shows the sublayering scheme used by Dempsey (Dempsey, 1969). In MEAPA, a similar sublayering scheme is used, where the sublayers were all 2 in thick until 73 inches of depth, after which the sublayers were 23.667 inches thick.

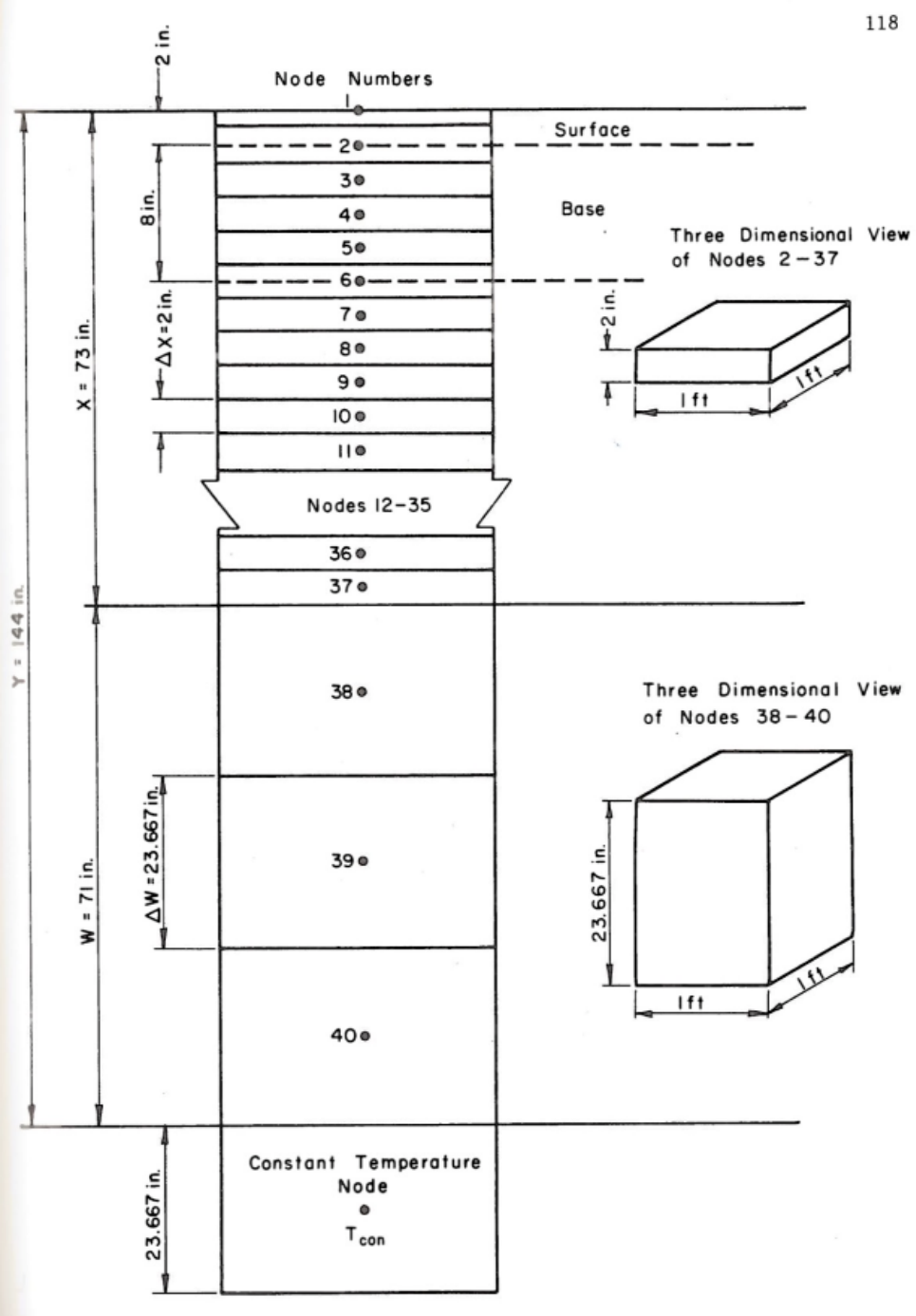

Figure 1. Pavement sublayering in the climatic model (Dempsey, 1969)**.**

3.1 Energy balance at the surface

At the surface of the pavement, the temperature is mostly affected by the convection and radiation. Figure 2 shows the conceptualized heat transfer phenomena between the pavement surface and the air and during a sunny/partly cloudy day.

$$Q_s + Q_a - Q_e \mp Q_c \mp Q_h \mp Q_g = 0 \quad [20]$$

where;

Q_a = heat flux resulting from long-wave radiation emitted by the atmosphere, Btu/ft2—hr;
Q_c = heat flux resulting from convective heat transfer, Btu/ft2-hr;
Q_e = heat flux resulting from long-wave radiation emitted by the pavement surface, Btu/ft2—hr
Q_g = heat flux conducted into pavement, Btu/ft2—hr;
Q_h = heat flux resulting from transpiration, condensation, evaporation, and sublimation, Btu/ft2-hr; (Q_h= assumed zero)
Q_s = net shortwave radiation entering into the energy balance at the pavement surface, Btu/ft2-hr;

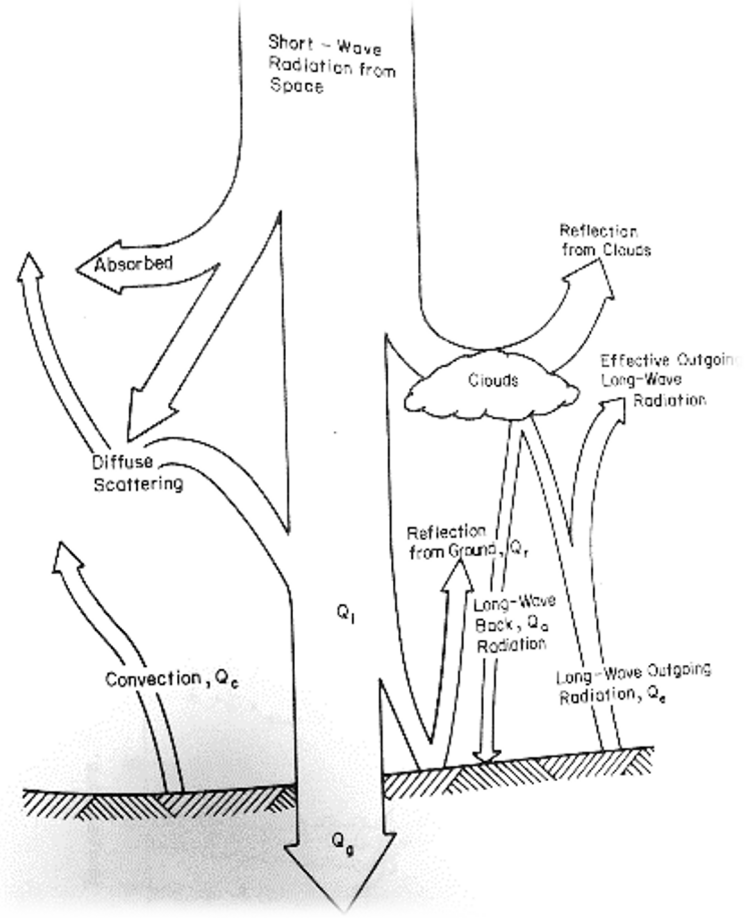

Figure 2. Heat flux boundary condition at the surface (Dempsey, 1969)

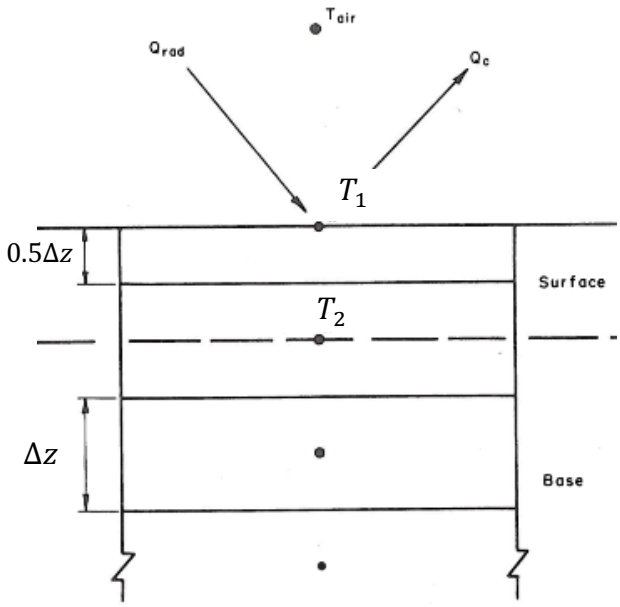

Figure 3. Illustration of the surface nodes used in the energy balance equation

Dempsey (Dempsey, 1969) provides an incremental formulation to solve for pavement surface temperature based on the net radiation flux (Q_{rad}):

$$T_1(t+\Delta t) = T_1(t)\left(1 - \frac{2K\Delta t}{\gamma C \Delta z^2} - \frac{2H\Delta t}{\gamma C \Delta z}\right) + T_2(t)\frac{2K\Delta t}{\gamma C \Delta z^2} + T_{air}(t)\frac{2H\Delta t}{\gamma C \Delta z} + Q_{rad}(t)\frac{2\Delta t}{\gamma C \Delta z} \quad [21]$$

where;

T_1 = surface temperature (˚F) – see Figure 3
T_2 = temperature of the first node within the pavement (˚F) – see Figure 3
H = Convection coefficient (btu/ft²-hr-F), which can be calculated using the following formula:

$$H = C_{unt}[0.00144V_m^{0.3}U^{0.7} + 0.00097(V_1 - V_{air})^{0.3}]$$

where;

V_{air} = air temperature (˚C)
V_1 = pavement surface temperature (˚C)
V_m = average air temperature and pavement surface temperature in Kelvin, where $V_m = 273.0 + \frac{V_1 + V_{air}}{2}$
U = average daily wind velocity in m/sec
C_{unt} = 122.93 (unit conversion coefficient from 'gm-cal/cm²-sec-C' to 'btu/ft²-hr-F'

T_{air} = air temperature (˚F) – see Figure 3
K = thermal conductivity (btu/(hr*ft*˚F))
C = heat capacity (btu/(lb*˚F))
Δz = spacing between the nodes (ft)
Q_{rad} = net radiation flux influencing heat transfer at a surface, Btu/ft²-hr, which is defined as follows:

$$Q_{rad} = Q_s + Q_a - Q_e \quad [22]$$

where;

Q_s = net shortwave radiation entering into the energy balance at the pavement surface, Btu/ft²-hr;
Q_a = heat flux resulting from long-wave radiation emitted by the atmosphere, Btu/ft²—hr;

Q_e = heat flux resulting from long-wave radiation emitted by the pavement surface, Btu/ft²—hr

where

$$Q_s = Q_i - Q_r = a * R_h(t) * \left(A + B * \frac{s}{100}\right) \quad [23]$$

where

Q_i = heat flux resulting from incident short-wave radiation, Btu/ft²-hr;
Q_r = heat flux resulting from reflected short-wave radiation, Btu/ft²-hr;
A = 0.202 (Dempsey, 1969)
B = 0.539 (Dempsey, 1969)
s = % sunshine
a = absorptivity of pavement surface = 0.85-0.9 for asphalt, 0.6-0.7 for concrete (Dempsey's dissertation); (The pavement surface thermal emissivity for estimating the longwave radiation intensity balance was equal to 0.9 and the solar absorption coefficient was equal to 0.95. (Minhoto et al., n.d.))
$R_h(t)$ = solar radiation at time t, Btu/ft²-hr– see discussion on this parameter later in this section.

There are two optional approaches in MEAPA to compute the Q_a and Q_e.

'Original' Method

This is the method implemented in the original MEPDG formulations, where the following formulations were used to compute the Q_a and Q_e:

$$Q_a = Q_z \quad [24]$$

$$Q_e = Q_x * \left(1 - N * \frac{100 - s}{100}\right) \quad [25]$$

where

N = cloud base factor, which ranges from 0.8 to 0.9 (assumed N = 0.8)
s = % sunshine
Q_x = long-wave radiation emitted from a surface without cloud cover correction, Btu/ft²-hr, which is defined as follows:

$$Q_x = \sigma\varepsilon * T_{1R}^4$$

where;

σ = 0.172x10^{-8} Btu/hr-ft²-R⁴ (Stefan-Boltzmann constant)
ε = Emissivity. Emissivity values are typically between 0.93 and 0.98 (assumed $\varepsilon = 0.95$) (Marchetti et al., 2004)
T_{1R} = Rankine temperature of surface node

Q_z = long-wave back radiation not corrected for cloud cover, Btu/ft2—hr, which is defined as follows:

$$Q_z = \sigma * T_{airR}^4 * [G - J * (10^{-\rho p})]$$

where;

G= 0.77
J= 0.28
ρ= 0.074
p= vapor pressure = 1-10 mmHg
T_{airR}= Rankine temperature of air

'Revised' Method

This is an improved (more physically consistent compared to the original EICM) method that can better consider the effects cloud cover (Forman & Margulis, 2010; Sugita & Brutsaert, 1993). In this method, the following formulations were used to compute the Q_a and Q_e:

$$Q_a = Q_z * \left(1 + N_{rev} * \frac{100 - s}{100}\right) \quad [26]$$

$$Q_e = Q_x \quad [27]$$

where

N_{rev} = Revised cloud base factor, which is equal to 0.17.

s = % sunshine

Q_x = long-wave radiation emitted from a surface without cloud cover correction, Btu/ft²-hr, which is defined as follows:

$$Q_x = \sigma\varepsilon * T_{1R}^4$$

where;

σ = 0.172x10^{-8} Btu/hr-ft²-R⁴ (Stefan-Boltzmann constant)

ε = Emissivity. Emissivity values are typically between 0.93 and 0.98 (assumed $\varepsilon = 0.95$) (Marchetti et al., 2004)

T_{1R} = Rankine temperature of surface node

Q_z = long-wave back radiation not corrected for cloud cover, Btu/ft2—hr, which is defined as follows (Idso, 1981):

$$Q_z = \sigma * T_{airR}^4 * [0.74 + 0.0049 * p_{mb}]$$

where;

p_{mb} = vapor pressure in Millibar (1mm-Hg = 1.3322 Millibar)

T_{airR} = Rankine temperature of air

Numerical Stability

It should be noted that for numerical stability of the finite difference formulation given in equation [21] , the following condition must be met:

$$\Delta t \leq \frac{\gamma C \Delta z}{2(H + \frac{K}{\Delta z})} \quad [28]$$

3.1.1 Daily and hourly solar radiation (R)

Daily solar radiation is computed using the following formula Diefenderfer and Al-Qadi, IL, "Development and Validation of a Model to Predict Pavement Temperature Profile." (kJ/m^2-day or Btu/ft^2-day (1 kJ/m^2-day = 0.088055075028155 Btu/ft^2-day)):

$$R = \frac{24}{\pi} I_{sc} E_o \sin\phi \sin\delta \left[\frac{\omega_s \pi}{180} - \tan\omega_s\right] \quad [29]$$

where;

R = Average daily solar radiation on a horizontal surface (kJ/m²-day). R is parabolic during the day, equal to zero during the night.

I_{sc} = solar constant = 4871 kJ/m²-hr (= 442 Btu/ft²-hr)

ϕ = latitude (degrees)

E_o = eccentricity factor:

$$E_o = 1.000110 + 0.034221\cos\Gamma + 0.001280\sin\Gamma + 0.000719\cos 2\Gamma + 0.000077\sin 2\Gamma$$

Γ = $\frac{2\pi d_{n-1}}{365}$ = day angle (rad)

d_n = The day number of the year ranging from 1 to 365

δ = Solar declination (degrees)

$$\delta = (0.006918 - 0.399912\cos\Gamma + 0.070257\sin\Gamma - 0.006758\cos 2\Gamma + 0.000907\sin 2\Gamma - 0.002697\cos 3\Gamma + 0.00148\sin 3\Gamma)$$

ω_s = sunrise hour angle (degrees);

$$\omega_s = \cos^{-1}(-\tan\phi\tan\delta)$$

Few example daily solar radiation values are illustrated in Table 3.

Table 3. Daily solar Radiation Values for Four Locations in the Eastern United States

Location	Latitude, °N	H_0, kJ/m^{2}day		
		January 1	May 1	September 1
Caribou, ME	46.87	9580	36095	31820
Washington, DC	38.95	14461	37661	34214
Blacksburg, VA	37.19	15554	37927	34664
Tampa, FL	27.97	21207	38801	36505

In order to be able to calculate the hourly temperature with depth, the daily solar radiation needs to be converted to hourly solar radiation for each day. For this, Dempsey (Dempsey, 1969) assumed a parabolic shape, as shown in Figure 4, between sunrise and sunset times. There is no information in Dempsey's dissertation as to how the sunrise and sunset times are determined (Dempsey, 1969). In Figure 4, it is shown that 6am is the assumed sunrise time and 6pm is the assumed sunset time. In this project, an algorithm (see Figure 5) was used to compute the sunrise and sunset times based on latitude, longitude, date and time in a year.

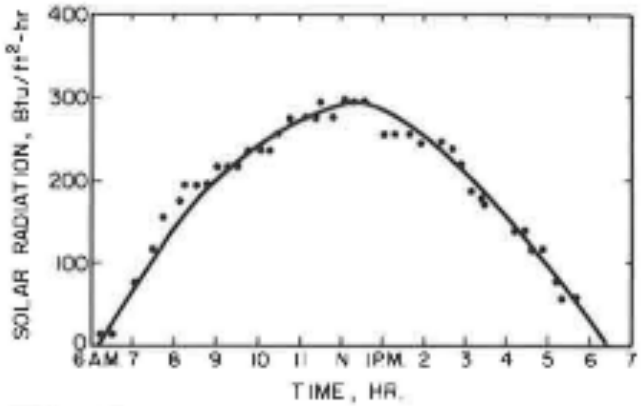

Figure 4. Assumed variation of intensity of solar radiation in Dempsey's dissertation (Dempsey, 1969)**.**

```
function [rise_time, set_time] = f_sun_up_down(date, latitude, longitude, daylight_saving, UTC)
% example inputs:
% date = '2009-05-20'
```

```
% latitude = 42.699013;
% longitude  = -84.412416;
% daylight_saving = 1
% UTC = -5
%Calculates Julian Day Number (jdn)
    date_str = strsplit(date, '-');
    year = str2double(char(date_str(1)));
    month = str2double(char(date_str(2)));
    day = str2double(char(date_str(3)));

    a = floor((14 - month)/12);
    y = year + 4800 - a;
    m = month + 12*a - 3;

    jdn = day + floor((153*m + 2)/5) + 365*y + floor(y/4) - floor(y/100) + ...
          floor(y/400) - 32045;

%Calculate days since 1st Jan 2000
    n = jdn - 2451545 + 0.0008;
    J_star = n - longitude/360;
    M = mod(357.5291 + 0.98560028*J_star, 360);
    C = 1.9148 * sind(M) + 0.0200 * sind(2*M) + 0.0003 * sind(3*M);
    lambda = mod(M + C + 180 + 102.9372, 360);
    J_transit = 2451545.5 + J_star + 0.0053*sind(M) - 0.0069*sind(2*lambda);
    delta_sin = sind(lambda)*sind(23.44);
    omega_0_cos = (sind(-0.83) -
sind(latitude)*delta_sin)/(cosd(latitude)*cosd(asind(delta_sin)));
    J_set = J_transit + acosd(omega_0_cos)/360;
    J_rise = J_transit - acosd(omega_0_cos)/360;

    rise_time = (J_rise - jdn)*24 + daylight_saving + UTC;
    set_time = (J_set -jdn)*24 + daylight_saving + UTC;
```

Figure 5. A MATLAB algorithm to calculate sunrise and sunset times.

Figure 6 shows an example sunrise and sunset times in a year for Lansing, MI.

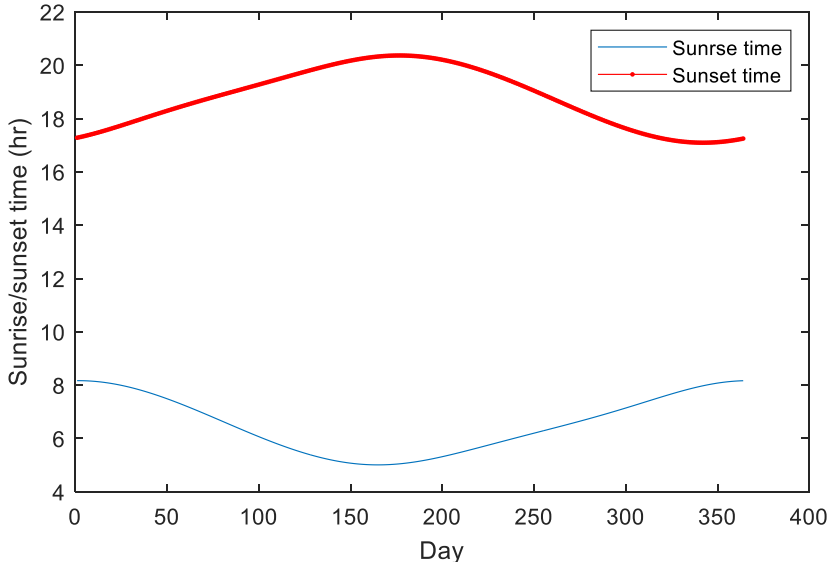

Figure 6. Example sunrise and sunset times for Lansing, MI (daylight savings time is ignored)

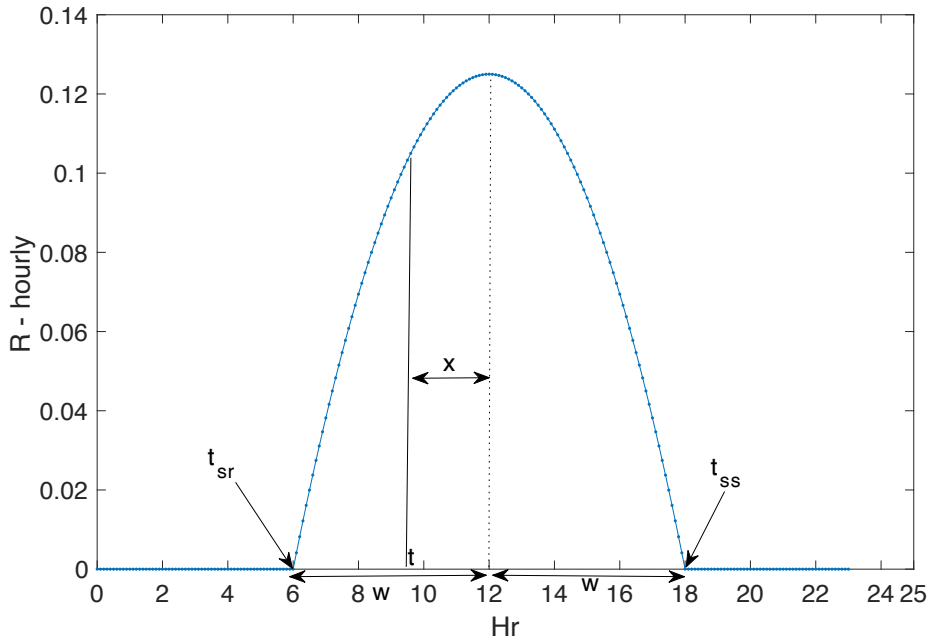

Figure 7. Parabolic shape of the hourly solar radiation variation

Once the sunrise and sunset times in a given day are obtained, the total daily solar radiation is converted into hourly solar radiation using the following parabolic formula (derived from the Fortran source code in dissertation by Dempsey 1969) (see Figure 7):

$$R_h(t) = \frac{3R}{4w^3}(w^2 - x^2) \qquad [30]$$

where;

$R_h(t)$ = solar radiation at time t, Btu/ft²-hr
x, w = see Figure 7
w = $(t_{ss} - t_{sr})/2$
x = $(t - t_{peak})$
t_{sr} = sunrise time
t_{ss} = sunset time
t_{peak} = time when sun is at its peak = $(t_{ss} + t_{sr})/2$
R = total solar radiation per day Btu/ft²-day

Note that $R(t) = 0$ *if* $t < t_{sr}$ *or* $t > t_{ss}$

3.2 Propagation of surface temperature into the pavement layers

Conduction is the dominant mechanism for propagation of the surface temperature into the pavement structure. For this, the one-dimensional Fourier heat-transfer finite difference equation is used:

$$\frac{\partial^2 T}{\partial z^2} = \frac{1}{\alpha}\frac{\partial T}{\partial t} \qquad [31]$$

The equation above can be discretized into the following set of equations, based on the sublayer definitions illustrated in Figure 8.

$$\frac{\partial T}{\partial t} = \frac{\alpha}{\Delta z^2}(T_{n-1} - 2T_n + T_{n+1}) \text{ for nodes n} = 2 \ldots \text{N} - 1 \quad [32]$$

$$\frac{\partial T}{\partial t} = \frac{\alpha}{\Delta z^2}(T_{n-1} - 2T_n + T_{con}) \text{ for node n} = \text{N} \quad [33]$$

$$T_n(t + \Delta t) = T_n(t) + \frac{\partial T}{\partial t}\Delta t \quad [34]$$

where;

N = total number of nodes
α = thermal diffusivity (ft^2/hr) ($\alpha = K/C\gamma$)
T_{surf} = surface temperature ($^\circ$F)
T_{con} = 51^{o}F = constant temperature at a depth of 144 inches ($^\circ$F)

For numerical stability, time step should be kept below a certain value, as described below:

$$\Delta t \leq \frac{\gamma C \Delta z^2}{2K} \quad [35]$$

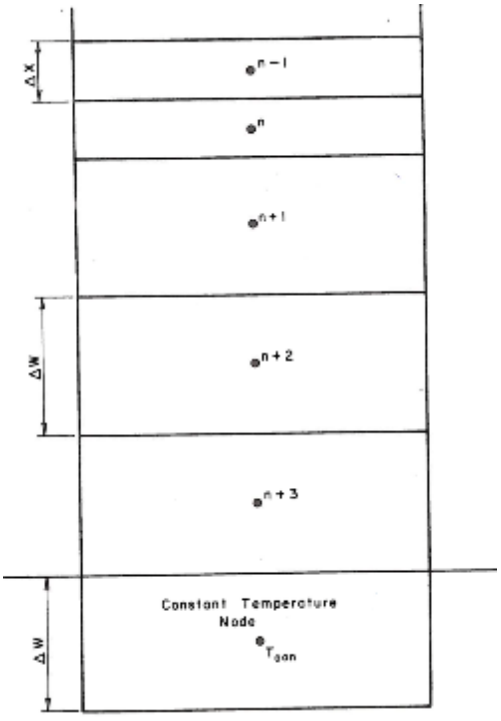

Figure 8. Pavement sublayers used in the climatic model

At the interface between two layers of asphalt or interface between the base/asphalt etc., the following equation is used to propagate the temperature (for nodes n=2…N-1)

$$\frac{\partial T}{\partial t} = \frac{1}{\Delta z^2 (C_{n-1}\gamma_{n-1} + C_{n+1}\gamma_{n+1})} (T_{n-1}2K_{n-1} - 2T_n(K_{n-1}+K_{n+1}) + T_{n+1}2K_{n+1}) \quad [36]$$

For stability of the equation above, the following equation must be hold:

$$\Delta t \leq \frac{(C_{n-1}\gamma_{n-1} + C_{n+1}\gamma_{n+1})\Delta z^2}{2(K_{n-1} + K_{n+1})} \quad [37]$$

3.3 Example runs and validation

Figure 9 illustrates an example pavement structure with temperature variation with depth, at specific time (t=46 hrs after the beginning of the simulation). In AC modeling, histogram of the hourly temperatures are computed for each month (see Step 2 in Figure 9), then the histogram is divided into five equal intervals, i.e., quintiles. Then the temperature at the center of each quintile is computed. The pavement structural models in AC is run using the moduli that correspond to each quintiles and distresses are computed at each of the five quintiles.

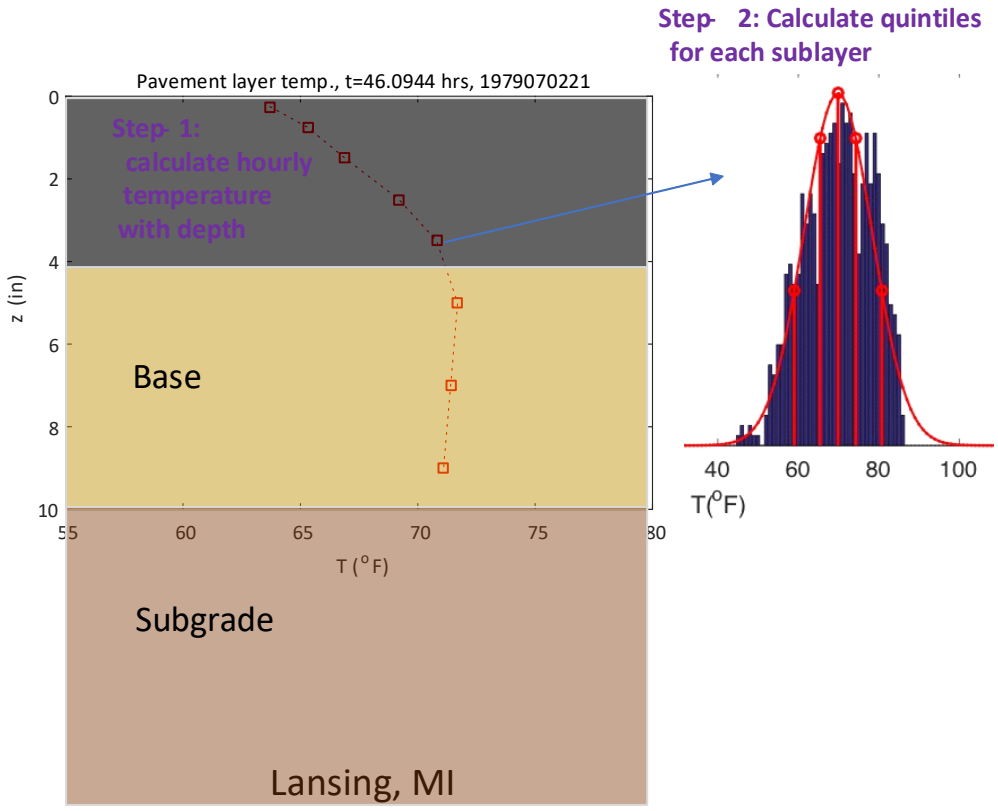

Figure 9. An example temperature profile computed by the climatic model and illustration of the determination of the temperatures at each quintile.

A comparison of the temperatures in different quintiles computed by the EICM model and the MCLIM climatic model coded herein are shown in Figure 10 for several depths. As shown, a very good match is visible at depths closer to the surface. The difference increases with increasing depth.

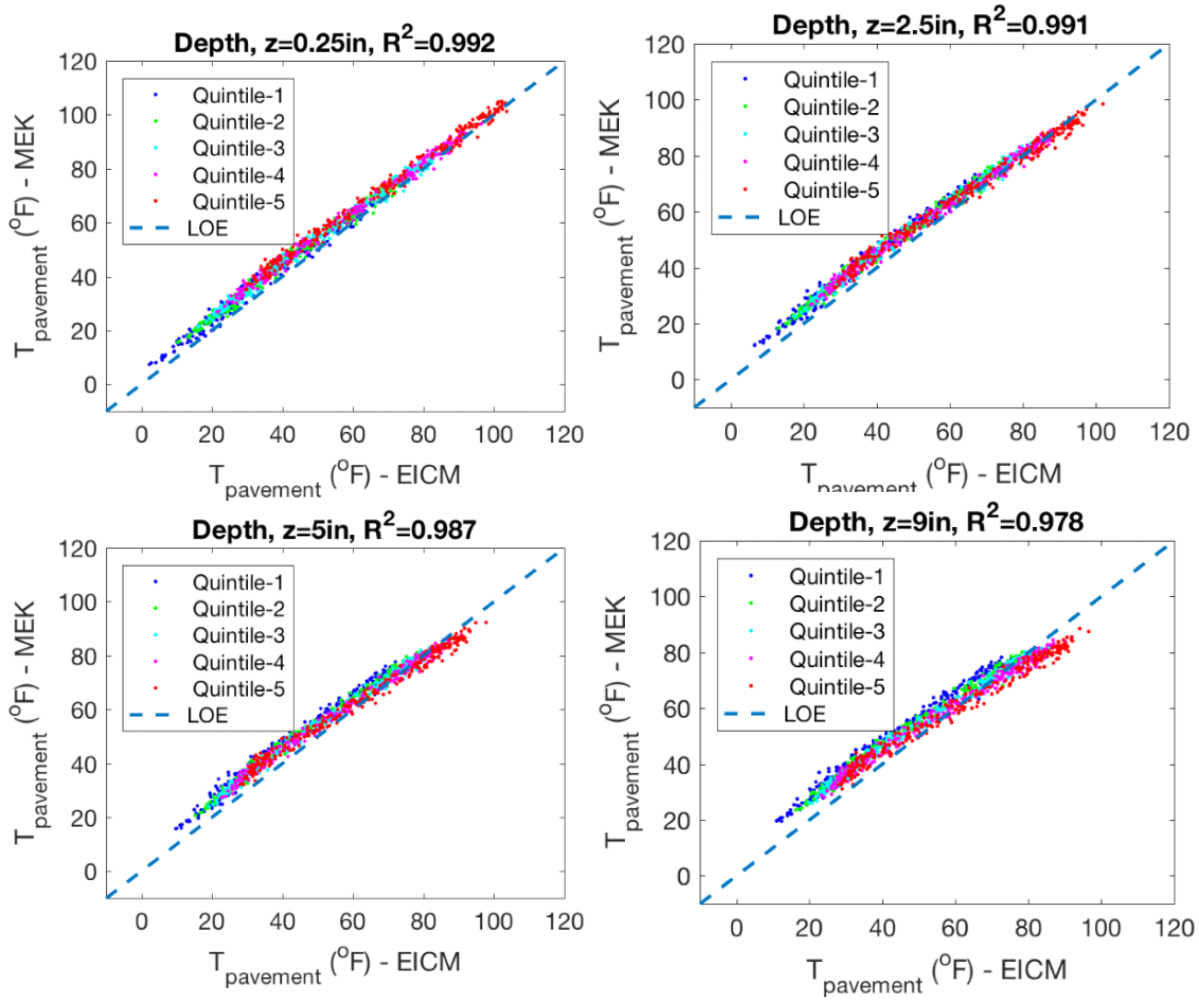

Figure 10. Comparison of EICM and the MEAPA climatic model at different quintiles, at different depths.

4. MODELING AC-GB: ASPHALT CONCRETE OVER GRAVEL BASE

As mentioned previously, the following distresses are computed for the pavement type AC-GB (Asphalt Concrete over Gravel Base):

1. AC top-down fatigue cracking (ft/mile)
2. AC bottom-up fatigue cracking (%)
3. AC thermal cracking (ft/mile)
4. Rutting – AC, base, subbase, subgrade (in)
5. International Roughness Index (IRI) (in/mile)

The general steps of the algorithm are as follows:

1. Development of the |E*| master curves for the AC layer(s)
2. Sublayering of the structure
3. Calculating equivalent frequencies and load correction factors using the MEPDG procedure
4. Running the climatic model and obtaining temperature at the center of each sublayer
5. Running the Global Aging System (GAS) model
6. Calculation of the elastic moduli in five quintiles in a given month using the temperature at each quintile, frequency and the |E*| master curve coefficients.
7. Defining the critical strain locations for each type of distress
8. Running the thermal cracking model
9. Running the MatLEA structural response model at each quintile of each month, then:
    a. Compute the top-down cracking increment
    b. Compute the bottom-up cracking increment
    c. Compute the AC rutting increment
    d. Compute the base/subbase rutting (same model) increment
    e. Compute the subgrade rutting increment.
    f. Summation of the distresses computed during 5 quintiles of each month to compute the cumulative monthly distresses.
10. Compute IRI values for each month

4.1 Development of the |E*| master curve(s) for the AC layer(s)

The following sigmoid formulation is used to construct the |E*| master curves for each AC layer:

$$log(|E^*|) = c1 + \frac{c2}{1+e^{c3+c4log((t_r)}} \quad [38]$$

where;

$|E^*|$ = Dynamic modulus.
t_r = Time of loading at the reference temperature.
$c1$ = Minimum value of E^*.
$c1 + c2$ = Maximum value of E^*.
$c3, c4$ = Parameters describing the shape of the sigmoidal function.

The reduced time (t_r) is essentially equivalent to stress pulse duration, and defined using the following formula:

$$log(t_r) = log(t) - log[a(T)] \quad [39]$$

where;

t_r = Time of loading at the reference temperature.
t = Time of loading at a given temperature of interest. It is assumed that $t = 1/f$ where f = frequency (Hz) at the center of the sublayer.
$a(T)$ = Shift factor as a function of temperature.
T = Temperature of interest.

The shift factor coefficient is a function of the temperature:

$$log(a(T)) = a_1\left(T^2 - T_{ref}^2\right) + a_2(T - T_{ref}) \quad [40]$$

where;

$a(T)$ = Shift factor, as a function of temperature.
a_1, a_2 = Constants.
T_{ref} = Reference temperature

In addition, a gaussian function is fit to the phase angles, to develop a phase angle master curve:

$$\phi = d_1 e^{-\frac{(d_2+logt_r)^2}{2d_3^2}} \quad [41]$$

where;

ϕ = Phase angle (degrees).
d_1, d_2, d_3 = Constants.
$logt_r$ = Logarithm of the reduced time

An example |E*| and phase angle inputs and corresponding |E*| and phase angle master curves are shown in Figure 11.

Mixture |E*| (psi)				
T (F) \ f(Hz)	0.1	1	10	25
14	2080818	2576683	2965251	3089022
40	884204	1415009	1981830	2196098
70	196099	416308	790492	981083
100	45980	98647	218399	296475
130	17794	32017	65494	89249

Mixture Phase Angle (degrees)				
T (F) \ f(Hz)	0.1	1	10	25
14	11.0	7.0	4.1	3.2
40	22.0	16.9	11.9	10.1
70	29.3	27.1	23.0	21.0
100	27.1	29.3	29.2	28.4
130	20.4	25.1	28.4	29.2

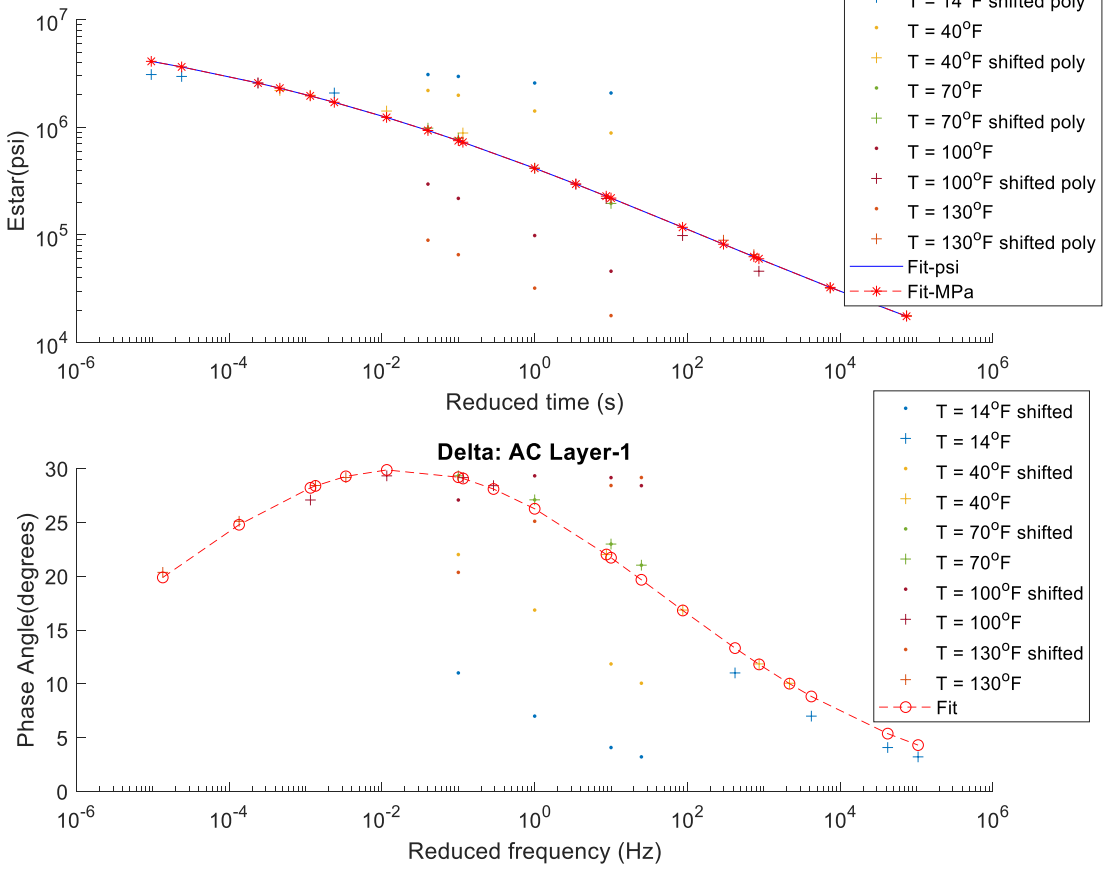

Figure 11. An example |E*| and phase angle input and corresponding |E*| and phase angle master curves

4.2 Sublayering Pavement Structure and Analysis Points

Pavement layers are sublayered into several layers. This is needed for:

- Calculation of temperature, frequency and then the moduli of each AC sublayer using the |E*| master curve coefficients.
- Calculation of the rutting at the center of each sublayer in all pavement layers
- Calculation of thermal stresses at the center of each sublayer in thermal cracking model.

The sublayering is done using the following rules:

- Top layer:
    - If the thickness is greater than 1.5", subdivide into layers with 0.5", 0.5", 1" layers and the remaining thickness. For example, if the thickness is 1.75", the sublayers are 0.5", 0.5" and 0.75". If the thickness is 4.25", the sublayers are 0.5", 0.5", 0.25", 1", 1" and 1".
    - If the thickness is less than 1.5", there is no sublayering. Entire layer is treated as one sublayer.
- Subsequent layers:
    - If the thickness is greater than 2", subdivide into multiple 2" sublayers and remaining thickness. One exception is that if the remaining thickness is between 2" and 4", entire remaining thickness is treated as one sublayer.
    - If the thickness is less than 2", there is no sublayering. Entire layer is treated as one sublayer.

Figure 12 shows example sublayering of a three-layer structure. Figure 12 also shows the structural analysis points for a single axle, dual tire. The analysis points for the single axle dual tire are selected as follows:

- In z-direction: At the surface, center of each sublayer, at the bottom of the AC layer and the top of the subgrade
- In x-direction: At the center between the dual tire, halfway between the center of the dual tire and the edge of the tire, at the edges of the tire, at the center of the tire, then 4", 8", 16", 24" and 32" away from the outer edge of the tire.

Figure 13 shows the analysis points for the single, tandem, tridem and quad axles. In z- and x-directions, the points are selected same as the single axle and this set is herein called the XZ point cloud. In tandem axle, 3 sets of XZ point clouds are placed; two at the centerlines of the two dual tires and one at the midpoint between the axles.

Similarly, in tridem and quad axles, the XZ point clouds are placed along the centerlines of the dual tires and at the midpoint between the dual tires in the y-direction. As a result, 5 sets of XZ point clouds are generated in tridem axle and 7 sets of XZ point clouds are generated for the quad axle, as shown in Figure 13.

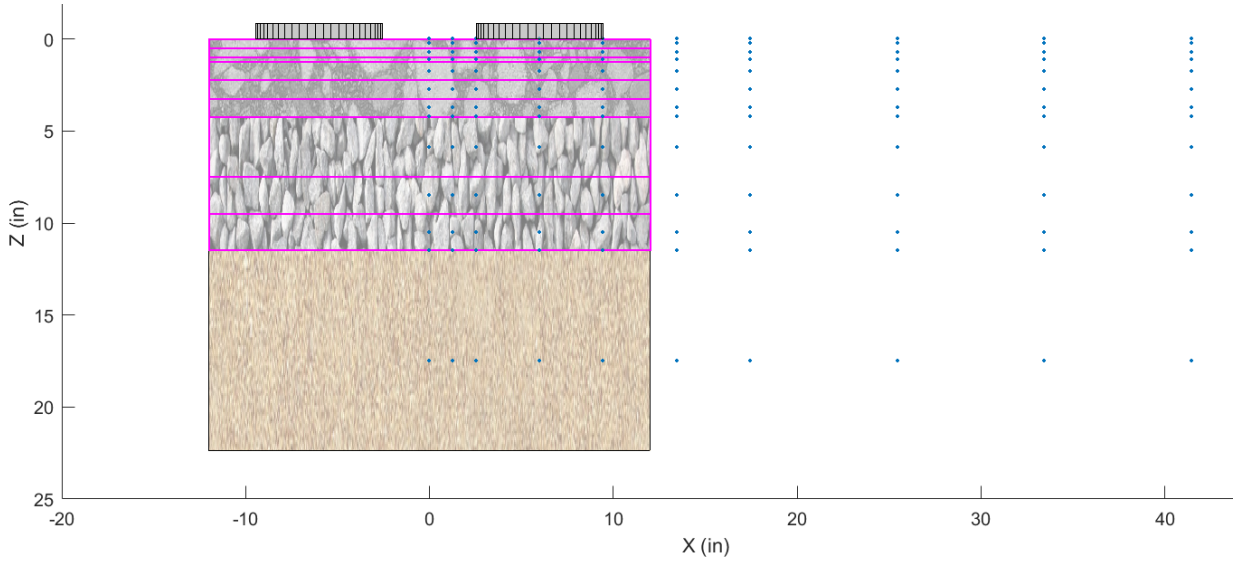

Figure 12. Example sublayering of a three-layer structure and analysis points for the single axle dual tire configuration

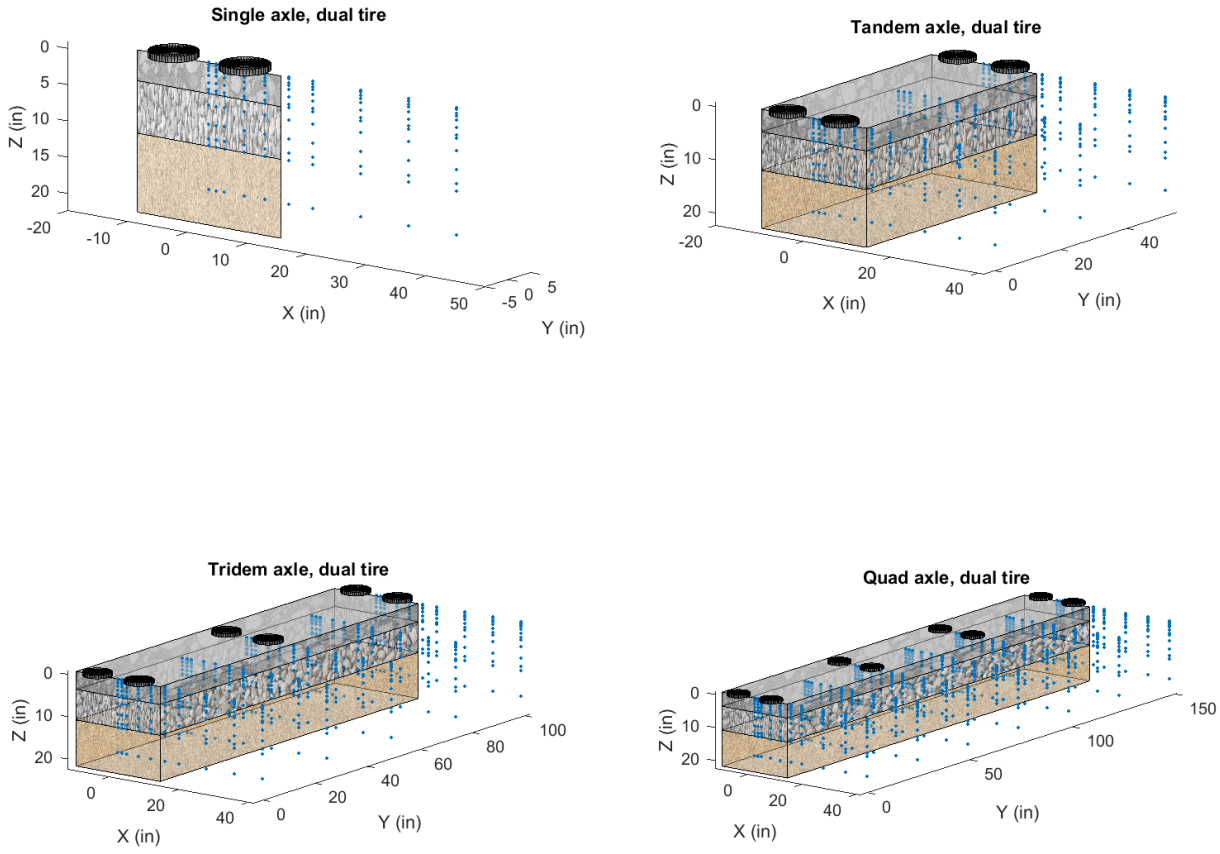

Figure 13. Analysis points for the single, tandem, tridem and quad axle configurations.

4.3 Calculation of the loading frequency

The calculation of the loading frequency is based on the concepts used by the MEPDG, where the stress pulse is assumed to be haversine, and its duration depends upon the vehicle speed and the depth of the point of interest below the pavement surface. The following equation relates the time of load to the vehicle speed, and the effective length of the pulse.

$$t = \frac{L_{eff}}{17.6\, v_s} \quad [42]$$

where;

t= Duration of load (sec)
L_{eff}= Effective length (inch)
v_s= Velocity (mph)

The calculation of the effective length at a given point is described in the next paragraphs. The loading frequency (f, in Hz) is based on the base time of the loading pulse, according to the following relationship:

$$f = \frac{1}{t} \quad [43]$$

The traffic load applied on top of the pavement surface produces stresses in the underlying layers. These stresses spread as a function of the stiffness: stiffer materials tend to distribute the stresses over a much wider area compared to the less stiff material. The effective length (L_{eff}) is defined as the extent of the stress pulse at a specified depth within the pavement system.

Based on its definition, the slope of the stress distribution as a function of material stiffness is needed for the estimation of the effective length. Since no relationship exists to relate the stiffness to the slope of the stress distribution, a simplified approach was used to overcome this problem: the concept of equivalent thickness. This concept was first established by Odemark in 1949. Odemark's method is based on the assumption that the stresses and strains below a layer depend on the bending stiffness of that layer only. If the thickness, modulus and Poisson's ratio of a layer are changed, but the bending stiffness remains unchanged, the stresses and strains below the layer should also remain unchanged. The stiffness of a layer is proportional to $\frac{h^3 E}{1-\upsilon^2}$, where h is the thickness, E is the modulus and υ is the Poisson's ratio of the layer. The transformation shown in Figure 14 should not influence the stresses or strains in layer 2 provided that:

$$\frac{h_1^3 E_1}{1-v_1^2} = \frac{h_e^3 E_2}{1-v_2^2} \quad [44]$$

or

$$h_e = h_1 \sqrt[3]{\frac{E_1}{E_2} \times \frac{1-v_2^2}{1-v_1^2}} \quad [45]$$

where he is known as the "equivalent" thickness.

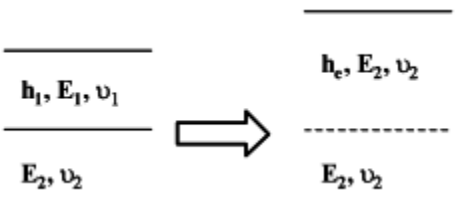

Figure 14. Transformation of a layered system using the Odemark's method

Using the concept presented by Odemark, any pavement structure can be transformed into an equivalent structure having the subgrade modulus and a total thickness given by equivalent thickness, h_e. For simplicity, the stress distribution for a typical subgrade soil is assumed to be at 45 degrees and using this stress distribution the effective length can be computed at any depth.

4.3.1 Effective Depth and Length for Single and Tandem Axles

For any pavement layer, the effective length of the stress pulse is computed at a specific depth for which the loading frequency is needed for the computation of the modulus and the following linear elastic analysis. This depth is called effective depth (Z_{eff}) and computed by the following relationship:

$$Z_{eff} = \sum_{i=1}^{n-1}\left(h_i \sqrt[3]{\frac{E_i}{E_{SG}}}\right) + h_n \sqrt[3]{\frac{E_n}{E_{SG}}} \quad [46]$$

For example, in the case of a three asphalt layers pavement structure and for the calculation of the tensile strains at the bottom of the asphalt layers, the Equation [5] is:

$$Z_{eff} = \sum_{i=1}^{2}\left(h_i \sqrt[3]{\frac{E_i}{E_{SG}}}\right) + h_3 \sqrt[3]{\frac{E_n}{E_{SG}}} \quad [47]$$

The effective length of the load pulse at a specific depth under the wheel load is a function of the axle configuration. The approach of calculating the effective length of the loading pulse is based on the following assumptions:

1. No overlap occurs between axles at an effective depth smaller than the free distance between axles.
2. Complete overlap occurs at effective depths larger than two times the distance between axles.
3. In the interval between depths defined in 1 and 2, the effective length varies linearly with depth on a log-log scale.

Thus, the effective length computation is a function of the axle type. In case of a single axle, no overlap of stresses occurs at any depth because any other axle is very far. The effective length is schematically shown in Figure 15 and mathematically defined by the following equation:

$$L_{eff} = 2.(a_c + Z_{eff}) \quad [48]$$

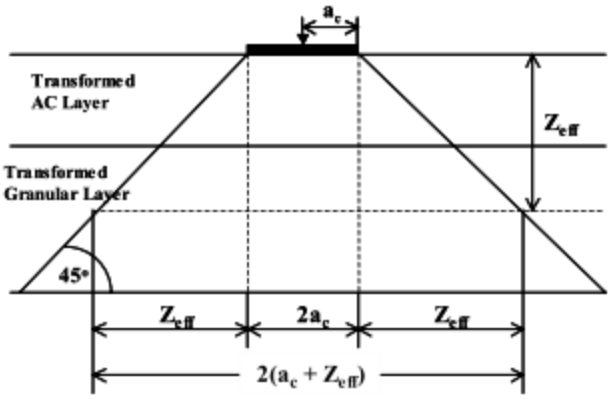

Figure 15. Effective length computation - Single Axle

Figure 16 shows the layout of the tandem wheel configuration where "S_T" is the tandem spacing between the axles in the direction of travel. Two stress distributions are formed because of this configuration. No overlap between the two distributions occurs close to the pavement surface. Then, stresses start to overlap until a complete overlap occurs at an effective depth larger than two times the distance between axles (2 S_T).

Near the pavement surface, in the "no overlap" zone, two distinct stress pulses will be observed. In this situation, the traffic repetitions must be multiplied by a factor of two (traffic multiplier, N). At depths greater than 2 S_T, in the "full overlap" zone, this axle configuration will generate only one stress pulse. The traffic multiplier in this situation is one (N =1). Between these two limits ("partial overlap" zone), the effective length of the stress pulse and the traffic multiplier are the functions of the amount of overlap of the stress pulses caused by the configuration. The effective length and the traffic multiplier can be calculated in the three zones mentioned above as follows.

4.3.1.1 No overlap zone: $Z_{eff} < S_T/2 - a_c$

The effective length for this condition is defined by the following equation:

$$L_{eff} = 2.(a_c + Z_{eff}) \quad [49]$$

As mentioned earlier, two distinct stress pulses can be observed resulting from the tandem axle configuration. In this situation, the traffic count for the tandem axle is multiplied by 2, to account for the twin peaks at this depth interval.

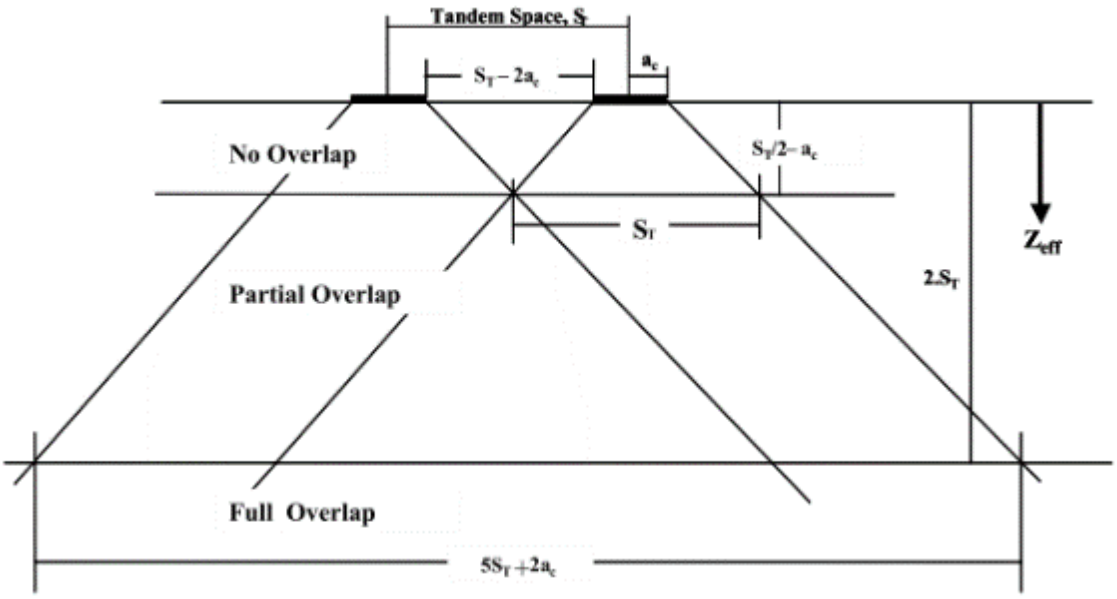

Figure 16. Effective length computation - Tandem Axle

4.3.1.2 Partial overlap zone: $S_T/2 - a_c < Z_{eff} < 2\ S_T$

As shown in Figure 16, at $S_T/2 - a_c$, the effective length can mathematically be defined as S_T, while at a depth of 2 S_T, the effective length is $5S_T + 2a_c$. Based on the third assumption presented earlier, between these two points the effective length varies linearly with depth on a log-log scale. Thus, the effective length can be calculated using the following equations:

$$\log(L_{eff}) = a\log(Z_{eff}) + b \quad [50]$$

$$a = \frac{log\frac{5S_T + 2a_c}{S_T}}{log\frac{2S_T}{\frac{S_T}{2} - a_c}} \quad [51]$$

$$b = \log S_T - alog\left(\frac{S_T}{2} - a_c\right) \quad [52]$$

The traffic multiplier for the partial overlap is given by the following relationships.

$$\log N = a\log Z_{eff} + b \quad [53]$$

$$a = \frac{\log 0.5}{\log\left(\frac{2S_T}{\frac{S_T}{2} - a_c}\right)} \quad [54]$$

$$b = \log 2 - a\log\left(\frac{S_T}{2} - a_c\right) \quad [55]$$

4.3.1.3 Partial overlap zone: Zeff => 2 ST

The effective length for this condition is defined by the following equation:

$$L_{eff} = S_T + 2a_c + 2Z_{eff} \quad [56]$$

Since full overlap occurs beyond this depth, only single resultant stress pulse occurs. Thus, the traffic multiplier is one (N = 1).

4.3.2 Effective length for any Number of Axles

Generalized equations for multiple axles (n) are similar to those of the tandem axle and summarized in Table 4.

Table 4. Generalized formulations for n number of axles (n=3 for tridem, n=4 for quad).

Zone	Equation	Note
No overlap zone: $Z_{eff} < S_T/2 - a_c$	$L_{eff} = 2.(a_c + Z_{eff})$	The traffic multiplier is equal to the number of axles (n) of the axle configuration.
Partial overlap zone: $S_T/2 - a_c < Z_{eff} < 2\,(n\text{-}1)\,S_T$	$\log L_{eff} = a \log Z_{eff} + b$ where $a = \frac{\log \frac{5S_T(n-1)+2a_c}{S_T}}{\log\left(\frac{2S_T(n-1)}{\frac{S_T}{2}-a_c}\right)}$ $b = \log S_T - a \log\left(\frac{S_T}{2} - a_c\right)$	Traffic multiplier (N) is $\log N = a \log Z_{eff} + b$ where $a = \frac{\log \frac{1}{n}}{\log\left(\frac{2S_T(n-1)}{\frac{S_T}{2}-a_c}\right)}$ $b = \log n - a \log\left(\frac{S_T}{2} - a_c\right)$
Partial overlap zone: $Z_{eff} => 2\ S_T\ (n\text{-}1)$	$L_{eff} = S_T(n-1) + 2a_c + 2Z_{eff}$	The number of loading peaks and the traffic multiplier is always equal to one (N = 1).

4.3.3 Selection of the frequency for the analysis

Figure 17 shows variation of frequency at different load levels in single axle load spectra, for each depth (at the center of sublayer). As shown, different load levels in the axle load spectra of single, tandem, tridem and quad axles will produce different magnitudes of the frequencies. This

is because it is assumed that the tire contact pressure is constant, as a result, the contact radius will be different in different load levels. Considering different frequencies in different load levels would significantly increase the computation time. Therefore, it is assumed that 'equivalent' frequency to be used in computation of the moduli of the AC layer is the frequency that corresponds to the 18 kip single axle dual tire load (see the cross section of the red dotted line with the curves in Figure 17).

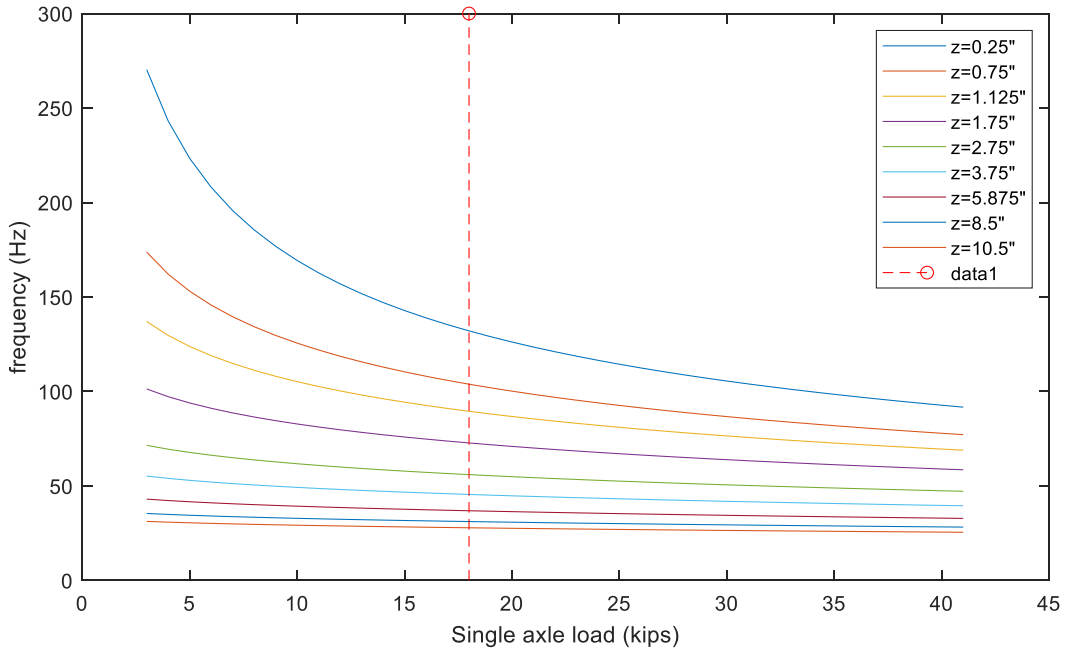

Figure 17. Variation of frequency with load levels in single axle load spectra and depth.

4.4 Effect of aging on the |E*| of the AC sublayers: Global Aging System (GAS) Model

Effect of aging (due to heat and oxidation) on the modulus of the AC sublayers is considered using the Global Aging System (GAS) Model. In the GAS model, the aged viscosity of the binder is calculated and subsequently used in the |E*| master curve sigmoid formulation. The GAS model includes four components:

- Original viscosity to mix/lay-down viscosity model
- Surface aging model
- Air void adjustment
- Viscosity-depth model

4.4.1 Original viscosity to mix/lay-down viscosity model

Asphalt binder viscosity at HMA placement is estimated as follows:

$$log\ (log(\eta_{t=0}) = a_0 + a_1\ log\ log\ (\eta_{orig}) \quad [57]$$

$$a_0 = 0.054405 + 0.004082 \times code \quad [58]$$

$$a_1 = 0.972035 + 0.010886 \times code \quad [59]$$

where;

$\eta_{t=0}$ = mix/lay-down viscosity, cP (centiPoise)
η_{orig} = original viscosity, cP (centiPoise)
code = hardening ratio (0 for average)

Codes used in original viscosity to mix/lay-down viscosity model are shown in Table 5. In order to simplify the inputs and not requiring Hardening Ratio as an input, code = 0 is used in the models. In addition, equation above is based on the original viscosity (η_{orig}). However, often times the binder |G*| is measured on RTFO aged binder and used in calculation of η_{orig}. In such case, a0 = 0 and a1 = 1 is used in algorithms. So RTFO parameter is an input to the algorithms. RTFO = 1 means RTFO aging is performed a0 = 0 and a1 = 1 is used, otherwise equations above are used to calculate a0 and a1.

Table 5. Codes used in original viscosity to mix/lay-down viscosity model

Mix/Lay-Down Hardening	Hardening Ratio (HR)	Code
Excellent to Good	HR ≤ 1.030	-1
Average	1.030 < HR ≤ 1.075	0
Fair	1.075 < HR ≤ 1.100	1
Poor	HR > 1.100	2

Viscosity of the original asphalt binder is calculated from |G*| at a frequency of 10 rad/s using the following relationship:

$$\eta_{orig} = 1000 * \frac{|G^*|}{10}\left(\frac{1}{sin\delta}\right)^{4.8628} \quad [60]$$

where;

η_{orig} = viscosity, cP (centiPoise)
δ = binder phase angle

It is noted that if η_{orig} value calculated using equation above is above 2.7x10^{12} cP, it is set equal to 2.7x10^{12} cP.

Once η_{orig} is computed for different values of $|G^*|$ corresponding to different temperatures (T_R), A and VTS values are computed by fitting a linear equation and determining the slope and intercept, using the A-VTS relationship shown below:

$$log\ log(\eta_{orig}) = A + VTS * log\ (T_R) \quad [61]$$

Where;

η_{orig} = mix/lay-down viscosity, cP (centiPoise)
T_R = Temperature in Rankine (^{o}R = ^{o}F + 459.67)
A = Intercept of viscosity-temperature relationship
VTS = Slope of viscosity-temperature relationship

4.4.2 Surface aging model

Asphalt binder viscosity at the pavement surface at certain pavement age is calculated as follows:

$$\log\ (log(\eta_{aged})) = \frac{log\ log(\eta_{t=0}) + At}{1 + Bt} \quad [62]$$

where;

$A = -0.004166 + 1.41213(C) + (C)\ log(MAAT) + (D)\ loglog(\eta_{t=0})$
$B = 0.197725 + 0.068384log(C)$
C = $10^{(274.4946 - 193.831\ log(T_R) + 33.9366\ log(T_R)^2)}$
D = $14.5521 + 10.47662\ log(T_R) - 1.88161\ log(T_R)^2$
η_{aged} = aged viscosity, cP (centiPoise)
$\eta_{t=0}$ = viscosity at mix/lay-down, cP (centiPoise)
MAAT= mean annual air temperature, °F
T_R = temperature in Rankine (^{o}R = ^{o}F + 459.67)
t = time in months

It is noted that if η_{aged} value calculated using equation above is above 2.7x10^{12} cP, it is set equal to 2.7x10^{12} cP.

4.4.3 Air void adjustment

Asphalt binder viscosity at the surface is corrected for air voids using the following relationship:

$$\log\left(log\left(\eta'_{aged}\right)\right) = F_v log\left(log\left(\eta_{aged}\right)\right) \quad [63]$$

$$F_v = \frac{1+1.0367\times10^{-4}(VA)(t)}{1+6.1798\times10^{-4}(t)} \quad [64]$$

$$VA = \frac{VA_{orig}+0.011(t)-2}{1+4.24\times10^{-4}(t)(MAAT)+1.169\times10^{-3}\left(\frac{t}{\eta_{orig,77}}\right)} + 2 \quad [65]$$

where;

η'_{aged} = viscosity at the surface is corrected for air voids
VA_{orig} = initial air voids in HMA
t = time in months since
MAAT = mean annual air temperature, °F
$\eta_{orig,77}$ = original binder viscosity at 77 °F, MPoise (Mega Poise)

It is noted that the formulation above resulted in unreasonable results as described later in this section. Therefore, these equations were omitted in the models by simply equating F_v to unity (i.e., $F_v = 1$).

4.4.4 Viscosity-depth model

Aged viscosity as a function of depth based on the aged viscosity from the surface and viscosity at mix/lay-down is calculated using the following relationship:

$$\eta_{t,z} = \frac{\eta_t(4+E)-E(\eta_{t=0})(1-4z)}{4(1+Ez)} \quad [66]$$

where;

$\eta_{t,z}$ = aged viscosity at time t, and depth z, MPoise
η_t = aged surface viscosity, MPoise
z = depth, in
E = $23.83e^{(-0.0308\ MAAT)}$, where

It is noted that if any $\eta_{t,z}$ value calculated using equation above is above $2.7x10^{12}$ cP, it is set equal to $2.7x10^{12}$ cP.

4.4.5 Discussion on the GAS model

An observation was made when the GAS model was implemented by following exact steps described above. As shown in Figure 18, the modulus values actually decreased with time. An investigation of why this happened revealed that the Fv parameter (the air void adjustment) was causing this phenomenon. As shown in Figure 19, the air-void corrected viscosity starts to decrease after about 30 months. Figure 20 shows the change in air voids and parameter Fv with time, where significant decrease in Fv is observed. Since Fv is a multiplier to the aged viscosity, after certain months, it causes the viscosity to decrease. While reading through the original paper describing the GAS model (Mirza & Witczak, 1995) it was realized that this parameter was actually an 'optional' parameter. A screenshot of the AAPT paper Mirza and Witczak. discussion is shown in Figure 21. Therefore, it was decided to set Fv = 1, i.e., air void adjustment is ignored.

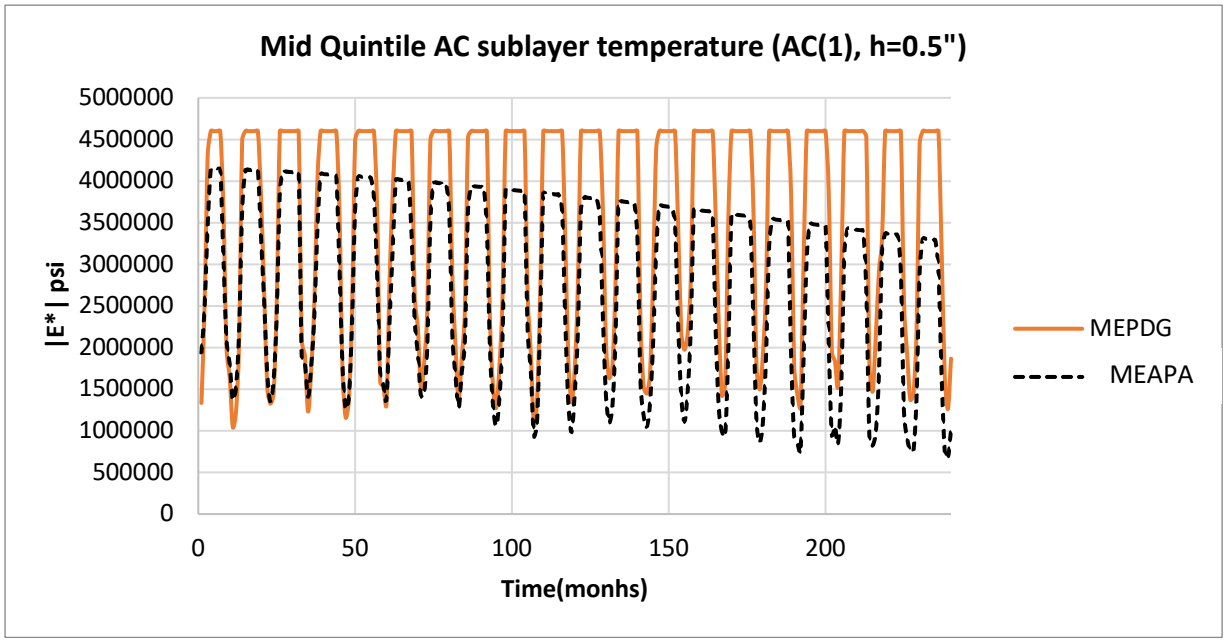

Figure 18. Comparison of MEPDG and MEAPA results for |E*| at top 0.5" sublayer, using the GAS model as described in the formulations. Climate: Lansing, MI.

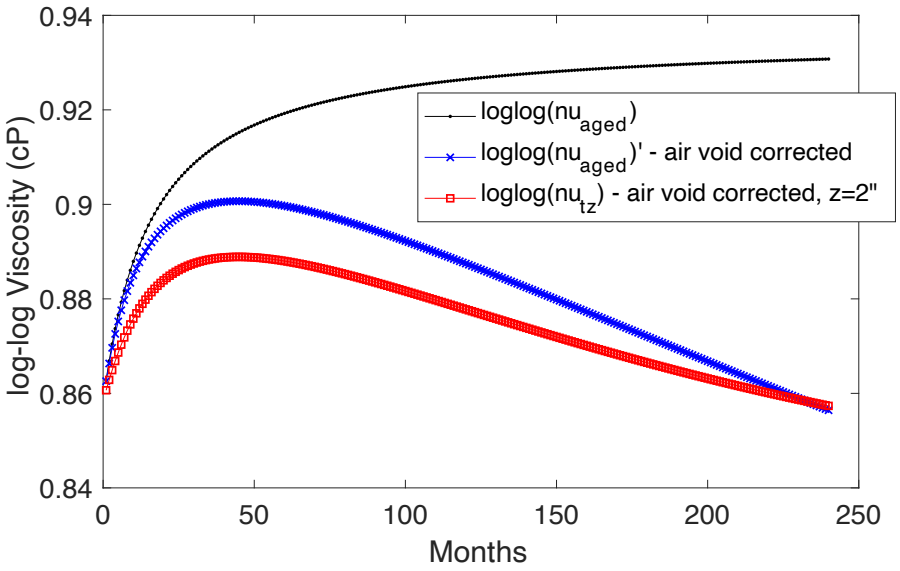

Figure 19. Comparison of viscosities with time

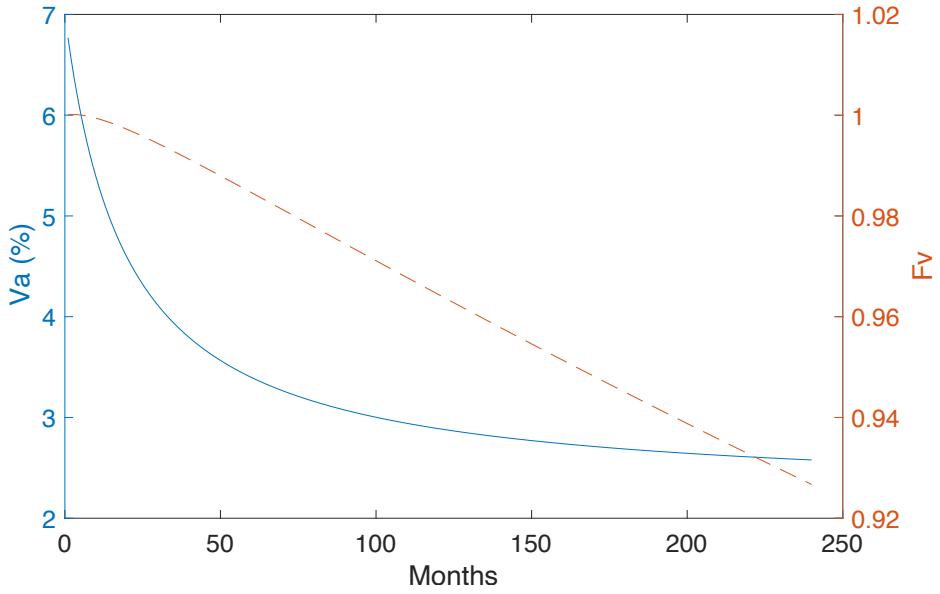

Figure 20. Change in air voids and parameter Fv with time.

DR. MIRZA: That is right if you have more permeable or higher air going into the mix it is going to be more oxidized and you are going to have a harder pavement at more deeper depths. That is why I had an adjustment factor to account for the air voids. I used this adjustment factor as an optional factor because a very limited number of data was available for the air voids which is, I believe, a very important factor in the age hardening properties of asphalt binders. In conclusion, I can say that the models developed were based on the data we can extract from the previous research studies. In fact, this study gives good guidelines for future research studies to include the variables that were not previously included in the research studies in the development of these models.

Figure 21. A snapshot from the discussion section of the AAPT paper Mirza and Witczak.

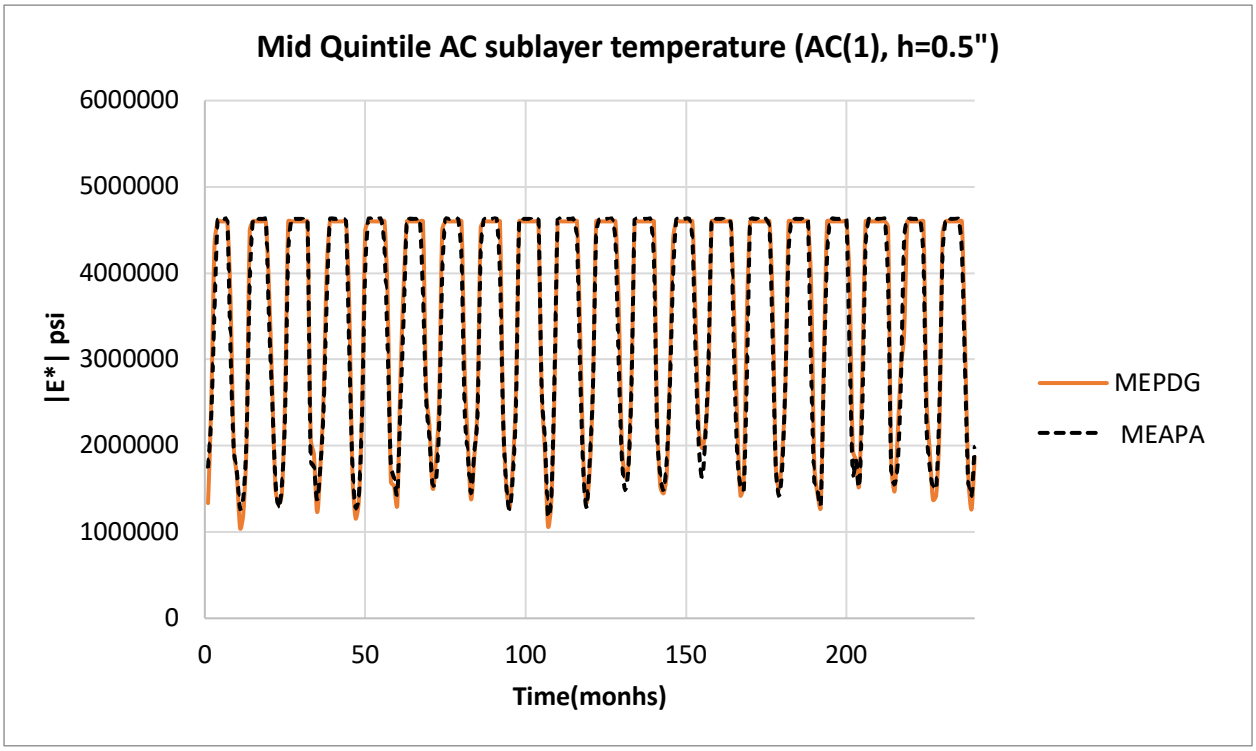

Figure 22. Mid Quintile AC sublayer temperature (AC(1), h=0.5") when Fv = 1 is used. Climate: Lansing, MI

4.5 Thermal Cracking

An overview of the thermal cracking model and basic formulations are shown in Figure 23. As shown, the basic propagation of the thermal crack length (C) within the depth of the pavement is based on a simplified Paris law. Once the C is computed, a probabilistic standard normal distribution is assumed and actual observed crack on the surface, in terms of ft per mile, is computed.

The thermal crack model includes the following basic steps:

1. Convert dynamic modulus |E*| to relaxation modulus E(t) using Prony-series based procedure
2. Calculate the thermal cracking fracture growth (Paris Law) parameters (e.g., m-value)
3. Calculate thermal strains caused by temperature fluctuations at different sublayers (using coefficient of thermal expansion/contraction)
4. Calculate reduced time using dynamic modulus master curve shift factor coefficients.
5. Solve convolution integral to compute the thermal stresses via state variable implementation (most time-consuming component)
6. Convert hourly stress fluctuations into daily max and daily minimum stresses.
7. Calculate maximum and minimum stress intensity factor (K) in a given day, then calculate $\Delta K = K_{max}-K_{min}$.
8. Calculate parameter A from the indirect tensile strength of the layer where the crack tip is, and m-value
9. Calculate ΔC and update the crack length $C \leftarrow C + \Delta C$
10. Calculate the observed amount of thermal cracking (C_f) using the standard normal distribution equation, and using the crack length C.

Crack growth model

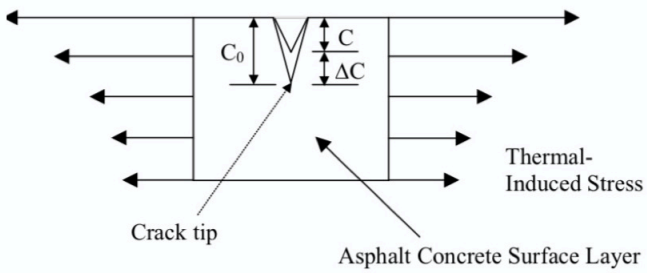

$$\Delta C = A(\Delta K)^n$$

where: ΔC = change in crack depth due to a cooling cycle

ΔK = change in stress intensity factor due to a cooling cycle

A,n = empirically determined fracture parameters

During a cooling cycle (daily), C is updated:
C ← C + ΔC

$$K = \sigma(0.45 + 1.99\, C_o^{0.56})$$

K	=	stress intensity factor
σ	=	far-field stress from pavement response model at depth of crack tip
C_o	=	current crack length

Probability-Based Thermal Cracking Model

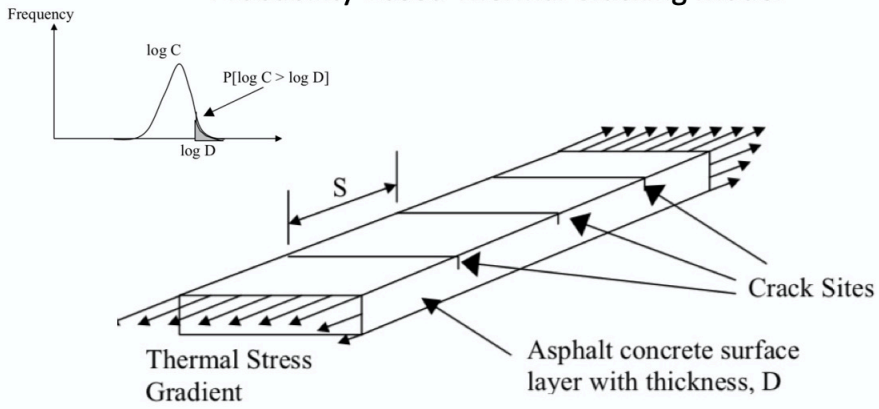

The amount of transverse cracking expected in the pavement system is predicted by relating the crack depth to an amount of cracking (crack frequency) by the following expression:

$$C_f = \beta_1 * N\left(\frac{\log C / h_{ac}}{\sigma}\right)$$

where:

C_f	=	Observed amount of thermal cracking.
β_1	=	Regression coefficient determined through field calibration.
$N(z)$	=	Standard normal distribution evaluated at (z).
σ	=	Standard deviation of the log of the depth of cracks in the pavement.
C	=	Crack depth.
h_{ac}	=	Thickness of asphalt layer.

Hierarchical Level	β_1	σ	E	β
1	400	0.769	10,000	5.0
2	400	0.769	10,000	1.5
3	400	0.769	10,000	3

Figure 23. An overview of the thermal cracking model and basic formulations.

4.5.1 Conversion of |E*| to E(t)

Since there is a correspondence between the |E*| and E(t), one can be computed from the other one. This eliminate the need for including the creep compliance (D(t)) as an input, as is done in MEPDG. In the conversion procedure, both |E*| and phase angle of the asphalt mixture is needed. Since phase angle is always measured during |E*| test, this does not constitute an additional input requirement. The |E*| to E(t) conversion procedure is originally described in the original paper by Park and Schapery (Park & Schapery, 1999). However, the steps were not very clear in the original paper and validation using asphalt mixtures was not given. A step-by-step description and laboratory validation of this procedure is given by Jamrah and Kutay (Jamrah & Kutay, 2015)

General steps of the interconversion procedure is given below:

1. Calculate the storage modulus($E'(\omega_R)$) as a function of reduced angular frequency (ω_R) using the dynamic modulus (|E*|) and phase angle (δ):

$$E'(\omega_R) = |E^*(\omega_R)|\cos\left(\delta(\omega_R)\right) \quad [67]$$

2. Fit a sigmoid function to the $E'(\omega_R)$ data in a log-log scale.
3. Obtain the equilibrium modulus E_∞ from the minimum value of sigmoid fitted *E'* in the log-log scale.
4. Define Prony series representation of storage modulus (*E'*) is:

$$E' = E_\infty + \sum_{i=1}^{n} \frac{E_i \omega_R^{\,2} \rho_i^{\,2}}{\omega_R^{\,2} \rho_i^{\,2} + 1} \quad [68]$$

5. Rearrange equation above:

$$E' - E_\infty = \sum_{i=1}^{n} \frac{E_i \omega_R^{\,2} \rho_i^{\,2}}{\omega_R^{\,2} \rho_i^{\,2} + 1} \quad [69]$$

   where ω_R=angular frequency, ρ_i relaxation times of each Maxwell element, which are selected to vary for several decades from 10^{-10} to 10^{10} s.
6. The relaxation strength (Prony series coefficients) E_i can be calculated by defining **[A]{X}=[C]** (matrix operations) such that:

$$A(j,i) = \frac{\omega_{R_j}^{\,2} \rho_i^{\,2}}{\omega_{R_j}^{\,2} \rho_i^{\,2} + 1} \quad [70]$$

$$X(i) = E_i \quad [71]$$

$$C(j) = (E'_j - E_\infty) \quad [72]$$

7. Solve for X in **[A] {X}= [C]** using least square method as follows:

$$\mathbf{X} = \left(\mathbf{A}^{\mathbf{T}}\mathbf{A}\right)^{-1}(\mathbf{AC}) \quad [73]$$

8. Knowing E_∞ and E_i, the relaxation modulus E(t) can be calculated using the following relationship:

$$E(t) = E_\infty + \sum_{i=1}^{n} E_i e^{(-t/\rho_i)} \quad [74]$$

where E_∞ is the long time elastic modulus, n is the number of elements in the Prony series (i.e. each Wiechert element) and ρ_i are the retardation time given by:

$$\rho_i = \frac{\eta_i}{E_i} \quad [75]$$

where η_i and E_i are the viscous damping and elastic coefficients of each Wiechert element (see Figure 25).

An example relaxation modulus (E(t)) master curve computed from |E*| and phase angle master curves is shown in Figure 24. One of the parameters used in thermal cracking fracture growth equation based on the Paris Law is the maximum slope (m) of the logE(t) -log(t) curve, which is computed using the minimum value of the derivative of the logE(t) -log(t), i.e., d(logE(t))/d(log(t)), as shown in Figure 24. Then the facture parameter (n) is computed using the following formula:

$$n = 0.8 * \left(1 + \frac{1}{m}\right) \quad [76]$$

where;
$n =$ fracture parameter used in the exponent of the law

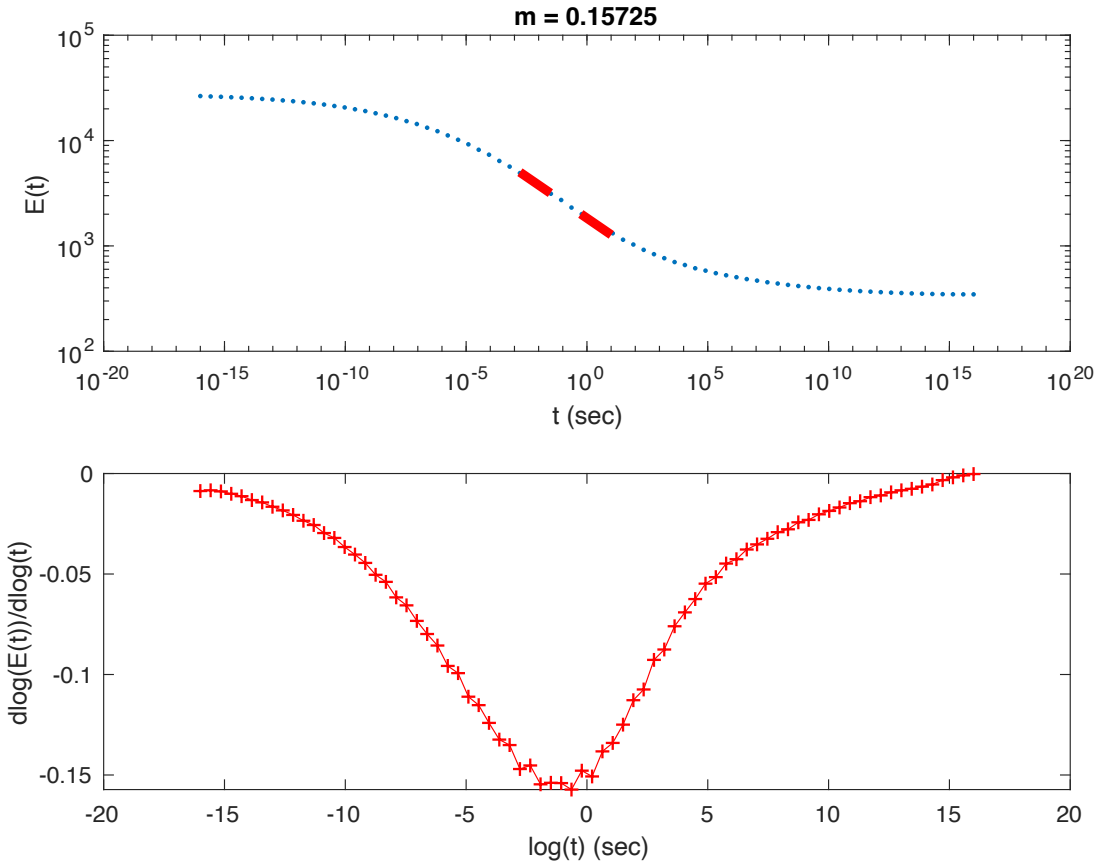

Figure 24. Relaxation modulus master curve computed from |E*| and phase angle master curves

4.5.2 Thermal strains caused by temperature fluctuations

The thermal strains at different depths caused by temperature fluctuations are computed by using temperature at each depth at each hour during the entire analysis duration. For each depth (e.g., at the center of a sublayer), this corresponds to 365 days * 24 hrs = 8,760 strain values for each year. For a typical pavement structure with 10 sublayers, and an analysis period of 20 years, total 1,752,000 strain values are computed. It is assumed that each sublayer is independently expanding/contracting like a series of horizontal rods, as illustrated in Figure 25.

Thermally induced strains for each rod are computed using the following one-dimensional expansion/contraction equation:

$$\varepsilon(t_R) = \alpha(\mathrm{T}(t_R) - \mathrm{T}_0) \qquad [77]$$

where

$\varepsilon(t_R)$=Thermal strain at the reduced time t_R

α =Coefficient of thermal contraction (1/C). For AC, it can be assumed $\alpha = 3\times10^{-5}$ 1/C (Islam & Tarefder, 2015)

$\mathrm{T}(t_R)$=Temperature of the sublayer at the reduced time of t_R

T_0 =Pavement temperature when the stress is zero. T_0=135°C, temperature right after the construction, can be assumed.

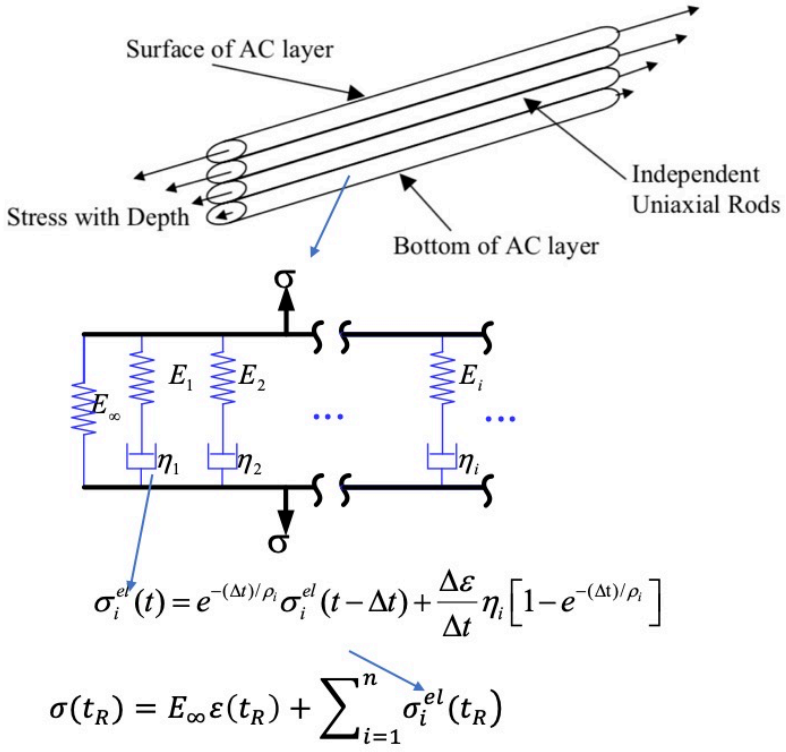

Figure 25. Illustration of the assumption of independent rods during calculation of thermal strains and stresses.

An example variation of thermal strains with time is shown in Figure 26.

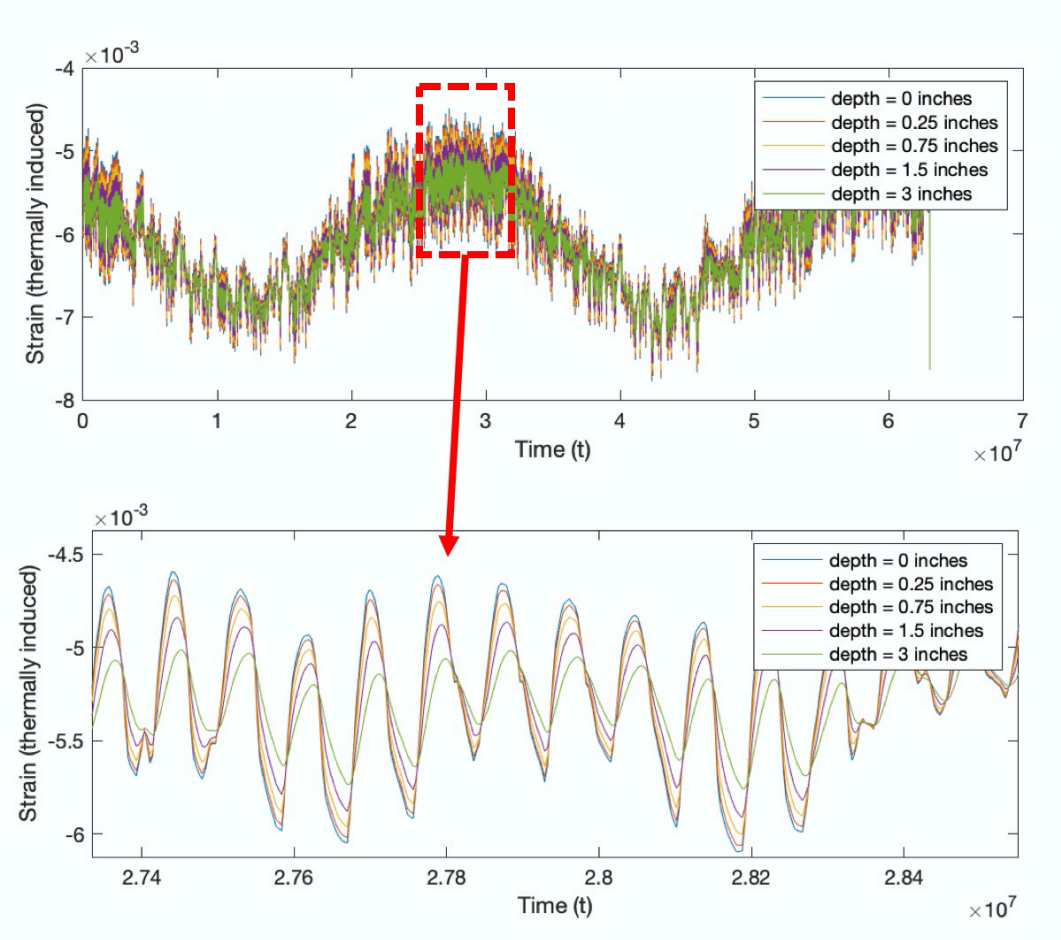

Figure 26. An example variation of thermal strains with time.

4.5.3 Calculate reduced time using dynamic modulus master curve shift factor coefficients.

The reduced time for each pavement sublayer with a different temperature ($T(t_R)$) is computed using the following formula:

$$t_R = \int_0^t \frac{dt}{a(T)} \quad [78]$$

where

$a(T)$ = Shift factor coefficient for each sublayer for each temperature T, $log(a(T)) = a_1(T^2 - T_{ref}^2) + a_2(T - T_{ref})$

It is noted that the reduced time for each sublayer has a different magnitude for a given time t, because of the temperature differences.

4.5.4 State variable implementation to solve for convolution integral for stresses

Viscoelastic stress response of each sublayer to thermal strains computed in the previous steps ($\varepsilon(t_R)$) is computed using the following convolution integral:

$$\sigma(t_R) = \int_0^{t_R} E(t_R - \tau)\frac{\partial \varepsilon}{\partial \tau} d\tau \quad [79]$$

where

$E(t_R - \tau)$ = Relaxation modulus evaluated at time $= t_R - \tau$
ε = Thermal strain at time $= t_R$, $\varepsilon(t_R)$)
$\sigma(t_R)$ = Thermal stress at time $= t_R$
τ = Time variable of the integration.

The equation above is impossible to solve tradionally for the duration of a typical analysis (e.g., for every hour for the duration of 20 years). Therefore, the state variable implementation, which converts the solution to an incremental solution, is used (see (M.E. Kutay & Lanotte, 2018)). In state variable implementation, the relaxation modulus is represented with a Wiechert (Generalized Maxwell) model (see Figure 25) using the Prony series: $E(t) = E_\infty + \sum_{i=1}^{n} E_i e^{(-t/\rho_i)}$.

$$\sigma(t_R) = E_\infty \varepsilon(t_R) + \sum_{i=1}^{n} \sigma_i^{el}(t_R) \quad [80]$$

where $\sigma(t_R)$ is viscoelastic stress at a reduced time t_R (for each depth), E_∞ is the long-time elastic modulus, *n* is the number of elements in the Prony series (i.e., Generalized Maxwell model), and $\sigma_i^{el}(t)$ is the stress in each Maxwell element at time *t*, which is computed using the following incremental formulation:

$$\sigma_i^{el}(t) = e^{-(\Delta t)/\rho_i}\sigma_i^{el}(t-\Delta t) + \frac{\Delta\varepsilon}{\Delta t}\eta_i\left[1 - e^{-(\Delta t)/\rho_i}\right] \quad [81]$$

where ρ_i, η_i and E_i, respectively, are the retardation time, viscous damping and elastic coefficients of each Generalized Maxwell element.

An example variation of viscoelastic stresses due to thermally induced strains is shown in Figure 27.

4.5.5 Daily maximum and minimum stresses and stress intensity factor

At this stage, hourly viscoelastic thermal stresses are used to compute the maximum and minimum thermal stresses in a given day. Figure 28 illustrates the daily maximum (σ_{max}) and minimum (σ_{min}) thermal stresses used in the thermal cracking formulations. Next step is to compute the stress intensity factor (K). Stress intensity factor, K, is computed using a simplified equation developed from theoretical finite element studies:

$$K_{min} = \sigma_{min}(0.45 + 1.99 * C_o^{0.56}) \quad [82]$$

$$K_{max} = \sigma_{max}(0.45 + 1.99 * C_o^{0.56}) \quad [83]$$

where;

K_{max}, K_{min} = Daily maximum and minimum stress intensity factor at depth of crack tip.
$\sigma_{max}, \sigma_{min}$ = Daily maximum and minimum viscoelastic thermal stress at depth of crack tip, psi.
C_o = Current crack depth for a given day, in.

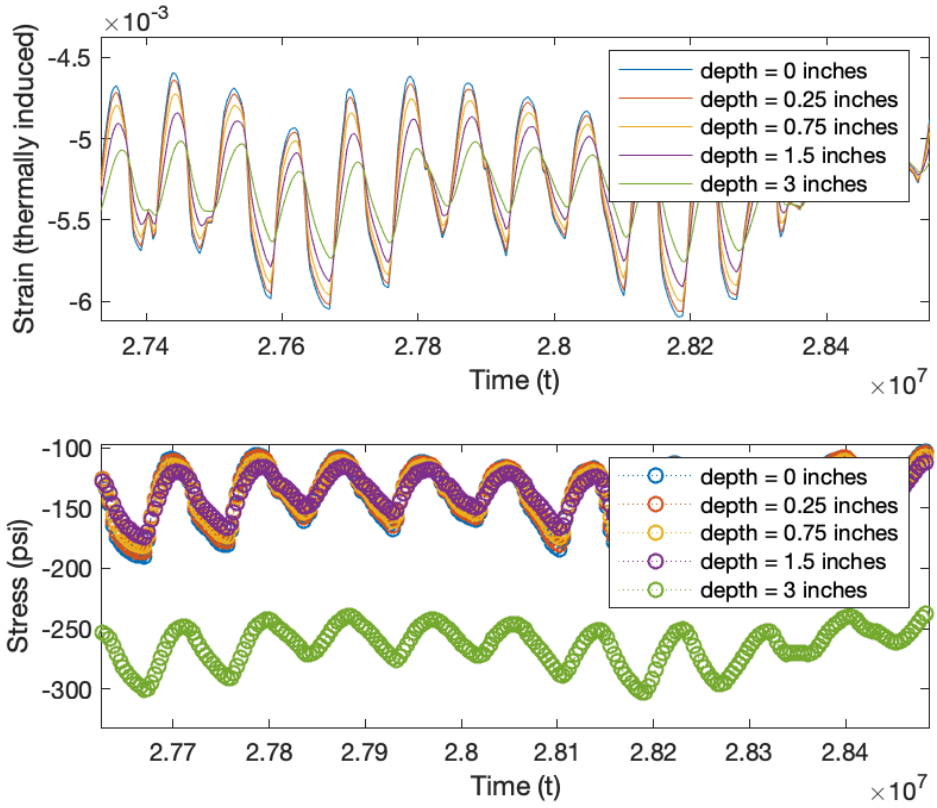

Figure 27. An example variation of viscoelastic stresses due to thermally induced strains. Please note that, in this example, there is a different asphalt layer at depth = 3", which is the reason for less stress response compared to the other depths.

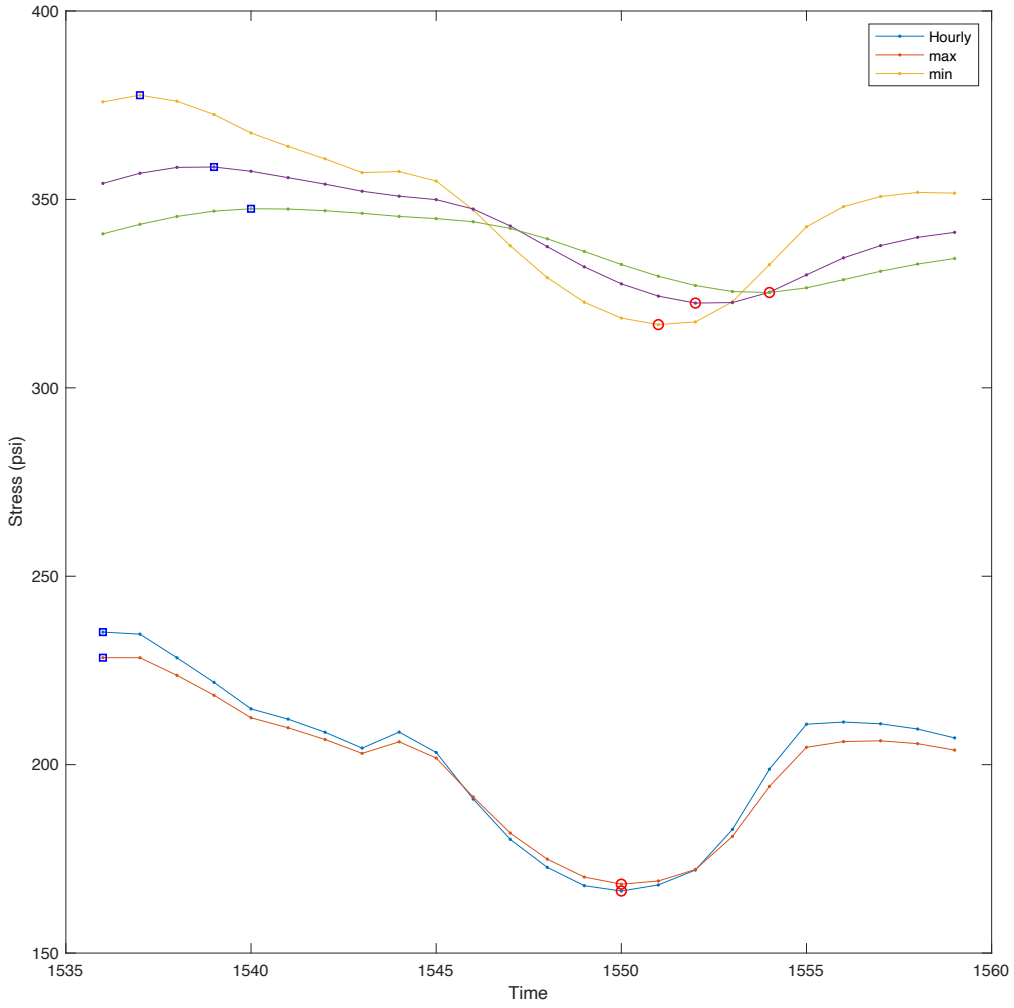

Figure 28. Illustration of the daily maximum and minimum thermal stresses used in the thermal cracking formulations.

4.5.6 Calculation of crack depth (C_o)

After calculation of daily maximum and minimum stress intensity factors, the stress intensity increment is calculated:

$$\Delta K = K_{max} - K_{min} \quad [84]$$

Then the parameter A is calculated from the indirect tensile strength of the layer where the crack tip is, and n-value:

$$A = 10^{4.389-2.52*\log(10000*IDT*n)} \quad [85]$$

where;

IDT = Indirect tensile strength of the layer where the crack tip is, in psi.
n = Fracture parameter(n= $0.8 * (1 + 1/m)$)

Change in the crack depth is computed using the simplified Paris law:

$$\Delta C = \left(K\beta_t\right)^{n+1} A \cdot \Delta K^n \quad [86]$$

ΔC = Change in the crack depth due to a cooling cycle.
ΔK = Change in the stress intensity factor due to a cooling cycle.
A, n = Fracture parameters for the HMA mixture.
β_t = Global calibration factor, equal to 16.
K = Local calibration factor (an input)

The depth of the crack length is updated for each day:

$$C_o\left(t_{day}+1\right) = C_o\left(t_{day}\right) + \Delta C \quad [87]$$

C_o = Crack depth, in.
t_{day} = Time, days
ΔC = Change in the crack depth due to a cooling cycle in a day

Finally, the observed amount of thermal cracking (C_f) is computed using the standard normal distribution equation:

$$C_f = C_f^{max} * \frac{1}{s_t\sqrt{2\pi}} e^{-\frac{(x_c-\mu_c)^2}{2s_t^2}} \quad [88]$$

C_f = Crack length, ft/mile.
C_f^{max} = 2112 ft/mile (maximum possible observed crack length)
x_c = Normalized crack depth fr a given day, in (see equation elow)
s_t = Standard deviation of the normal distribution, $s_t = 0.769/2$
μ_c = Mean of the normal distribution, which is equal to zero in this case.

$$x_c = \frac{1}{0.769}\log_{10}\left(\frac{C_o}{h_{ac}}\right) \quad [89]$$

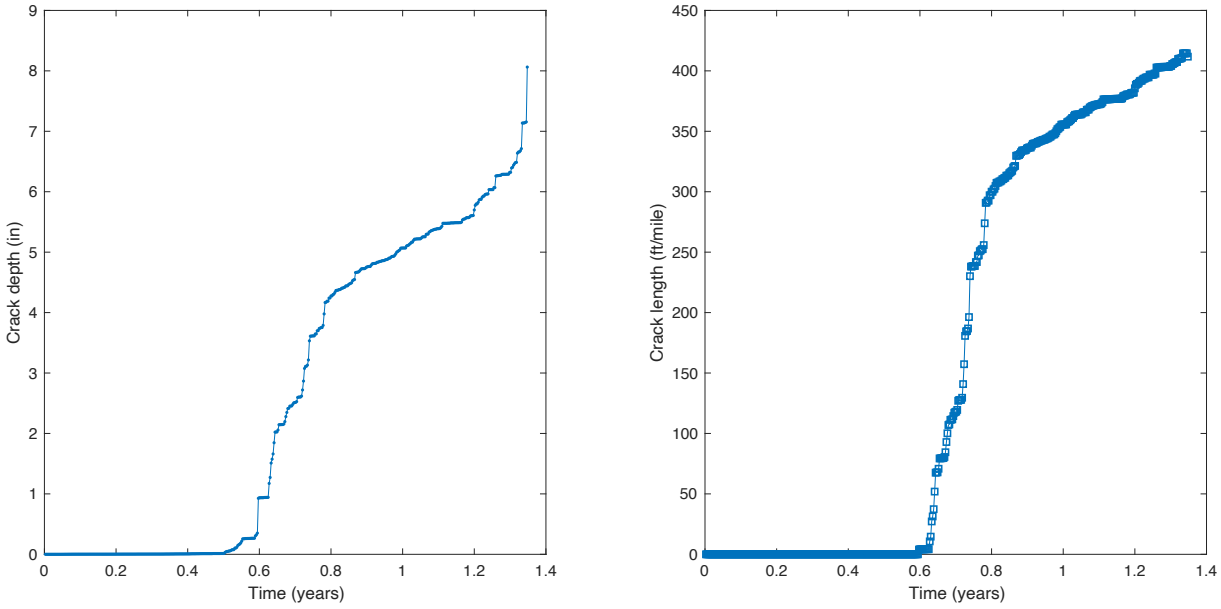

Figure 29. An example variation of computed thermal crack depth (C_o) and observed crack length (C_f)

4.6 Layered Elastic Analysis program: MatLEA

A computationally efficient layered elastic analysis program, called MatLEA (coded in MATLAB) was used in this work. The MatLEA is publicly available and formulations and computational steps are almost identical to those of the MnLayer software (Khazanovich & Wang, 2007). The concept is based on the Burmister's multi layered elastic theory (Burmister, 1945) and MatLEA solution procedure is described in Appendix G. The main differences between the MnLayer software and MatLEA are:

- A, B, C, D parameters (as described in described in Appendix G) are computed via 3D matrix inversion (making the program faster)
- The integration over the 'm' (the inverse Henkel transform variable) is done via bulk matrix operations.

An example run results of MatLEA for a 3-layer structure is shown in Figure 30. The evaluation points are shown as black dots in the figures. The response of total 315 points were computed (9 Z-coordinates and 35 R-Coordinates). Runtime for this particular run was 137 milliseconds.

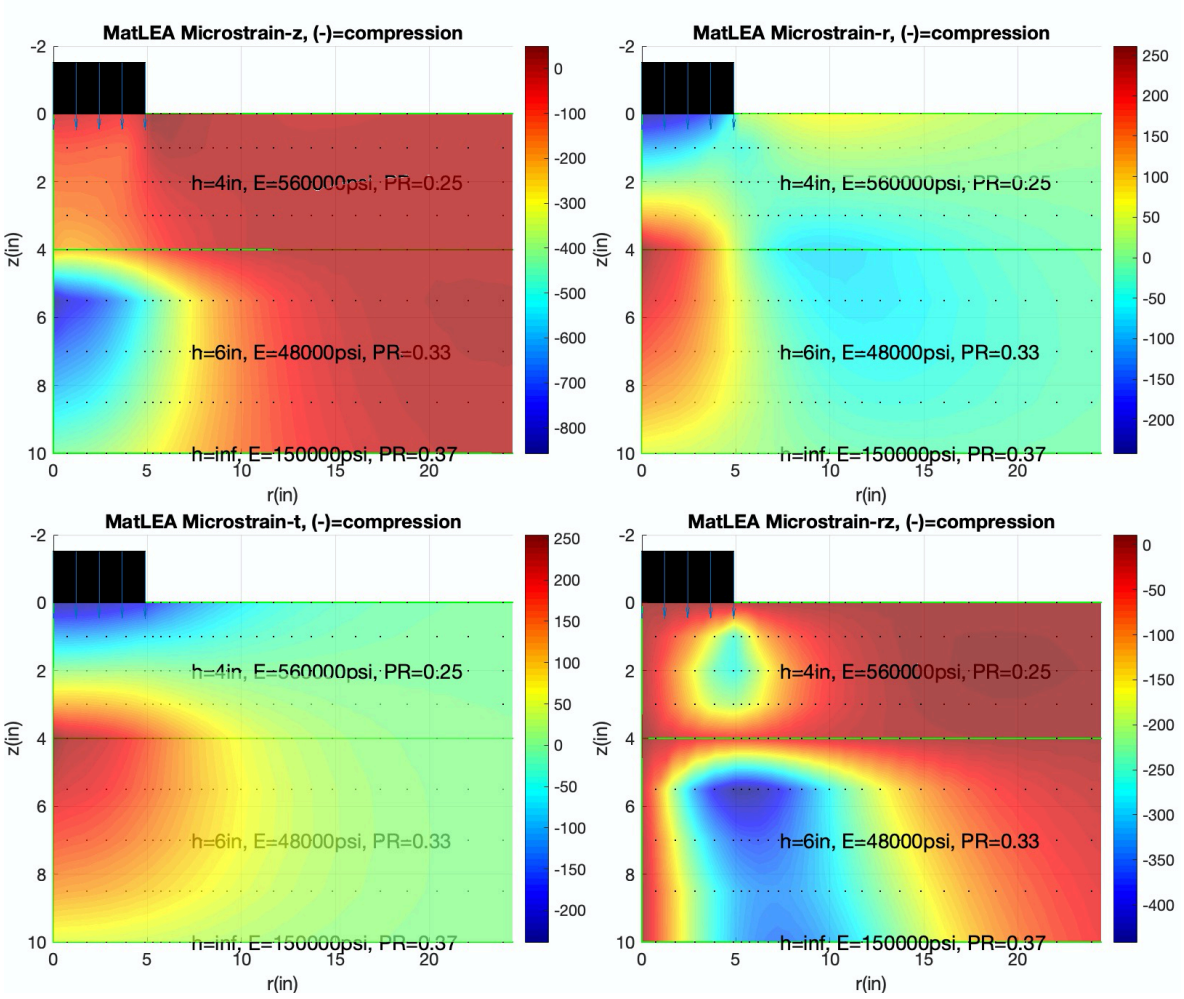

Figure 30. An example run of MatLEA for a 3-layer structure

A comparison of MatLEA results with those of CHEVLAY2 for radial microstrain is shown in Figure 31. Comparisons of MatLEA results with CHEVLAY2 and JULEA programs for microstrains in other directions are shown in Appendix H. As shown, a perfect match between the MatLEA and CHEVLAY2 is visible. Even though generally there is a good match between MatLEA and JULEA, some differences were observed (see Appendix H). Given the fact that MatLEA and CHEVLAY2 agree with each other very well, the errors are possibly due to the computational issues with JULEA program.

The MatLEA run time within MEAPA is about 100 milliseconds in the first run in a computer with Intel Core I7 processor with 2.5GHz speed (16 GB RAM). However, in subsequent runs in the 'for loop' that is going over the quintiles and months, it takes about 30 milliseconds for each run.

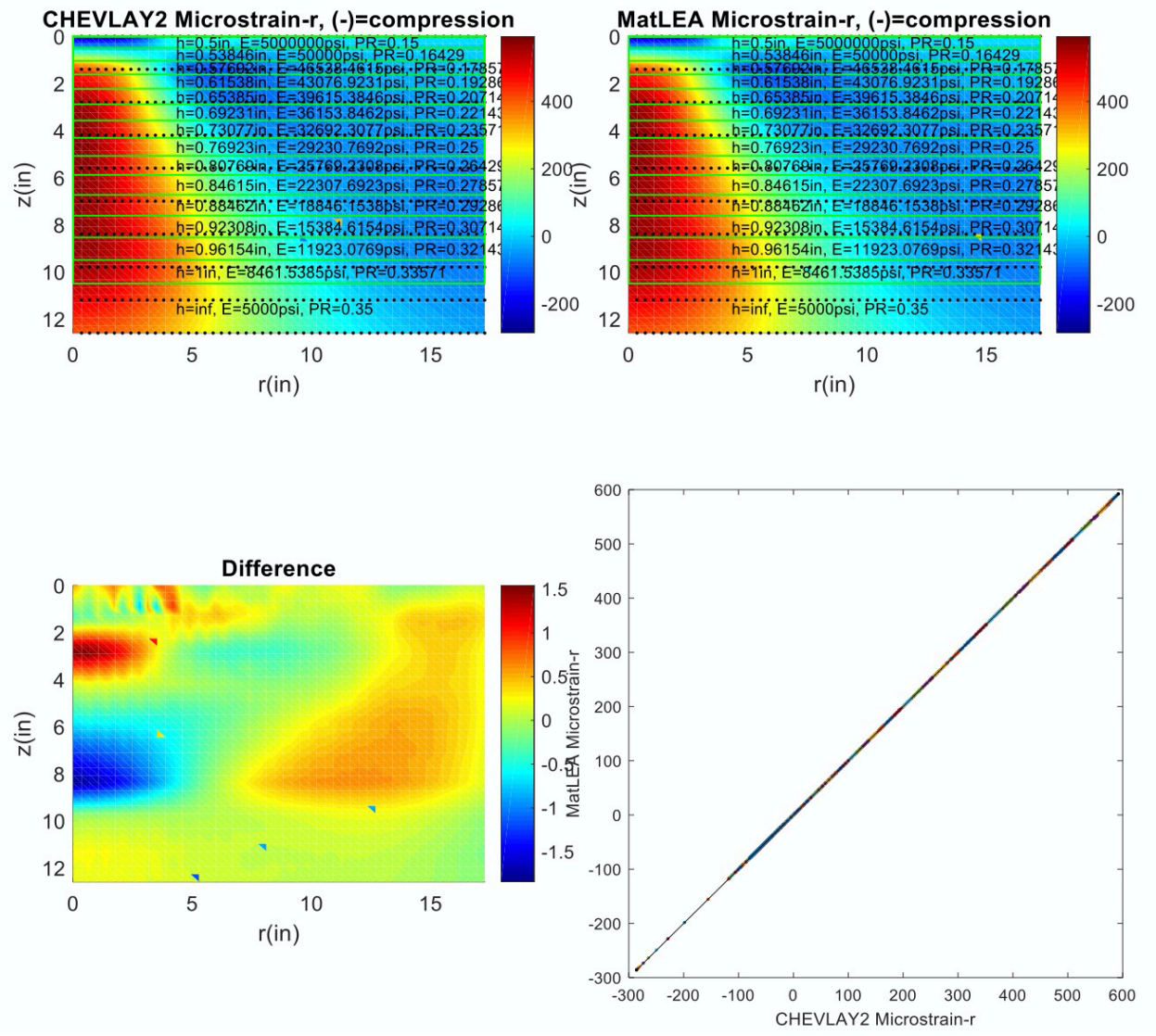

Figure 31. A comparison of MatLEA results with those of CHEVLAY2 for radial microstrain (which is used in models of bottom-up and top-down cracking)

4.7 Bottom-up Fatigue Cracking

The bottom up fatigue cracking is based on the traditional fatigue life formulation, Miner's law of linear damage growth and transfer functions converting damage to observed fatigue cracking in the field. The material level traditional fatigue life formulation used herein are as follows:

$$N_f = C_H C \beta_{f1} k_{f1} \left(\frac{1}{\varepsilon_t}\right)^{\beta_{f2} k_{f2}} \left(\frac{1}{E}\right)^{\beta_{f3} k_{f3}} \quad [90]$$

$$C = 10^{4.84\left(\frac{V_{be}}{V_a + V_{be}} - 0.69\right)} \quad [91]$$

$$C_{H-bu} = \left(b_{bu1} + \frac{b_{bu2}}{1 + e^{(b_{bu3} - b_{bu} h_{ac})}}\right)^{-1} \quad [92]$$

where,

ε_t	=	tensile strain at the bottom of AC
N_f	=	Number of cycles to failure, for bottom-up cracks
kf1, kf2, kf3	=	Global field calibration parameters (from the NCHRP 1-40D re-calibration; kf1 = 0.007566, kf2 = -3.9492, and kf3 = -1.281).
βf1, βf2, βf3	=	Local or mixture specific field calibration constants; for the global calibration effort, these constants were set to 1.0.
hac	=	height of the AC layer
b_{bui}	=	Coefficients: b_{bu1}=0.000398, b_{bu2}=0.003602, b_{bu3}=11.02, b_{bu4}=3.49
E	=	Equivalent modulus of bottom layer (at the given temperature/frequency)
V_{be}	=	Effective asphalt content by volume, %
Va	=	Percent air voids in the HMA mixture, %

The critical strain at the bottom of AC is computed at several analysis locations for single, tandem, tridem and quad axles. For each axle, the simulation is done for dual tires.

4.7.1 Calculation of Damage

Figure 32, Figure 33, Figure 34, and Figure 35 show critical strains computed by single, tandem, tridem and quad axles, respectively. As shown, the critical strains are computed at different X and Y locations at the bottom of the AC layer. This is needed for simulation of wheel wander and include its effect in the accumulated damage. For each axle, the maximum strain profile in Y direction is identified. An example of maximum strain profile for different axles is shown in Figure 36. This strain profile is used to calculate the number of cycles to failure for different locations in X direction, which is subsequently used in calculation of bottom-up damage due to each axle using the following formula:

$$D_{bu}^{\boldsymbol{single}}(X) = \frac{N_{i,t,w_k}^{\boldsymbol{single}}}{N_f(X)} \quad [93]$$

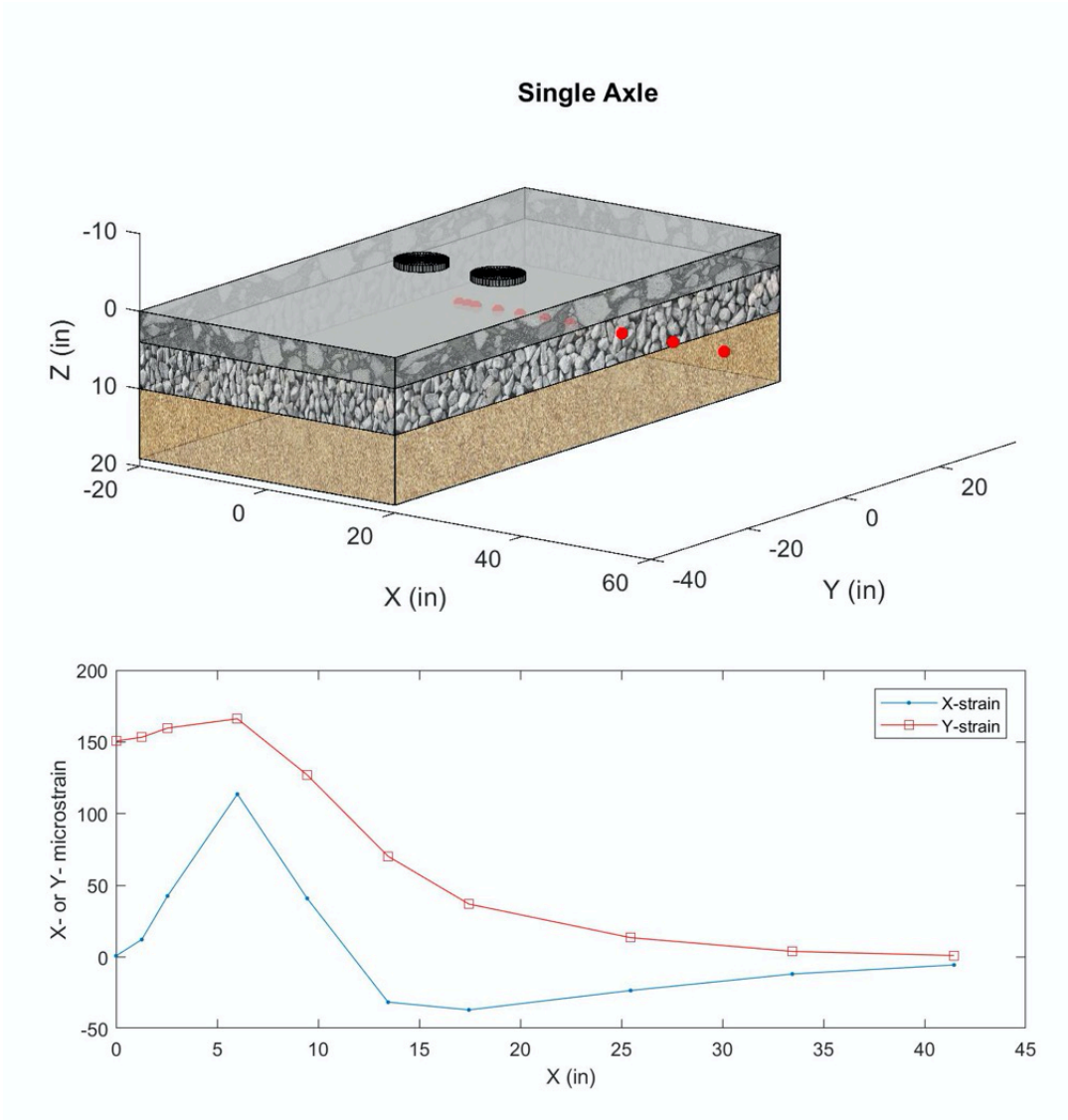

Figure 32. Critical strains computed at the bottom of AC due to single axle dual tire

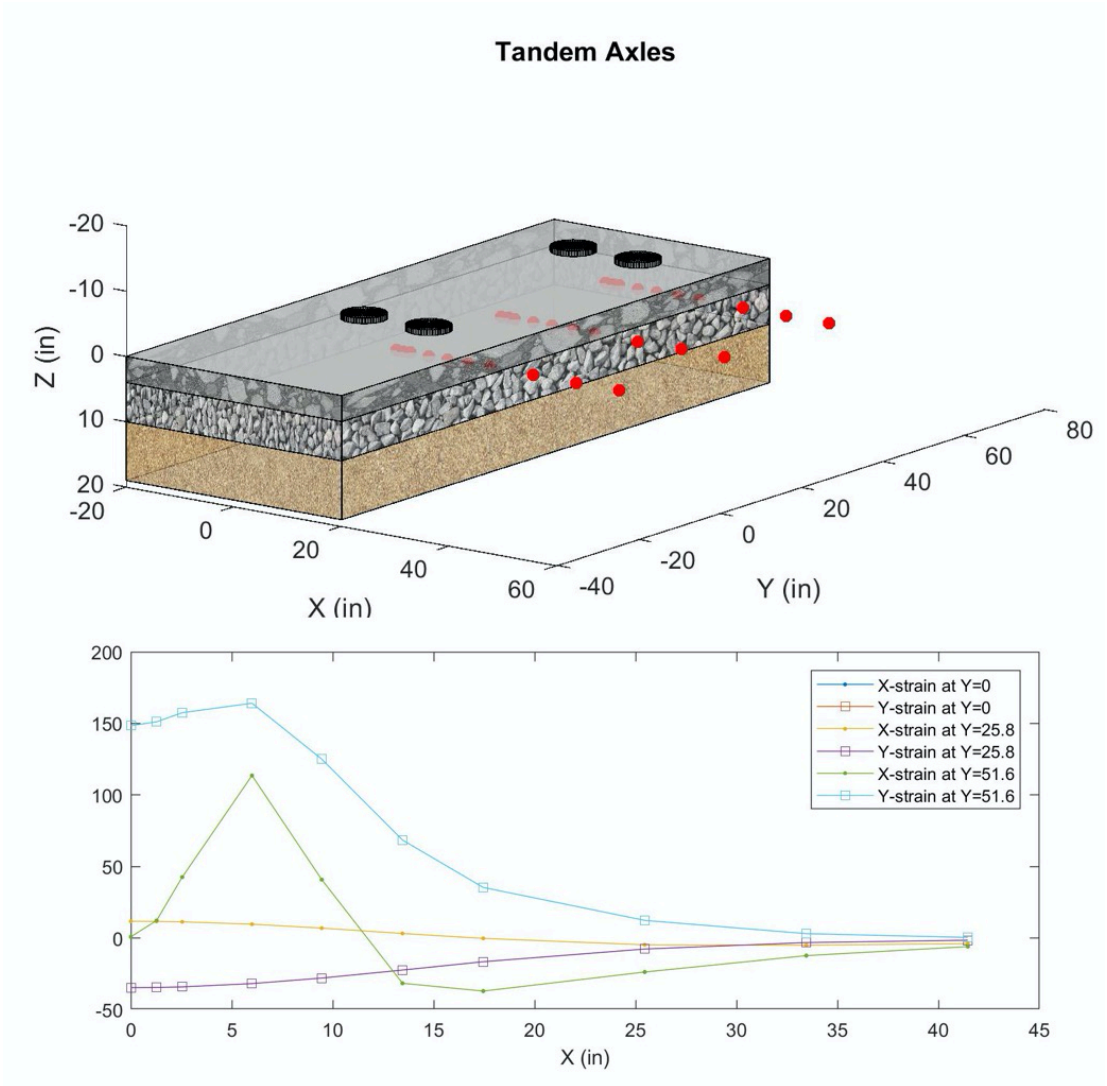

Figure 33. Critical strains computed at the bottom of AC due to tandem axle dual tire

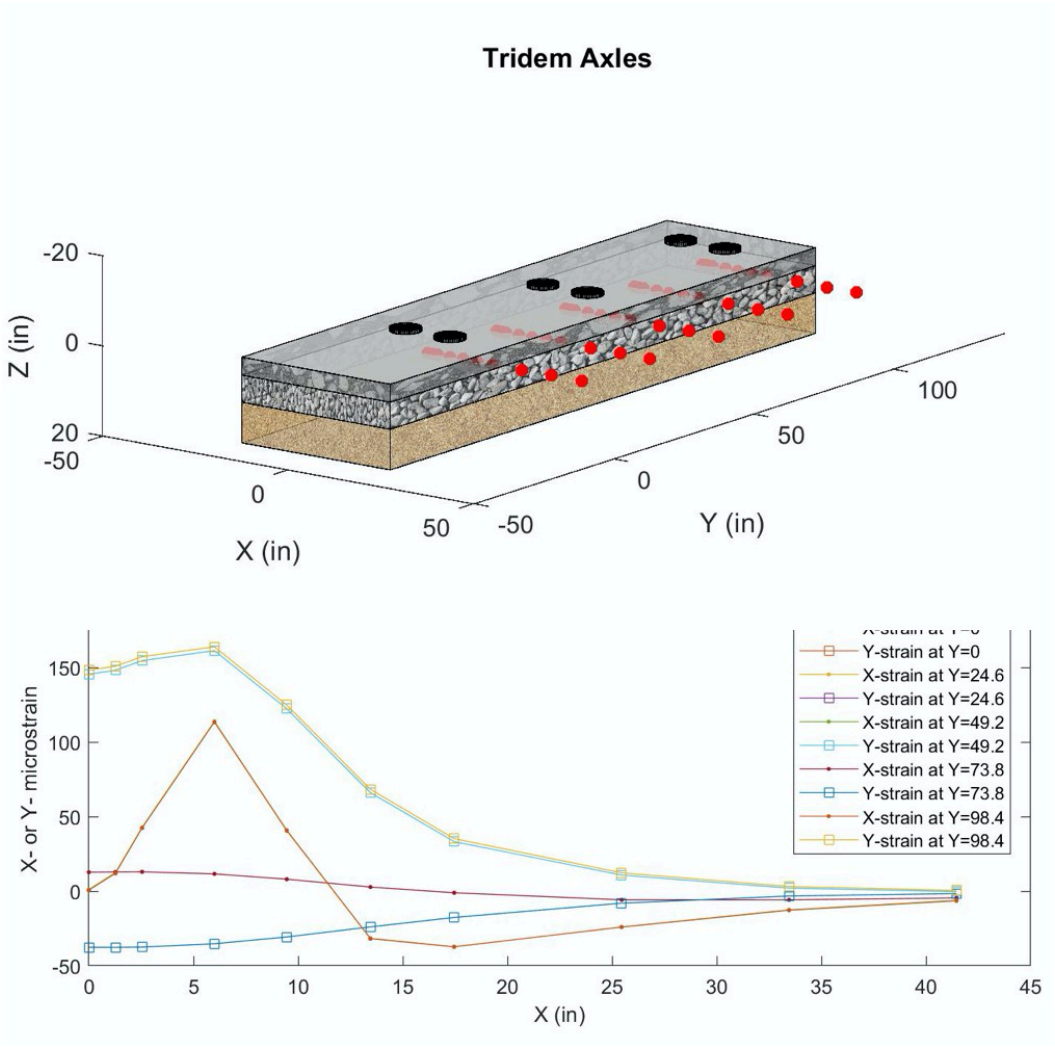

Figure 34. Critical strains computed at the bottom of AC due to tridem axle dual tire

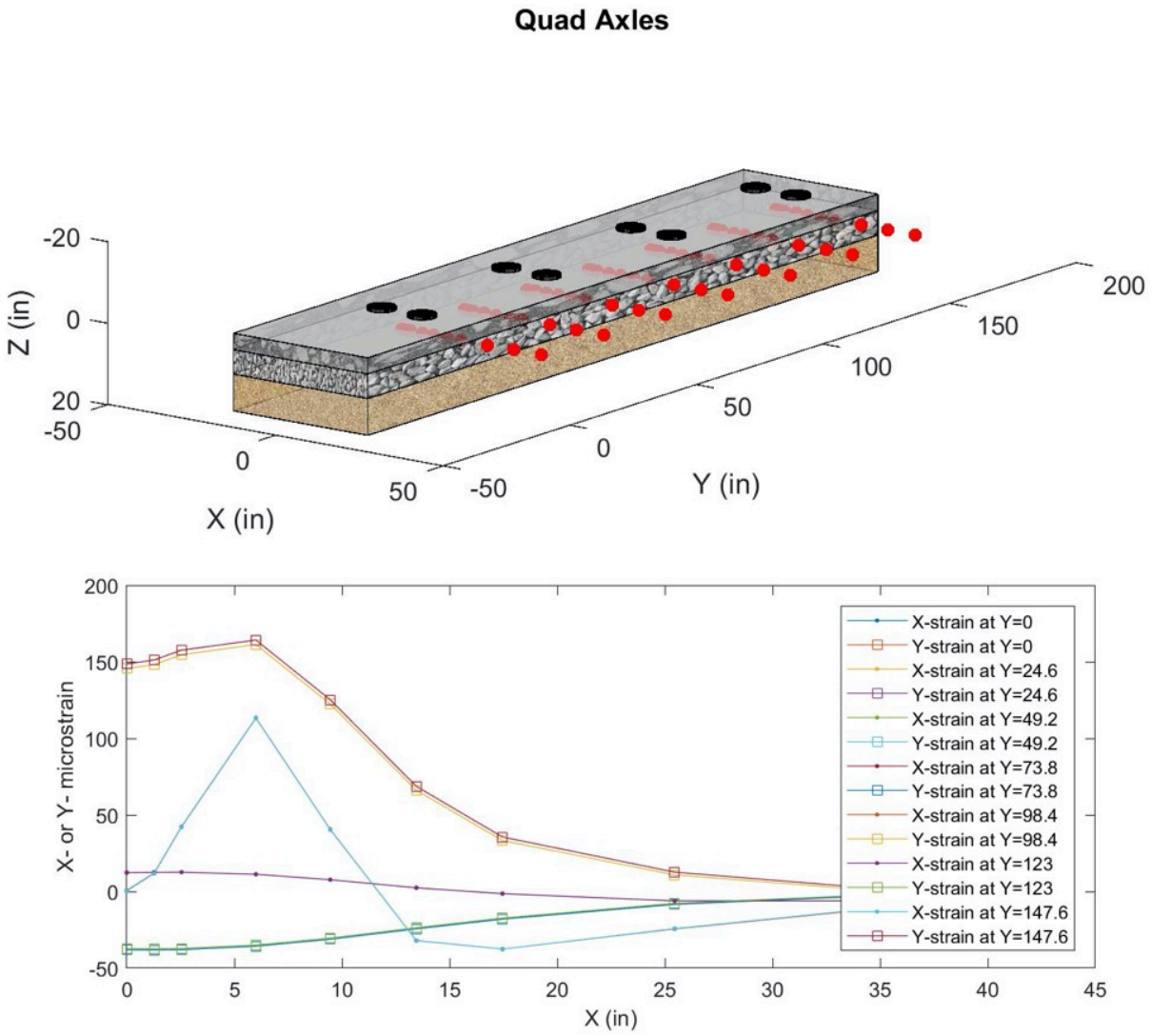

Figure 35. Critical strains computed at the bottom of AC due to quad axle dual tire

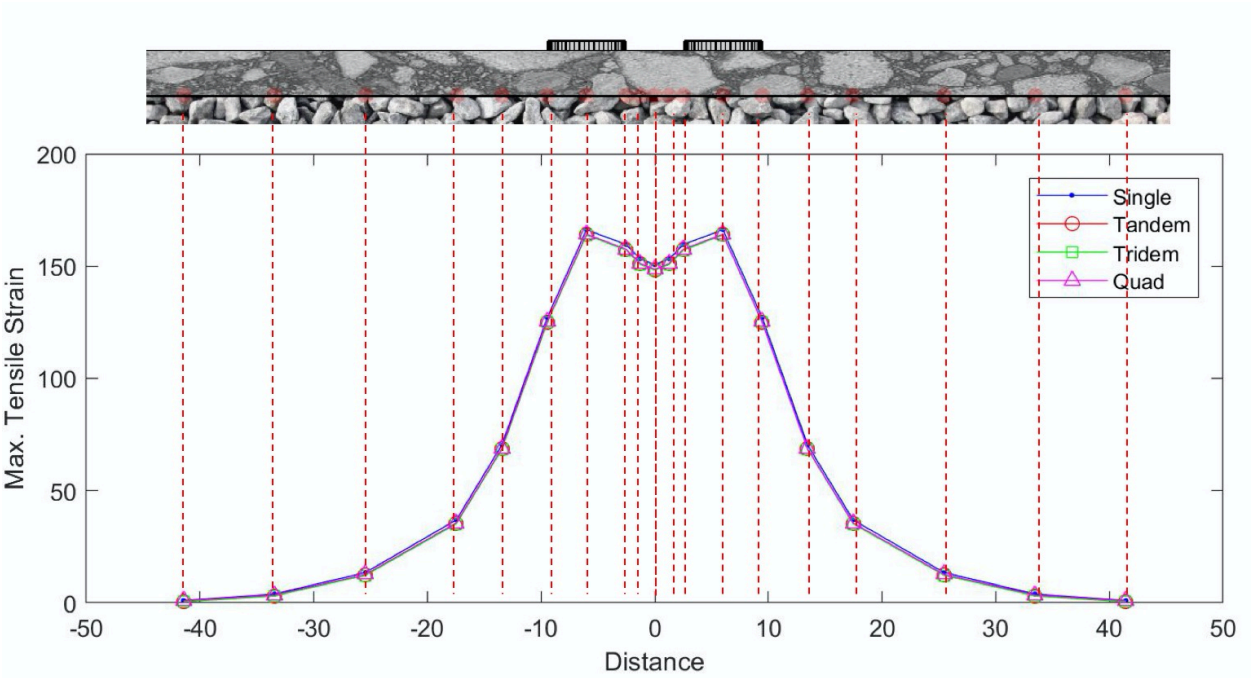

Figure 36. Maximum strain profile for different axles.

$$D_{bu}^{\boldsymbol{tandem}}(X) = \frac{N_{i,t,w_k}^{\boldsymbol{tandem}}}{N_f(X)} \quad [94]$$

$$D_{bu}^{\boldsymbol{tridem}}(X) = \frac{N_{i,t,w_k}^{\boldsymbol{tridem}}}{N_f(X)} \quad [95]$$

$$D_{bu}^{\boldsymbol{quad}}(X) = \frac{N_{i,t,w_k}^{\boldsymbol{quad}}}{N_f(X)} \quad [96]$$

where;

$N_f(X)$ = Number of cycles to failure based on the tensile strain each location in X direction.

N_{i,t,w_k}^{single} = Number of single axles for each month i ($i = 1 \dots 12$), for year t ($t = 1 \dots t_a$, where t_a is analysis duration), corresponding to axle weight w_k Where $k = 1 \dots 39$ and $w_k = 3000, 4000, \dots 41000$ (lb).

N_{i,t,w_k}^{tandem} = Number of tandem axles for each month i ($i = 1 \dots 12$), for year t ($t = 1 \dots t_a$, where t_a is analysis duration), corresponding to axle weight w_k Where $k = 1 \dots 39$ and $w_k = 6000, 8000, \dots 82000$ (lb).

N_{i,t,w_k}^{tridem} = Number of tridem axles, for each month i ($i = 1 \dots 12$), for year t ($t = 1 \dots t_a$, where t_a is analysis duration), corresponding to axle weight w_k, where $k = 1 \dots 31$ and $w_k = 12000, 15000, \dots 102000$ (lb).

N_{i,t,w_k}^{quad} = Number of quad axles i, for each month i ($i = 1 \dots 12$), for year t ($t = 1 \dots t_a$, where t_a is analysis duration), corresponding to axle weight w_k Where $k = 1 \dots 31$ and $w_k = 12000, 15000, \dots 102000$ (lb).

An example bottom-up damage due to a single axle ($D_{bu}^{\boldsymbol{single}}(X)$) is shown in Figure 37.

4.7.2 Inclusion of the Effect of Wheel Wander

In order to simulate the effect of wheel wander, a standard normal distribution is used. The area under a standard normal distribution curve can be divided into five equal intervals, with normalized center points of -1.2816, -0.5244, 0, 0.5244 and 1.2816. Wheel wander is simulated by multiplying the wheel wander standard deviation (S_d), which is an input, by -1.2816, -0.5244, 0, 0.5244 and 1.2816 and subtracting from each X-coordinate. Then total computed damage (D) in Figure 37 is divided by 5 and shifted damage curves (D_1, D_2, D_3, D_4 and D_5) are obtained, as shown in Figure 38.

$$D_{bu,i}^{single}(X) = \frac{1}{5} D_{bu}^{single}(X - S_d * \rho_i) \quad [97]$$

$$D_{bu,i}^{tandem}(X) = \frac{1}{5} D_{bu}^{tandem}(X - S_d * \rho_i) \quad [98]$$

$$D_{bu,i}^{tridem}(X) = \frac{1}{5} D_{bu}^{tridem}(X - S_d * \rho_i) \quad [99]$$

$$D_{bu,i}^{quad}(X) = \frac{1}{5} D_{bu}^{quad}(X - S_d * \rho_i) \quad [100]$$

where;

$D_{bu,i}^{single}$ (X) = Damage in position X, in t^{th} month, j^{th} quintile (temperature), due to single axle, at shifted location.

$D_{bu,i}^{tandem}$ (X) = Damage in position X, in t^{th} month, j^{th} quintile (temperature), due to tandem axle, at shifted location.

$D_{bu,i}^{tridem}$ (X) = Damage in position X, in t^{th} month, j^{th} quintile (temperature), due to tridem axle, at shifted location.

$D_{bu,i}^{quad}$ (X) = Damage in position X, in t^{th} month, j^{th} quintile (temperature), due to quad axle, at shifted location.

S_d = Wheel wander standard deviation, in.

ρ_i = Standard normal distribution center points: -1.2816, -0.5244, 0, 0.5244 and 1.2816

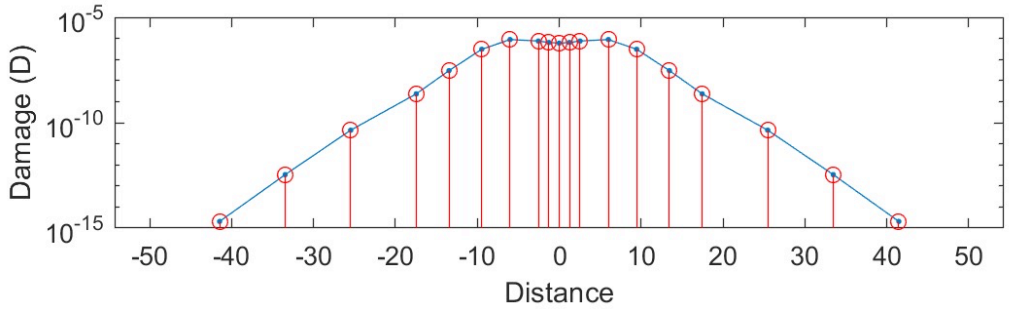

Figure 37. Damage distribution due to a single axle ($D_{bu}^{single}(X)$)

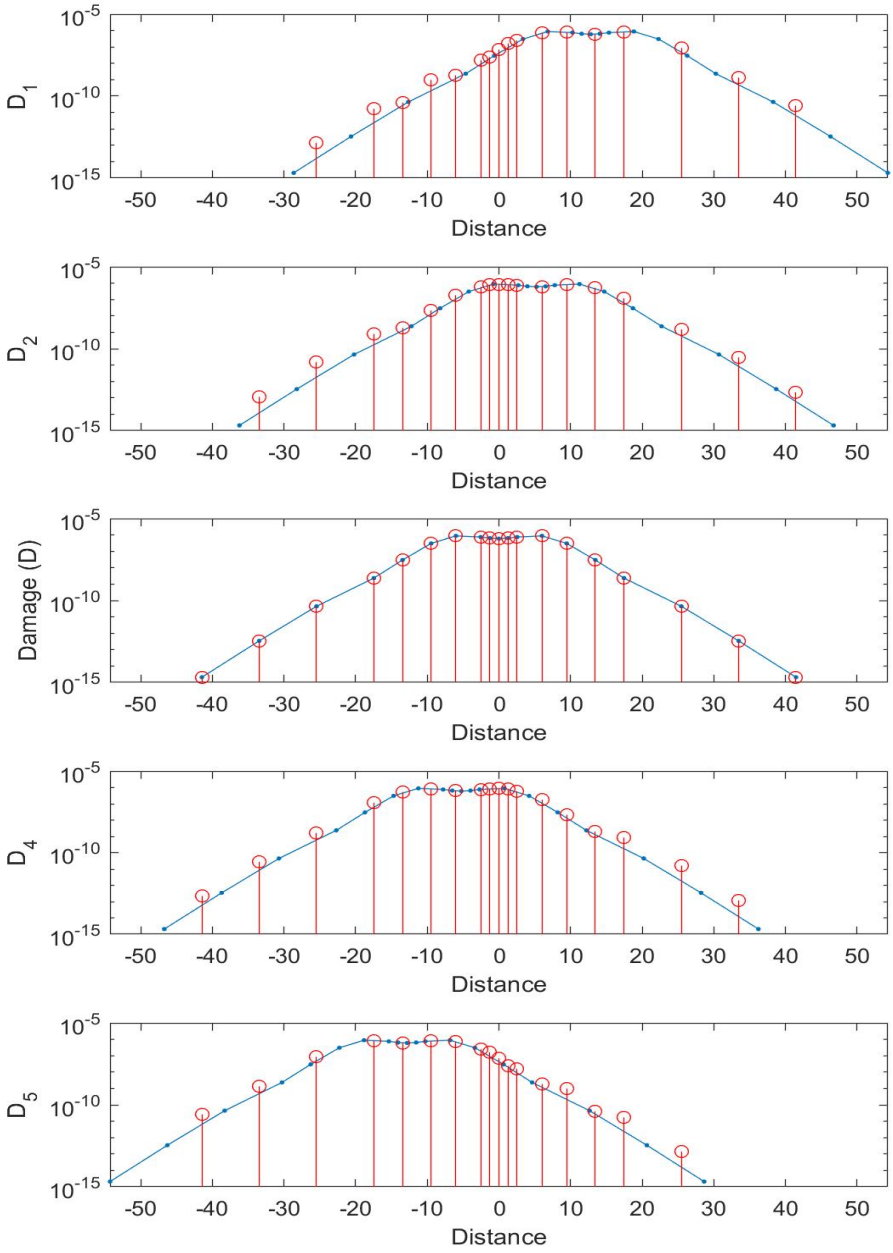

Figure 38. Simulation of wheel wander by shifting the damage distribution. Each subfigure shows $D_{bu,i}^{single}(X)$.

Then, via interpolation, damage at each original analysis point in X-direction is computed and all the damage is summed up as follows:

$$D_{jtw_k}^{single}(\mathrm{X}) = \sum_{i=1}^{5} D_{bu,i}^{single}(X) \qquad [101]$$

$$D_{jtw_k}^{tandem}(X) = \sum_{i=1}^{5} D_{bu,i}^{tandem}(X) \quad [102]$$

$$D_{jtw_k}^{tridem}(X) = \sum_{i=1}^{5} D_{bu,i}^{tridem}(X) \quad [103]$$

$$D_{jtw_k}^{quad}(X) = \sum_{i=1}^{5} D_{bu,i}^{quad}(X) \quad [104]$$

where;

$D_{jtw_k}^{single}$ (X) = Damage in position X, in t^{th} month, j^{th} quintile (temperature), due to single axle with weight w_k

$D_{jtw_k}^{tandem}$ (X) = Damage in position X, in t^{th} month, j^{th} quintile (temperature), due to tandem axle with weight w_k

$D_{jtw_k}^{tridem}$ (X) = Damage in position X, in t^{th} month, j^{th} quintile (temperature), due to tridem axle with weight w_k

$D_{jtw_k}^{quad}$ (X) = Damage in position X, in t^{th} month, j^{th} quintile (temperature), due to quad axle with weight w_k

An example $D_{jtw_k}^{single}$ (X) is shown in Figure 39. Once the damage distribution (after considering wheel wander) above is computed, then the maximum damage $D_{jtw_k-max}^{single}$, which is the maximum damage in t^{th} month, j^{th} quintile (temperature), due to k^{th} axle (single, tandem etc.) is computed, as illustrated in Figure 39. Then total damage in all quintiles, due to all weights in all axles is computed

$$D_{bu}(t) = \sum_{j=1}^{5} \sum_{k=1}^{NW} (D_{jtw_k-max}^{single} + D_{jtw_k-max}^{tandem} + D_{jtw_k-max}^{tridem} + D_{jtw_k-max}^{quad}) \quad [105]$$

$D_{bu}(t)$ = Total bottom-up damage in month t.

NW = Number of weight categories for each axle (equals to 39 for single and tandem, 31 for tridem and quad)

j = Quintile number

An example variation of damage with time ($D_{bu}(t)$) is shown in Figure 40.

Once the damage caused by the axles for each month is computed, cumulative damage is calculated using the following formula:

$$D_{cum}(t) = \sum_{i=1}^{t} D_{bu}(t_i) \quad [106]$$

where;

$D_{cum}(t)$ = Cumulative damage at the bottom of the HMA layers.

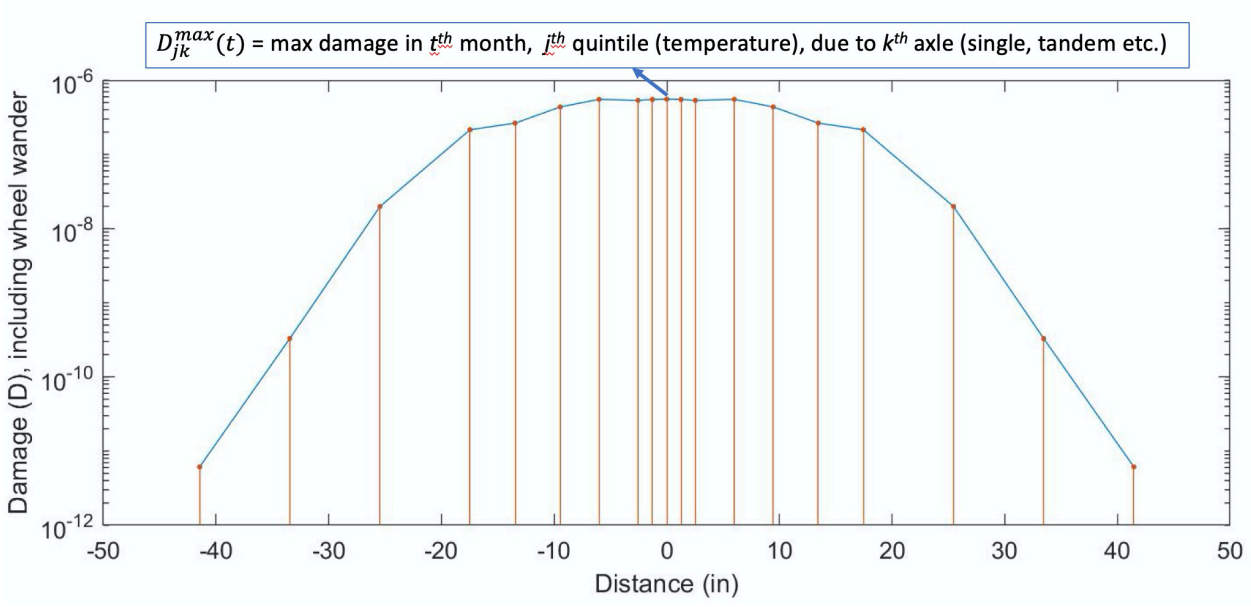

Figure 39. Total damage distribution after wheel wander.

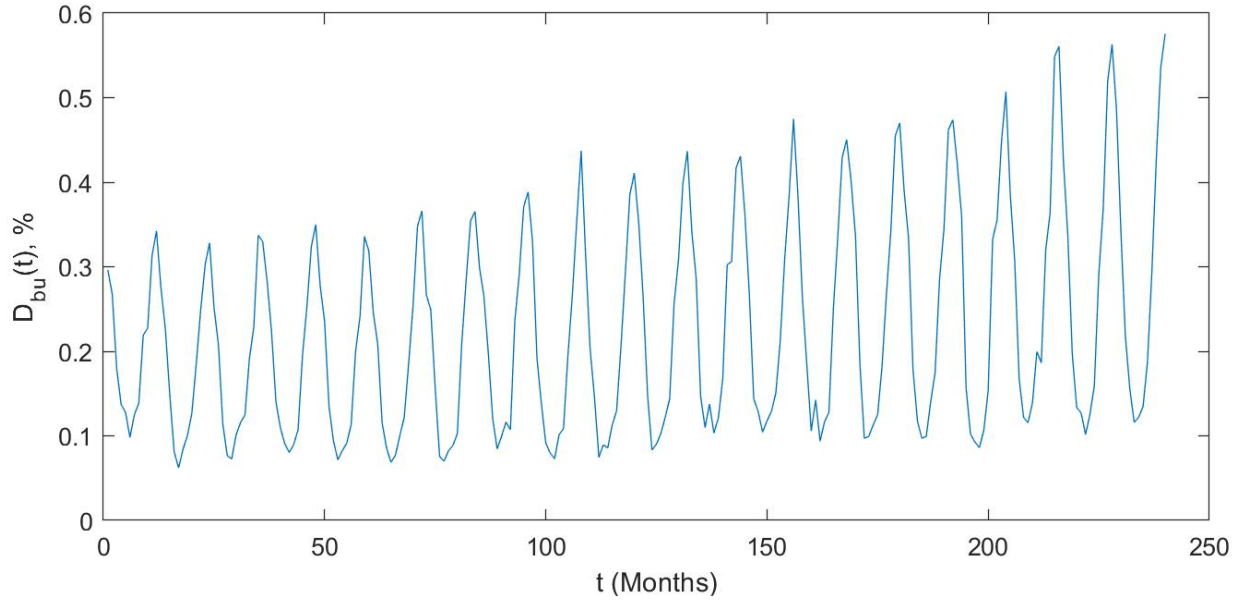

Figure 40. An example variation of bottom up damage with time.

4.7.1 Bottom-up Fatigue Cracking Transfer Function

The magnitude of bottom-up fatigue cracking us computed using the following empirical transfer function:

$$FC_{bottom-up}(t) = \left(\frac{1}{60}\right)\left(\frac{C_{4-bu}}{1 + e^{(C_{1-bu} * C_1^* + C_{2-bu}^* log\ (D_{cum}(t))}}\right) \quad [107]$$

where

$FC_{bottom-up}(t)$	=	Area of alligator cracking that initiates at the bottom of the HMA layers, percent of total lane area.
$D_{cum}(t)$	=	Cumulative damage at the bottom of the HMA layers.
$C_{i\text{-}bu}$	=	Transfer function regression constants; C4-bu = 6,000; C1-bu = 1.00; and C2-bu =1.00
C_1^*	=	$-2 * C_2^*$
C_2^*	=	$-2.40874 - 39.748(1 + h_{ac})^{-2.856}$

An example cumulative damage and bottom up fatigue cracking is shown in Figure 41.

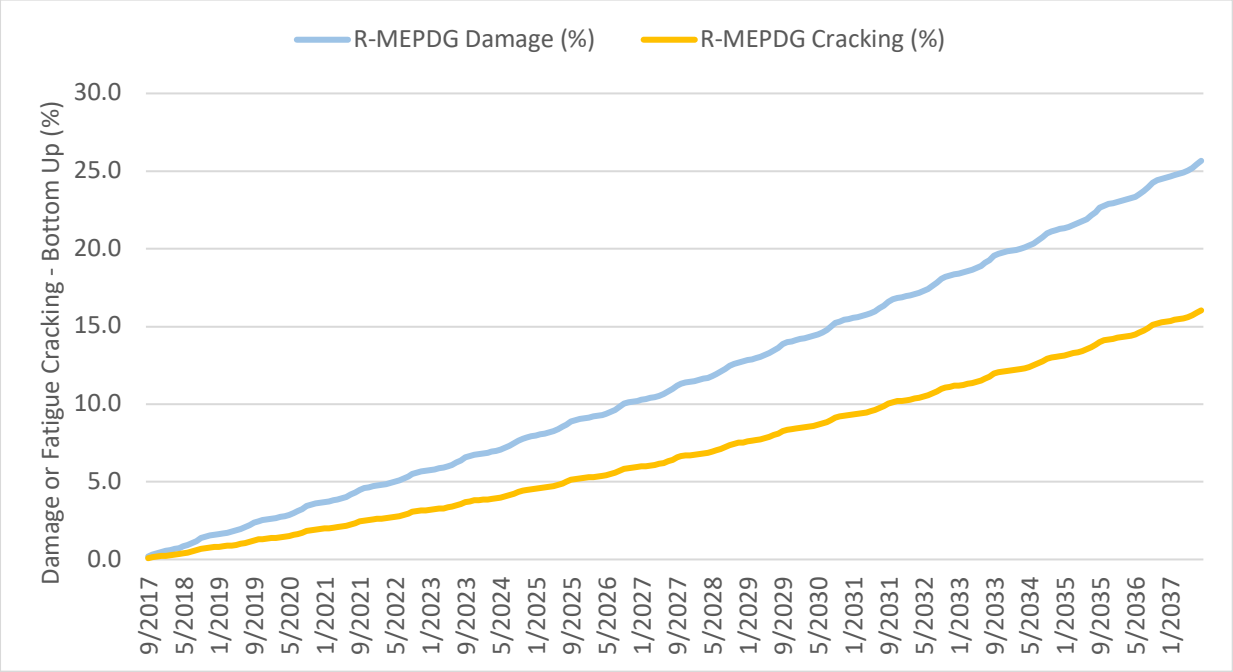

Figure 41. An example cumulative damage and fatigue cracking for a climate of Tampa, FL, structure of 4"AC (PG70-28), 6" Base, Subgrade, with full axle load spectra as input.

4.8 Top-Down Cracking

Longitudinal top-down cracking originates near the surface and it is thought to be due to maximum tensile strain near the surface. In MEPDG documentation, it is stated that maximum tensile strain at the surface between the tires was the maximum observed in the cases analyzed in NCHRP 1-37A project (ARA Inc. ERES Consultants Division, 2004). In this work this conclusion could not be replicated. It was observed in this work that the magnitudes of the maximum tensile strain values in X- and Y- directions were quite low (see Figure 42).

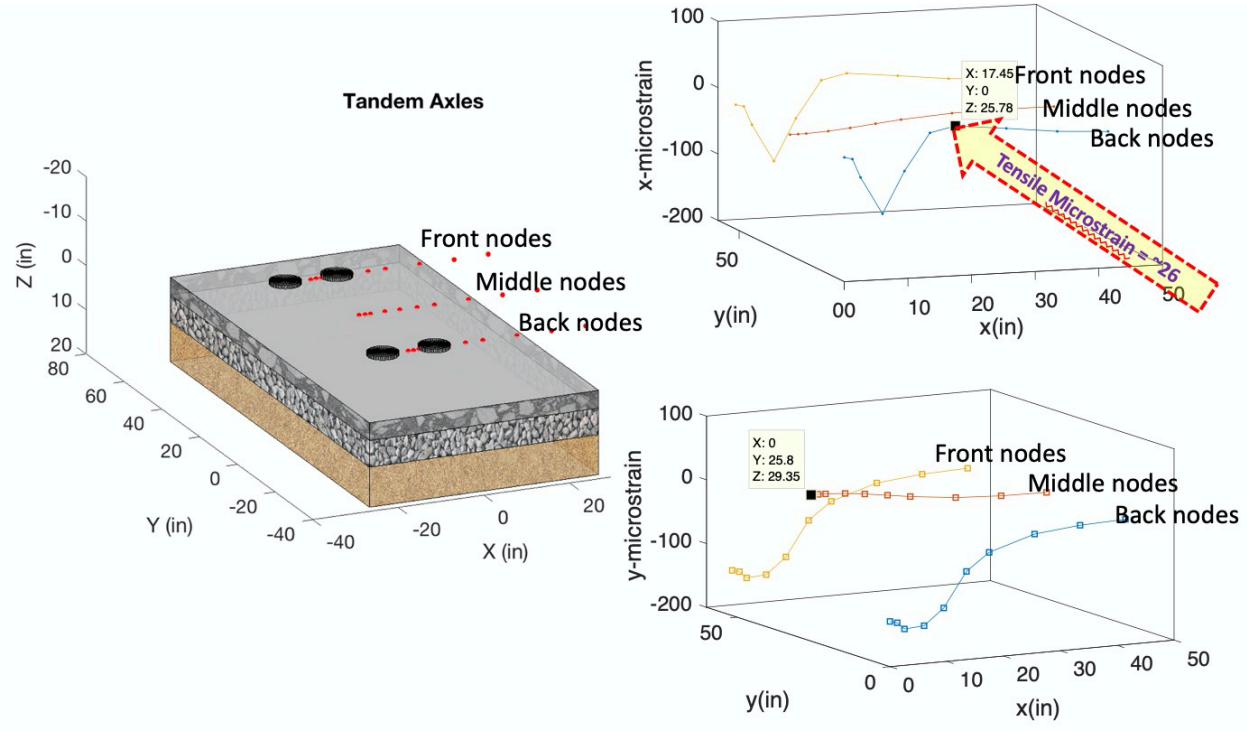

Figure 42. Critical strains computed at the top of AC due to tandem axle dual tire

Several researchers noted that three-dimensional stress state near the surface include significant shear as well as axial strains (Wang et al., 2012; Wang & Roque, 2011). In a paper by Wang and Roque (Wang & Roque, 2011), the importance of use of principal strains in top-down cracking modeling is noted as follows: *"…Study by the authors indicated that shear induced principal tensile stress (SIGMA-1) at tire edge could be 2 to 3 times greater than bending stress in magnitude at AC surface, which might be more likely responsible for the initiation of top-down cracking…"*. Strain distribution in cartesian coordinate system and in principal directions for an example 3-layer structure is shown in Figure 43. As shown, the large magnitudes of tensile strain are observed in principal directions near the surface. It is postulated that these strains near the surface cause crack initiation, in an inclined/diagonal direction (not X- or Y-direction), which is consistent with the conclusions of past researchers (Wang et al., 2012; Wang & Roque, 2011) who have significant experience in modeling top-down cracking.

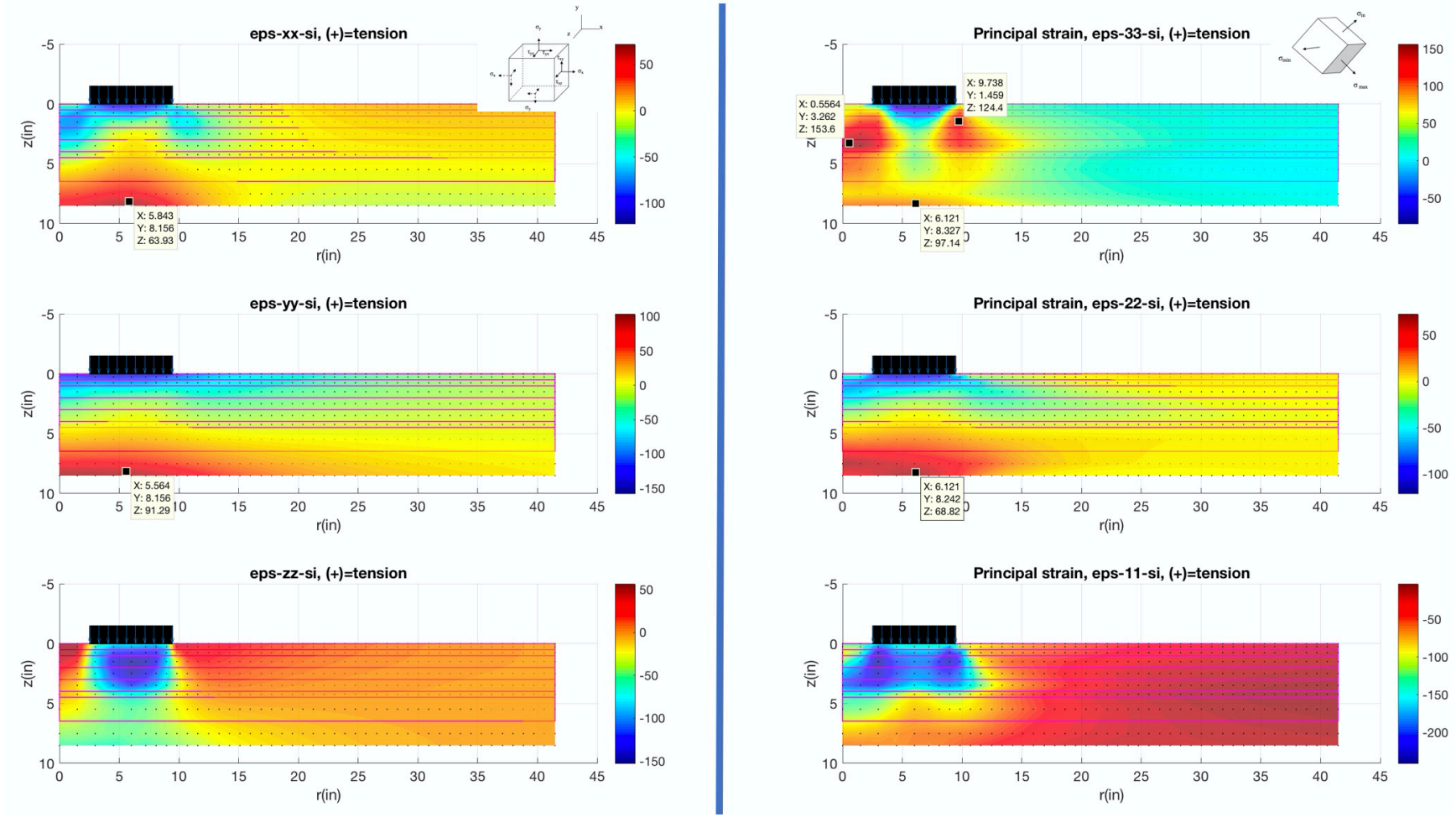

Figure 43. Strain distribution in cartesian coordinate system and in principal directions, for a 3-layer structure.

In MEAPA, for top-down cracking, maximum major *tensile principal strain* near the tire within top 0.5" of the asphalt pavement layer was used in the fatigue life formulation instead of the maximum horizontal tensile strain (X- or Y-direction) at the surface. A more recent top-down cracking model is the model developed as part of the NCHRP Project 01-52 (Robert L Lytton et al., 2018). However, NCHRP Project 01-52 project resulted in a procedure based on Paris's law of fracture growth and uses Artificial Neural Networks (ANNs) to estimate the J-integral. Unfortunately, trained ANN for the J-integral is not publicly available (only available to AASHTO). This makes it impossible for the results of NCHRP Project 01-52 to be used by any institution other than AASHTO. The use of maximum major principal strain near the pavement surface near the tire is the best intermediate solution until a more accurate and publicly available model is developed.

The material level traditional fatigue life formulation used herein for top-down cracking is the same as that of the bottom up cracking:

$$N_f = C_H C \beta_{f1} k_{f1} \left(\frac{1}{\varepsilon_{t-principal}} \right)^{\beta_{f2} k_{f2}} \left(\frac{1}{E} \right)^{\beta_{f3} k_{f3}} \quad [108]$$

$$C = 10^{4.84\left(\frac{V_{be}}{V_a + V_{be}} - 0.69\right)} \quad [109]$$

$$C_{H-td} = \left(b_{td1} + \frac{b_{td2}}{1 + e^{(b_{td3} - b_{td4} h_{ac})}} \right)^{-1} \quad [110]$$

where,

$\varepsilon_{t-principal}$	=	Maximum principal tensile strain at the within the top 0.5" of AC surface layer
N_f	=	Number of cycles to failure, for top-down cracks
kf1, kf2, kf3	=	Global field calibration parameters (from the NCHRP 1-40D re-calibration; kf1 = 0.007566, kf2 = -3.9492, and kf3 = -1.281).
βf1, βf2, βf3	=	Local or mixture specific field calibration constants; for the global calibration effort, these constants were set to 1.0.
hac	=	height of the AC layer
b_{tdi}	=	Coefficients: btd1= 0.01, btd2 =12, btd3 = 15.676 and btd4 = 2.8186
E	=	Equivalent modulus of AC surface layer (at the given temperature/frequency)
V_{be}	=	Effective asphalt content by volume for the AC surface layer, %
Va	=	Percent air voids in the HMA mixture for the AC surface layer, %

4.8.1 Calculation of Damage and Inclusion of the Effect of Wheel Wander

Similar to the procedure for bottom-up cracking, the critical strains were computed at several analysis locations near the surface for single, tandem, tridem and quad axles (using dual tires). Steps of calculation of damage due to different axles and simulation of wheel wander are identical to those of bottom-up cracking, therefore, they will not be repeated for brevity. See the subsections of Bottom-Up Cracking section titled "Calculation of Damage and Inclusion of the Effect of Wheel Wander" for the details.

4.8.2 Top-Down Fatigue Cracking Transfer Function

The magnitude of top-down fatigue cracking us computed using the following transfer function:

$$FC_{top-down}(t) = (10.56)\left(\frac{C_{4-\text{td}}}{1 + e^{(C_{1-\text{td}} - C_{2-\text{td}} log\,(D_{cum}(t))}}\right) \quad [111]$$

where

$FC_{top-down}(t)$	=	Length of longitudinal cracks that initiate at the top of the HMA layer, ft/mi.
$D_{cum}(t)$	=	Cumulative damage at the top of the HMA layers.
$C_{1-\text{td}}, C_{2-\text{td}}$ and $C_{4-\text{td}}$	=	Transfer function regression constants; $C_{4-\text{td}}$= 1,000; $C_{1-\text{td}}$=7.00; and $C_{2-\text{td}}$=3.5

An example top-down fatigue cracking for a long-life (perpetual) and standard thick asphalt pavement are shown in Figure 44.

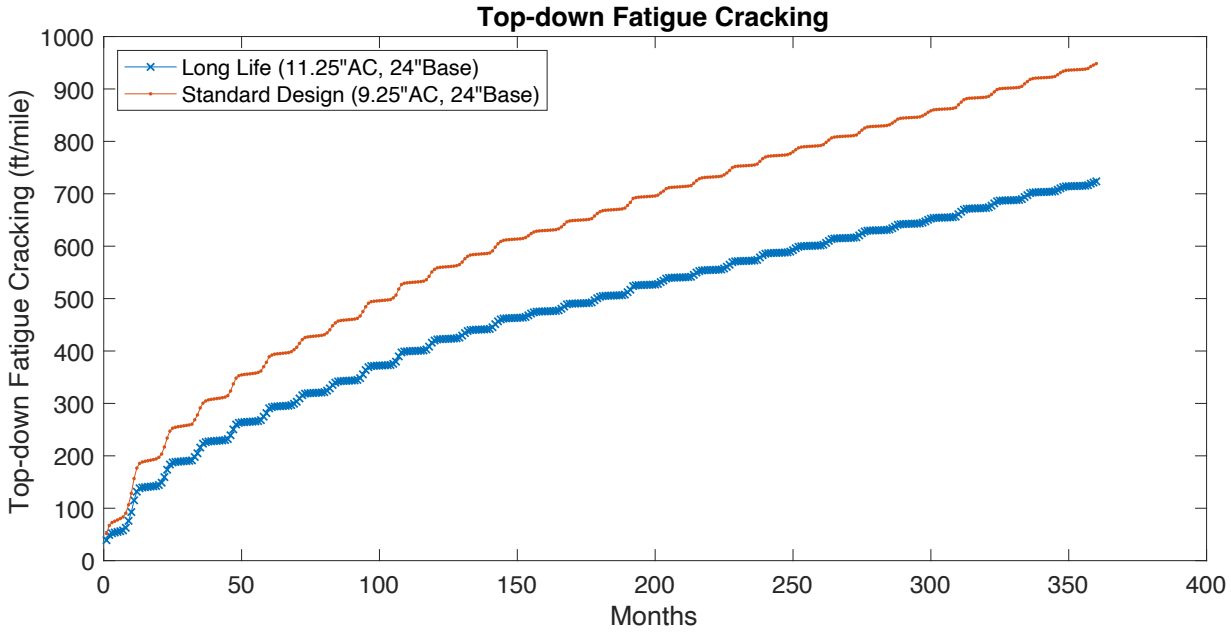

Figure 44. Example top-down cracking results for a long-life (perpetual) and standard thick asphalt pavement

4.8.3 Validation of the Top-Down Cracking Model

In order to validate the top-down cracking modeling procedure described above, pavement performance data from 13 freeway sections in different regions of Michigan was used. All the inputs were obtained from MDOT's database that was used in the previous Pavement ME calibration efforts (Buch et al., 2009; Haider et al., 2014, 2016; Jamrah et al., 2014; M Emin Kutay & Jamrah, 2013). Appendix I shows all the inputs used in the MEAPA for the pavement

sections included in the validation. Figure 45 shows a comparison of measured and predicted top down cracking, both using the MEAPA and the Pavement ME software. As shown, MEAPA predictions are much closer to the line of equality and R^2 is higher as compared to the Pavement ME. It is noted that, in this analysis, global calibration coefficients were used, i.e., local calibration was not done.

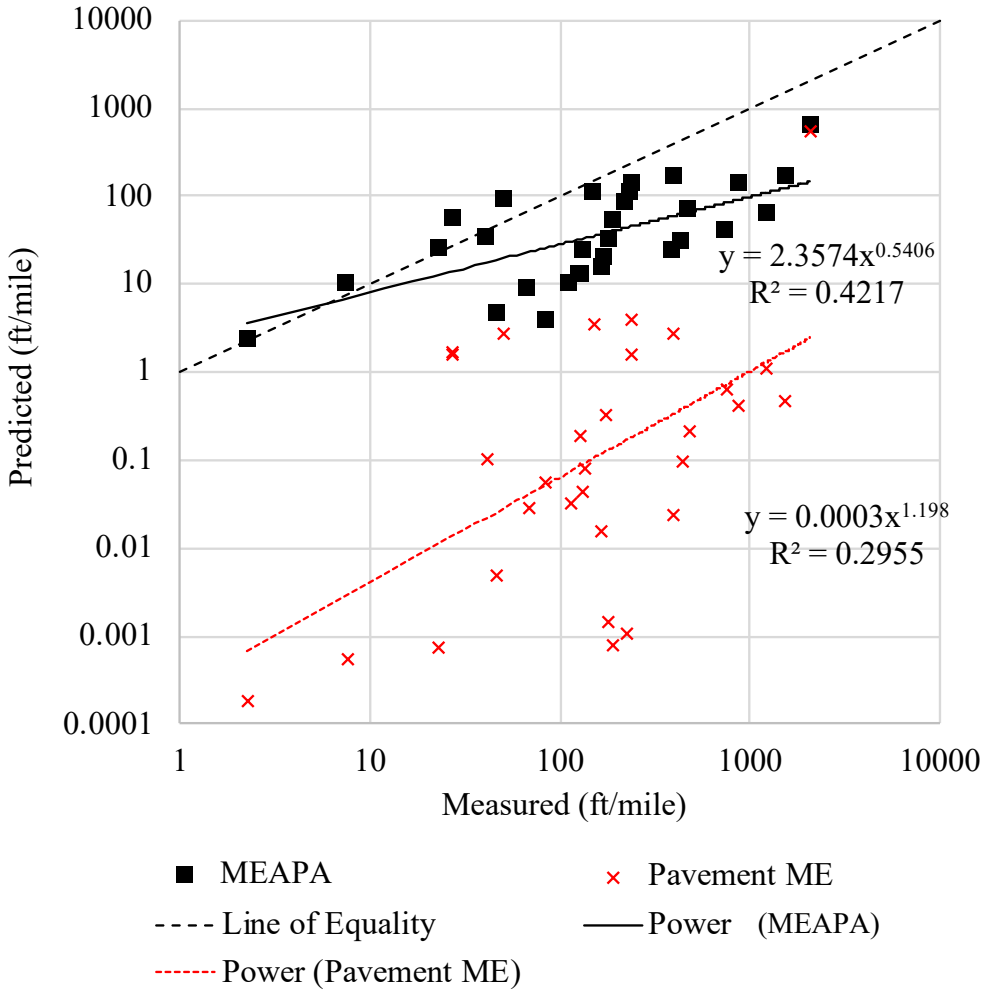

Figure 45. Comparison of the top down cracking predicted by the MEAPA model, Pavement ME and Measured values for 13 MDOT sections.

4.9 AC Rutting

AC rutting is primarily based on the vertical compressive strain and temperature of the AC layer. First, the vertical compressive strains at the center of the AC layers are calculated from the MatLEA analysis program. Then the following formula is used to compute the rutting ((Ayres Jr & Witczak, 1998; Kaloush & Witczak, 2000; Leahy, 1989):

$$\epsilon_{p(HMA)} = \epsilon_{r(HMA)} \cdot k_z \cdot \beta_{1r} \cdot 10^{k_{1r}} \cdot T^{(\beta_{2r} \cdot k_{2r})} n^{(\beta_{3r} \cdot k_{3r})} \quad [112a]$$

$$\Delta_{p(HMA)} = \epsilon_{p(HMA)} h_{HMA} \quad [112b]$$

where;

$\Delta_{p(HMA)}$ = Accumulated permanent or plastic vertical deformation in the HMA layer/sub-layer, in.

$\epsilon_{p(HMA)}$ = Accumulated permanent or plastic axial strain in the HMA layer/sub-layer, in/in.

$\epsilon_{r(HMA)}$ = Resilient or elastic strain calculated by the structural response model at the mid-depth of each HMA sub-layer, in/in.

$h_{(HMA)}$ = Thickness of the HMA layer/sub-layer, in.

n = Number of axle load repetitions.

T = Mix or pavement temperature, °F.

k_z = Depth confinement factor ($k_z = k_1$ below – Page 3.3.49 in MEPDG formulation).

$$k_1 = (C_1 + C_2 * depth) * 0.328196^{depth}$$

$$C_1 = -0.1039 * h_{ac}^2 + 2.4868 * h_{ac} - 17.342$$

$$C_2 = 0.0172 * h_{ac}^2 - 1.7331 * h_{ac} + 27.428$$

k1 = function of total asphalt layers thickness (hac, in) and depth (depth, in) to computational point, to correct for the confining pressure at different depths

$k_{1r,2r,3r}$ = Global field calibration parameters (from the NCHRP 1-40D recalibration; $k_{1r} = -3.35412$, $k_{2r} = 0.4791$, $k_{3r} = 1.5606$).

$\beta_{1r}, \beta_{2r}, \beta_{3r}$ = Local or mixture field calibration constants; for the global calibration, these constants were all set to 1.0.

Unlike the fatigue models where linear damage accumulation (Miner's law) is assumed, the propagation of rutting is a nonlinear process. The plastic strain in the AC layers are calculated by following equivalent cycles approach, which is described in the next subsection.

4.9.1 Equivalent Cycles Approach

The equivalent cycles approach is similar to the method described in the MEPDG documentation ((ARA Inc. ERES Consultants Division, 2004); Appendix GG). An illustration of the equivalent cycles approach for calculation of plastic strain is provided in Figure 46. As shown, for an HMA layer, the curves of the propagation of plastic strain in different months and quintiles (temperatures) are different. In order to account for these changes in the predicted permanent strain, the approach described below is used.

Total plastic strain $\epsilon_{p,i-1}$ at the end of sub-season $i-1$ is calculated using the total number of traffic repetitions $n_{t,i-1}$ (see point 1 in Figure 46), temperature of the particular season (T_{i-1}) and resilient (vertical) strain computed for this season ($\epsilon_{v,i-1}$):

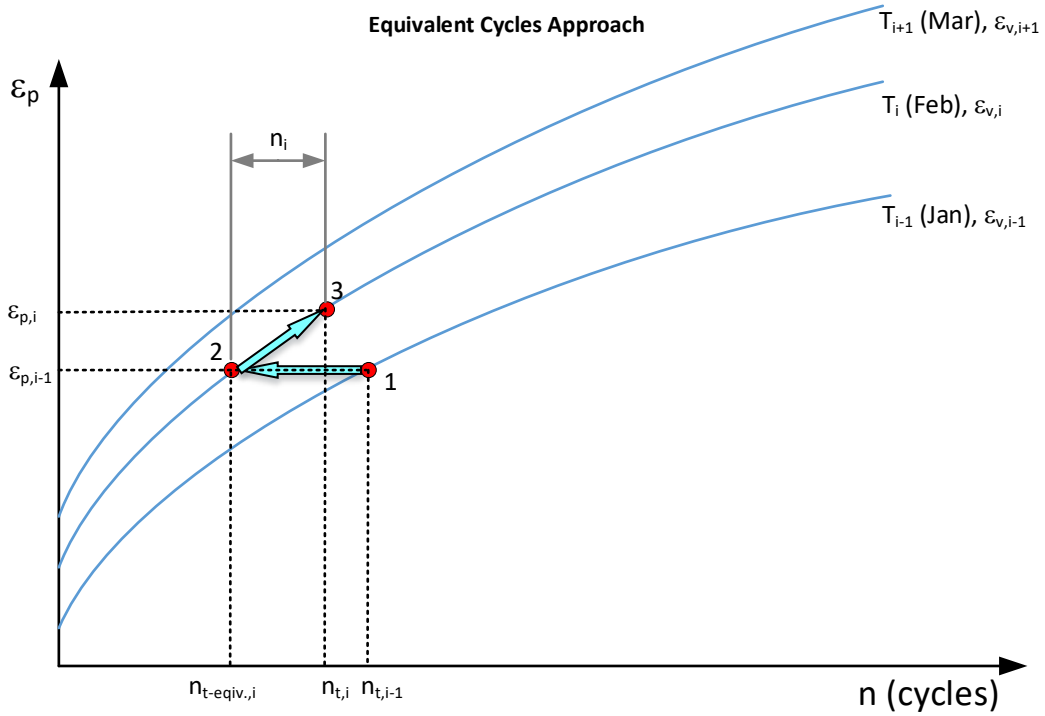

Figure 46. Illustration of the equivalent cycles approach for calculation of plastic strain in HMA

$$\epsilon_{p,i-1} = \epsilon_{v,i-1} \cdot k_z \cdot 10^{k_{1r}} \cdot {T_{i-1}}^{k_{2r}} \cdot n_{i-1}^{k_{3r}} \quad [113]$$

In the next sub-season i, the layer temperature is T_i and resilient (vertical) strain for load and material conditions is $\epsilon_{p,i}$. At the beginning of the next sub-season i (point 2), there is an equivalent number of traffic repetitions $n_{t-equiv,i}$ that corresponds to the total plastic strain at the end of sub-season i-1 but under conditions prevailing in the new sub-season (T_i, $\epsilon_{p,i}$). This $n_{t-equiv,i}$ can be calculated from the following equation:

$$n_{t-equiv,i} = \left(\frac{\epsilon_{p,i-1}}{k_z \epsilon_{v,i} 10^{k_{1r}} T_i^{k_{2r}}} \right)^{1/k_{3r}} \quad [114]$$

By adding the number of traffic repetitions at season i (n_i) to the total equivalent number of repetitions ($n_{t-equiv,i}$) and using it in the specific material model, it is possible to estimate point 3, which corresponds to the total plastic strain at the end of sub-season i ($\epsilon_{p,i}$):

$$n_{t,i} = n_{t-equiv,i} + n_i \quad [115]$$

$$\epsilon_{p,i} = \epsilon_{v,i} \cdot k_z \cdot 10^{k_{1r}} \cdot T_i^{k_{2r}} \cdot n_{t,i}^{k_{3r}} \quad [116]$$

An important note here is that since the process described above is nonlinear, order of loading and the temperature quintiles matters. Figure 47 shows the effect of order of loading on the predicted rutting, which can be significant. In this figure:

- Order 1 (default): For each month; calculations are done for quintile 1, quintile 2, quintile 3, quintile 4 and quintile 5, in this order. Within each quintile; single, tandem, tridem and quad axle repetitions are applied, in this order.
- Order 2 (reversed axle order): For each month; calculations are done for quintile 1, quintile 2, quintile 3, quintile 4 and quintile 5, in this order. Within each quintile; quad, tridem, tandem and single axle repetitions are applied, in this order.
- Order 3 (reversed quintile order): For each month; calculations are done for quintile 5, quintile 4, quintile 3, quintile 2 and quintile 1, in this order. Within each quintile; single, tandem, tridem and quad axle repetitions are applied, in this order.

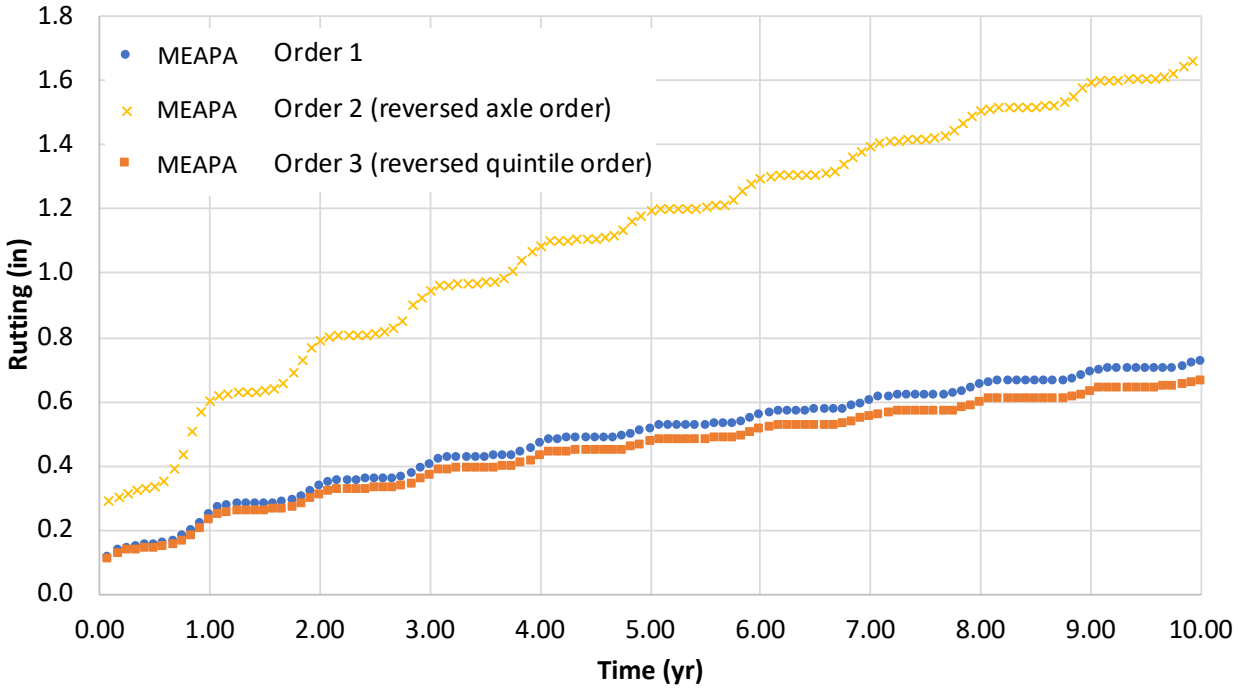

Figure 47. Effect of order of loading on the predicted rutting

In MEAPA, Order 1 above is used, which produced similar results as the Pavement ME software. A comparison between the Pavement ME and MEAPA results for AC rutting is shown in Figure 48.

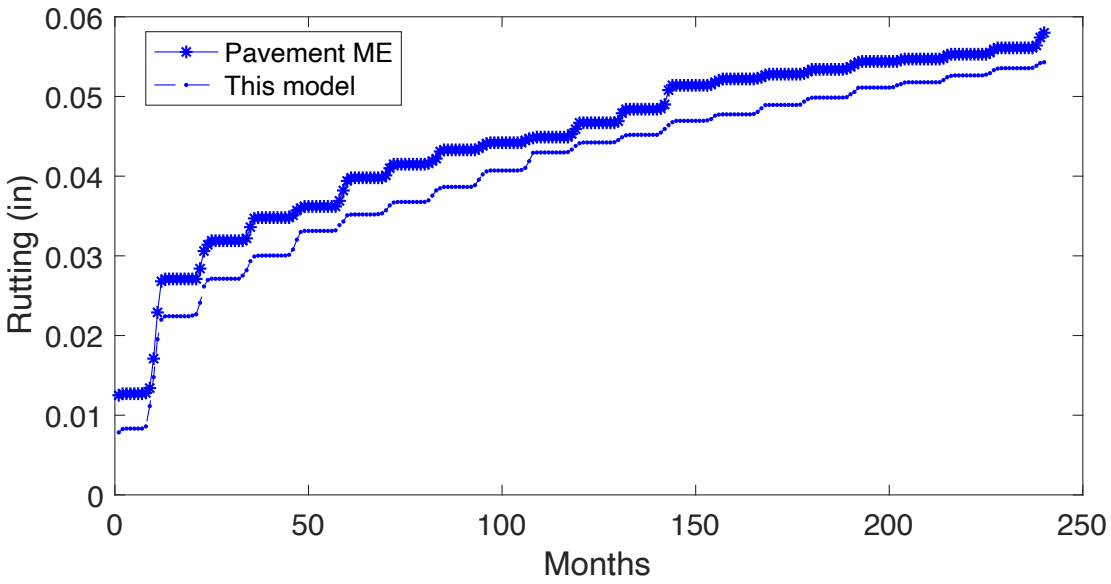

Figure 48. Comparison of Pavement ME and MEAPA for AC rutting.

4.10 Unbound Base and Subbase Layer Rutting

Unbound (base and subbase) layer rutting is computed using a procedure similar to the AC layer. The basic phenomenological relationship is the model developed by Tseng and Lytton (Tseng & Lytton, 1989), which is slightly modified during the NCHRP 1-37A project:

$$\varepsilon_p = \beta_{s1} k_{s1} \varepsilon_v R_e e^{-\left(\frac{\rho}{n}\right)^{\beta}} \quad [117]$$

$$\Delta_{p(unbound)} = h_{unbound} \varepsilon_p \quad [118]$$

where;

$\Delta_{p(unbound)}$	=	Permanent or plastic deformation for the unbound layer, in.
ε_p	=	Permanent or plastic strain, in/in.
n	=	Number of axle load applications.
ε_v	=	Average vertical resilient or elastic strain in the layer/sub-layer and calculated by the structural response model, in/in.
β	=	A parameter dependent on moisture content of the soil
ρ	=	A parameter related moisture content and resilient modulus of the soil
R_e	=	Ratio $R_e = \varepsilon_0/\varepsilon_r$, where; ε_o=Intercept determined from laboratory repeated load permanent deformation tests, in/in., ε_r=Resilient strain imposed in laboratory test to obtain material properties ε_o, β, and ρ, in/in.
$h_{unbound}$	=	Thickness of the unbound layer/sub-layer, in.
k_{s1}	=	Global calibration coefficients; k_{s1}=1.673 for granular materials and 1.35 for fine-grained materials.
β_{s1}	=	Local calibration constant for the rutting in the unbound layers; the local calibration constant was set to 1.0 for the global calibration effort.

The parameters β, ρ and $R_e = \varepsilon_0/\varepsilon_r$ are computed using the following relationships (ARA Inc. ERES Consultants Division, 2004):

$$\beta = 10^{-0.61119 - 0.017638 W_c} \quad [119]$$

$$\rho = 10^9 \left(\frac{\ln\left(\frac{a_1}{a_9}\right)}{1 - 10^{9\beta}} \right)^{\frac{1}{\beta}} \quad [120]$$

$$R_e = \frac{a_1 e^{\rho\beta} + a_9 e^{\left(\frac{\rho}{10^9}\right)^{\beta}}}{2} \quad [121]$$

$$W_c = 51.712 \left(\frac{Mr}{2555} \right)^{-0.5603 GWT^{0.1192}} \quad [122]$$

where;

W_c	=	Water content (%).
Mr	=	Resilient modulus of the layer/sublayer (psi).
GWT	=	Ground water table depth (ft).
a_1, a_9	=	Coefficients; $a_1 = 0.15$ and $a_9 = 20$

Since resilient modulus and moisture content can change from one month to another, a similar equivalent cycles approach is needed to compute the progression of plastic strain (i.e. rutting) with time.

4.10.1 Equivalent Cycles Approach

Total plastic strain $\varepsilon_{p,i-1}$ at the end of sub-season $i-1$ is calculated using the total number of traffic repetitions $n_{t,i-1}$, moisture content (and related parameters), and resilient (vertical) strain computed for this season ($\varepsilon_{v,i-1}$):

$$\varepsilon_{p,i-1} = \beta_{s1} k_{s1} (\varepsilon_{v,i-1})(R_{e,i-1}) e^{-\left(\frac{(\rho_{i-1})}{(n_{t,i-1})}\right)^{(\beta_{i-1})}} \quad [123]$$

At the beginning of the next sub-season i, there is an equivalent number of traffic repetitions $n_{t-equiv,i}$ that correspond to the total plastic strain at the end of sub-season i-1 but under conditions prevailing in the new sub-season ($R_{e,i}, \rho_i, \varepsilon_{v,i}$…etc.). This $n_{t-equiv,i}$ can be calculated from the following equation:

$$n_{t-equiv,i} = \frac{\rho_i}{A^{\frac{1}{\beta_i}}} \quad [124]$$

$$A = \ln\left(\frac{\beta_{s1} k_{s1} R_{e,i} \varepsilon_{v,i}}{\varepsilon_{p,i-1}}\right) \quad [125]$$

By adding the number of traffic repetitions at season i (n_i) to the total equivalent number of repetitions ($n_{t-equiv,i}$) and using it in the specific material model, it is possible to compute total plastic strain at the end of sub-season i ($\varepsilon_{p,i}$):

$$n_{t,i} = n_{t-equiv,i} + n_i \quad [126]$$

$$\varepsilon_{p,i} = \beta_{s1} k_{s1} (\varepsilon_{v,i})(R_{e,i}) e^{-\left(\frac{(\rho_i)}{(n_{t,i})}\right)^{(\beta_i)}} \quad [127]$$

An example base rutting progression with time is shown in Figure 49.

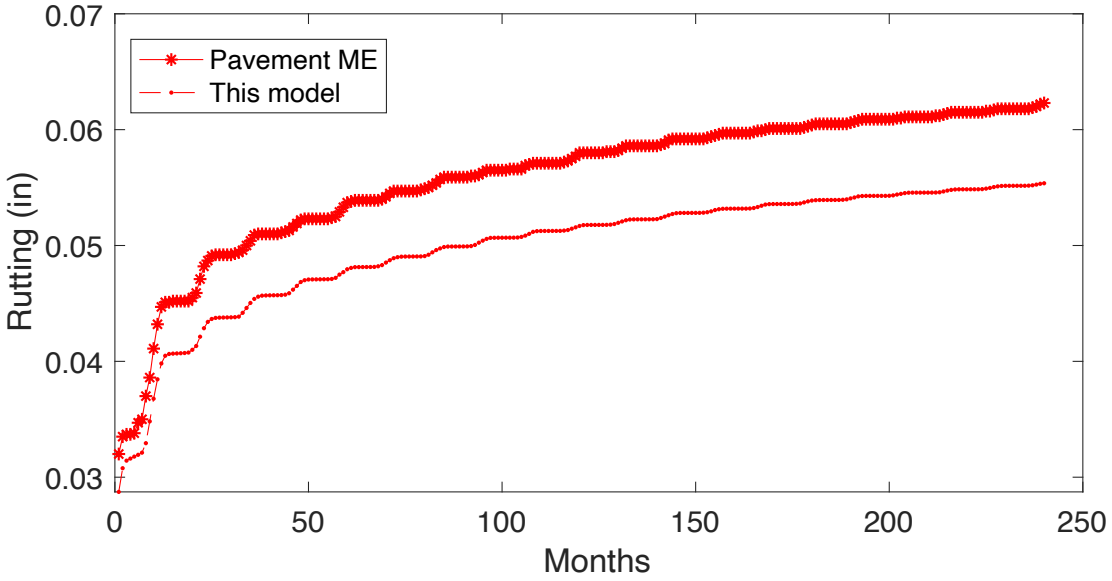

Figure 49. Comparison of Pavement ME and MEAPA for unbound layer rutting

4.11 Subgrade Layer Rutting

Subgrade layer rutting is computed using a procedure very similar to the unbound base and subbase layers. The same basic phenomenological relationship developed by Tseng and Lytton (Tseng & Lytton, 1989) is used to compute plastic strain:

$$\varepsilon_p = \beta_{subg1} k_{subg1} \varepsilon_v R_e e^{-\left(\frac{\rho}{n}\right)^{\beta}} \quad [128]$$

where;

ε_p	=	Permanent or plastic strain in subgrade layer, in/in.
n	=	Number of axle load applications.
ε_v	=	Average vertical resilient or elastic strain calculated by the structural response model, in/in.
β	=	A parameter dependent on moisture content of the soil
ρ	=	A parameter related moisture content and resilient modulus of the soil
R_e	=	Ratio $R_e = \varepsilon_0/\varepsilon_r$, where; ε_o=Intercept determined from laboratory repeated load permanent deformation tests, in/in., ε_r=Resilient strain imposed in laboratory test to obtain material properties ε_o, β, and ρ, in/in.
k_{subg1}	=	Global calibration coefficient $k_{subg1} = 1.35$ for fine-grained materials.
β_{sub1}	=	Local calibration constant for the rutting in the unbound layers; the local calibration constant was set to 1.0 for the global calibration effort. However, in this project, the β_{sub1}=0.6 was used since this value produced more realistic subgrade rutting.

The parameters β, ρ and $R_e = \varepsilon_0/\varepsilon_r$ are computed using the same relationships as those of the unbound layers described in the previous section.

For subgrade, vertical elastic strain (ε_v) is computed at two different locations: (i) top of subgrade and (ii) 6" below the top of the subgrade. The progression of plastic strain at these two locations were computed using the same procedure (i.e., equivalent cycles approach) described in the previous section. At each season, the following k_{subg} parameter was computed

$$k_{subg} = \frac{\ln\left(\frac{\varepsilon_{p,z=top-subgrade}}{\varepsilon_{p,z=(top-subgrade+6")}}\right)}{6} \quad [129]$$

where;

$\varepsilon_{p,z=top-subgrade}$	=	Plastic strain at the top of the subgrade, in/in
$\varepsilon_{p,z=(top-subgrade+6")}$	=	Plastic strain 6" below the top of the subgrade, in/in

It should be noted that the equation above assumes the strain on the top of the subgrade is more than the strain within the subgrade. This may not be true in certain conditions and the k_{subg} parameter may be negative, which is unrealistic. Therefore, if k_{subg} value is less than 10^{-6}, it is set to $k_{subg} = 10^{-6}$.

Finally, subgrade rutting is computed using the following relationship:

$$\Delta_{p(subgrade)} = \frac{\varepsilon_{p,z=top-subgrade}}{k_{subg}} \left(1 - e^{-k_{subg} h_{bedrock}}\right) \quad [130]$$

where;

$\varepsilon_{p,z=top-subgrade}$ = Plastic strain at the top of the subgrade, in/in
$\Delta_{p(subgrade)}$ = Subgrade rutting, in.
$h_{bedrock}$ = Depth to bedrock, ft.

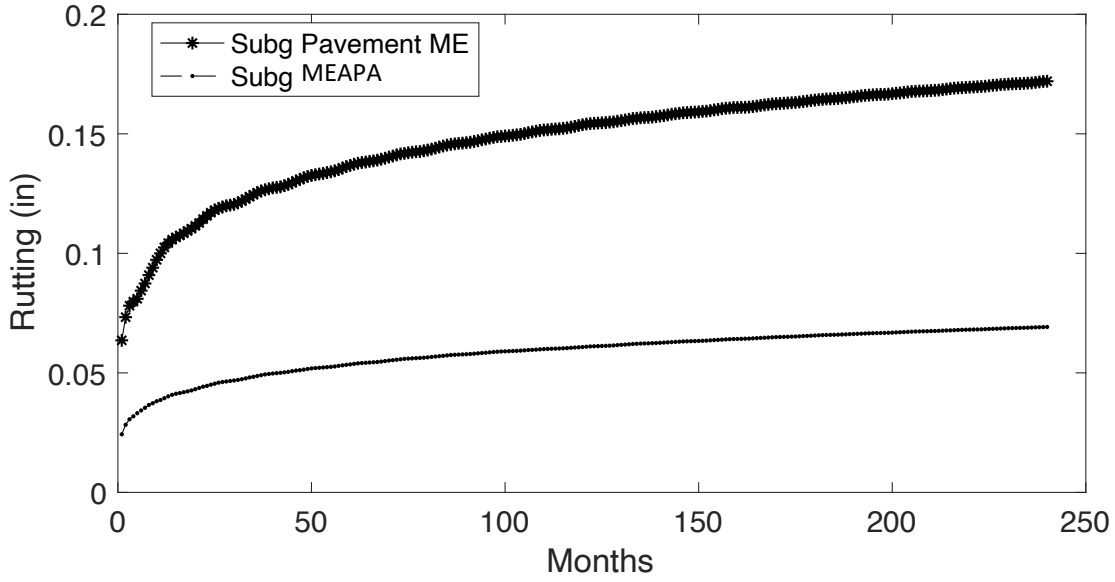

Figure 50. Comparison of Pavement ME and MEAPA for subgrade rutting

4.12 International Roughness Index (IRI)

The IRI for flexible pavements is calculated using the following formula:

$$IRI = IRI_o + C_1(RD) + C_2(FC_{total}) + C_3(TC) + C_4(SF) \quad [131]$$

where;

IRI	=	International roughness index, in/mile.
IRI_0	=	Initial IRI, in/mile
RD	=	Total rut depth, in = $\Delta_{p(HMA)} + \Delta_{p(unbound)} + \Delta_{p(subgrade)}$
FC_{total}	=	Total fatigue cracking (including bottom-up and top-down cracking), %
TC	=	Thermal cracking, ft/mile
SF	=	Site factor
C_i	=	Calibration coefficients. The default values of these coefficients are: C_1=40, C_2= 0.4, C_3=0.008 and C_4=0.015.

Total fatigue cracking in the IRI formulation above is computed using the formula below, which assumes 12 ft wide design lane (to convert FC_{td} from ft/mile to percentage):

$$FC_{total} = FC_{bu} + FC_{td}(\frac{ft}{mile})\frac{1ft\ (assumed\ TD\ cracking\ width)}{5280ft/mile * 12ft(lane\ width)} * 100 \quad [132]$$

Site factor is defined using the following set of equations:

$$SF = \left(Frost + Swell\right) \times Age^{1.5} \quad [133]$$

$$Frost = Ln\left[\left(Rain + 1\right) \times \left(FI + 1\right) \times P_4\right] \quad [134]$$

$$Swell = Ln\left[\left(Rain + 1\right) \times \left(FI + 1\right) \times P_{200}\right] \quad [135]$$

where;

SF	=	Site factor
Age	=	Pavement age (years)
FI	=	Freezing index, °F-days.
Rain	=	Mean annual rainfall (in.)
P_4	=	Percent material passing No. 4 sieve for the subgrade soil
P_{200}	=	Percent passing No. 200 sieve for the subgrade soil.

5. MODELING AC-CSM or AC-CSM-GB: ASPHALT CONCRETE OVER CHEMICALLY STABILIZED MATERIAL

The Chemically Stabilized Material (CSM) layers provide a stiff base layer that serve a good foundation for the overlying AC layers and help spread the load on a large area so that rutting in the base, subbase and subgrade are minimized. However, the CSM layers can degrade over time due to load-related fatigue cracking, which can propagate to the surface in the form of reflective cracks. Therefore, progression of reflective cracking over time is predicted, in addition to the other distresses. The following is the list of distresses computed for the AC-CSM and AC-CSM-GB pavement types:

1. AC reflective cracking due to the fatigue damage in the CSM layer
2. AC top-down fatigue cracking (ft/mile)
3. AC bottom-up fatigue cracking (%)
4. AC thermal cracking (ft/mile)
5. Rutting – AC, base, subbase, subgrade (in)
6. International Roughness Index (IRI) (in/mile)

The steps of the calculation of AC top-down fatigue cracking, bottom-up fatigue cracking, thermal cracking (ft/mile), and rutting of the AC, base and subgrade layers are identical to those of the AC-GB pavement type described in the previous section. Therefore, it will not be repeated here for brevity.

The general steps of the algorithm are as follows:

1. Development of the |E*| master curves for the AC layer(s)
2. Sublayering of the structure
3. Calculating equivalent frequencies and load correction factors using the MEPDG procedure
4. Running the climatic model and obtaining temperature at the center of each sublayer
5. Running the Global Aging System (GAS) model
6. Calculation of the elastic moduli in five quintiles in a given month using the temperature at each quintile, frequency and the |E*| master curve coefficients.
7. Defining the critical strain locations for each type of distress
8. Running the thermal cracking model
9. Running the MatLEA structural response model at each quintile of each month, then:
    a. Compute the top-down cracking increment
    b. Compute the bottom-up cracking increment
    c. Compute the AC rutting increment
    d. Compute the CSM layer damage and cracking increment
    e. Compute the base/subbase rutting (same model) increment
    f. Compute the subgrade rutting increment.
    g. Summation of the distresses computed during 5 quintiles of each month to compute the cumulative monthly distresses.
10. Compute IRI values for each month

5.1 Reflective Cracking due to the CSM Layer

The reflective cracking due to a CSM layer is computed via a set of equations that include a fatigue life formulation, Miner's law of linear damage growth and a convolution-like transfer function to convert damage to observed reflective cracking in the field. The material-level CSM fatigue life formulation used herein is as follows:

$$N_f^{CSM} = 10^{\frac{0.972\beta_{c1}-\frac{\sigma_t}{MoR}}{0.0825\beta_{c2}}} \quad [136]$$

where;

σ_t	=	tensile stress at the bottom of the CSM layer (psi)
N_f^{CSM}	=	Number of cycles to failure for the CSM layer
MoR	=	Modulus of Rupture (flexular strength) of the CSM layer, psi
β_{c1}, β_{c2}	=	Calibration factors, default equal to unity.

5.1.1 Calculation of Damage

The damage growth in the CSM layer is based on the Miner's law of linear damage growth, similar to the bottom-up fatigue cracking model in AC layer. Figure 32, Figure 33, Figure 34, and Figure 35 show critical strains computed by single, tandem, tridem and quad axles, respectively. For CSM layer, at each of these X- and Y locations, the maximum tensile stresses are computed at different X and Y locations at bottom of CSM, and used to calculate the number of cycles to failure using the following formula:

$$D_j^{\boldsymbol{single}} = \sum_{k=1}^{39} \frac{N_{i,t,w_k}^{\boldsymbol{single}}}{N_f^{CSM}} \quad [137]$$

$$D_j^{\boldsymbol{tandem}} = \sum_{k=1}^{39} \frac{N_{i,t,w_k}^{\boldsymbol{tandem}}}{N_f^{CSM}} \quad [138]$$

$$D_j^{\boldsymbol{tridem}} = \sum_{k=1}^{31} \frac{N_{i,t,w_k}^{\boldsymbol{tridem}}}{N_f^{CSM}} \quad [139]$$

$$D_j^{\boldsymbol{quad}} = \sum_{k=1}^{31} \frac{N_{i,t,w_k}^{\boldsymbol{quad}}}{N_f^{CSM}} \quad [140]$$

where;

N_f^{CSM} = Number of cycles to failure in CSM layer, based on the tensile stress at the bottom of CSM, in i^{th} month, j^{th} quintile due to axle weight w_k

N_{i,t,w_k}^{single} = Number of single axles for each month i ($i = 1 \dots 12$), for year t ($t = 1 \dots t_a$, where t_a is analysis duration), corresponding to axle weight $\boldsymbol{w_k}$ Where $k = 1 \dots 39$ and $\boldsymbol{w_k} = 3000, 4000, \dots 41000$ (lb).

N_{i,t,w_k}^{tandem} = Number of tandem axles for each month i ($i = 1 \dots 12$), for year t ($t = 1 \dots t_a$, where t_a is analysis duration), corresponding to axle weight $\boldsymbol{w_k}$ Where $k = 1 \dots 39$ and $\boldsymbol{w_k} = 6000, 8000, \dots 82000$ (lb).

N_{i,t,w_k}^{tridem} = Number of tridem axles, for each month i ($i = 1 \dots 12$), for year t ($t = 1 \dots t_a$, where t_a is analysis duration), corresponding to axle weight $\boldsymbol{w_k}$, where $k = 1 \dots 31$ and $\boldsymbol{w_k} = 12000, 15000, \dots 102000$ (lb).

$\boldsymbol{N_{i,t,w_k}^{quad}}$ = Number of quad axles i, for each month i ($i = 1 \dots 12$), for year t ($t = 1 \dots t_a$, where t_a is analysis duration), corresponding to axle weight $\boldsymbol{w_k}$ Where $k = 1 \dots 31$ and $\boldsymbol{w_k} = 12000, 15000, \dots 102000$ (lb).

Total damage in each quintile due to each axle are added to total damage

$$D_{csm}(t) = \sum_{j=1}^{5} \left(D_j^{\boldsymbol{single}} + D_j^{\boldsymbol{tandem}} + D_j^{\boldsymbol{tridem}} + D_j^{\boldsymbol{quad}} \right) \quad [141]$$

$D_{csm}(t)$ = Total CSM damage in month t.
k = k=1 for single, k=2 for tandem, k=3 for tridem and k=4 for quad axle
j = Quintile number

Once the damage caused by the axles for each month is computed, cumulative damage is calculated using the following formula:

$$D_{csm}^{cum}(t) = \sum_{i=1}^{t} D_{csm}(t_i) \quad [142]$$

where;
$D_{csm}^{cum}(t)$ = Cumulative damage in CSM layer.

5.1.2 Calculation of Reflective Cracking

First step in computing the reflective cracking on the AC surface is the computation of the cracked area within the CSM layer using the following formula:

$$CA_{csm}(t) = \frac{100}{1 + e^{6 - 6D_{csm}^{cum}(t)}} \quad [143]$$

where;
$D_{csm}^{cum}(t)$ = Cumulative damage in CSM layer.
$CA_{csm}(t)$ = Cracked area in CSM layer.

Then total reflected crack is computed using the following (convolution-like) equation:

$$TRA(t) = \sum_{\tau=1}^{t-1} RC(t-\tau) * \left(CA_{csm}(\tau+1) - CA_{csm}(\tau) \right) \quad [144]$$

where;
$TRA(t)$ = Total reflected crack area, %.
$CA_{csm}(t)$ = Cracked area in CSM layer, as decimal (not %).
$RC(t)$ = Percent cracking relected for age t

Percent cracking reflected for age t ($RC(t)$) can be computed using the following empirical formula (Part 3, Chapter 6 of (ARA Inc. ERES Consultants Division, 2004));

$$RC(t) = \frac{100}{1 + e^{a+bt}} \quad [145]$$

where;

$RC(t)$	=	Percent cracking reflected for age t
t	=	Time (in years)
a, b	=	Constants; $a = 3.5 + 0.75 * \mathrm{h_{AC}}$ and $b = -0.688584 - 3.37302 * \mathrm{h_{AC}^{-0.915469}}$ where hAC = total height of the AC layers above CSM layer.

5.1.3 Reduction of Modulus of CSM Layer Due to Damage

Typical CSM layer modulus is initially quite high. However, as fatigue damage grows within the CSM layer, this modulus decreases with time. Reduction of modulus of CSM layer is modeled using the following relationship:

$$E(t) = E_{min} + \frac{E_{max} - E_{\min}}{1 + e^{-4+14D_{csm}^{cum}(t)}} \quad [146]$$

where;

E_{max}	=	Maximum CSM modulus, psi
$E_{\min}$	=	Minimum CSM modulus, psi
$D_{csm}^{cum}(t)$	=	Cumulative damage in CSM layer, at the end of each month,t.

An example intermediate outputs of the CSM model is shown in Figure 51, which shows the reduction in CSM modulus with time, growth of cracked area in CSM with time and progression of reflective cracking.

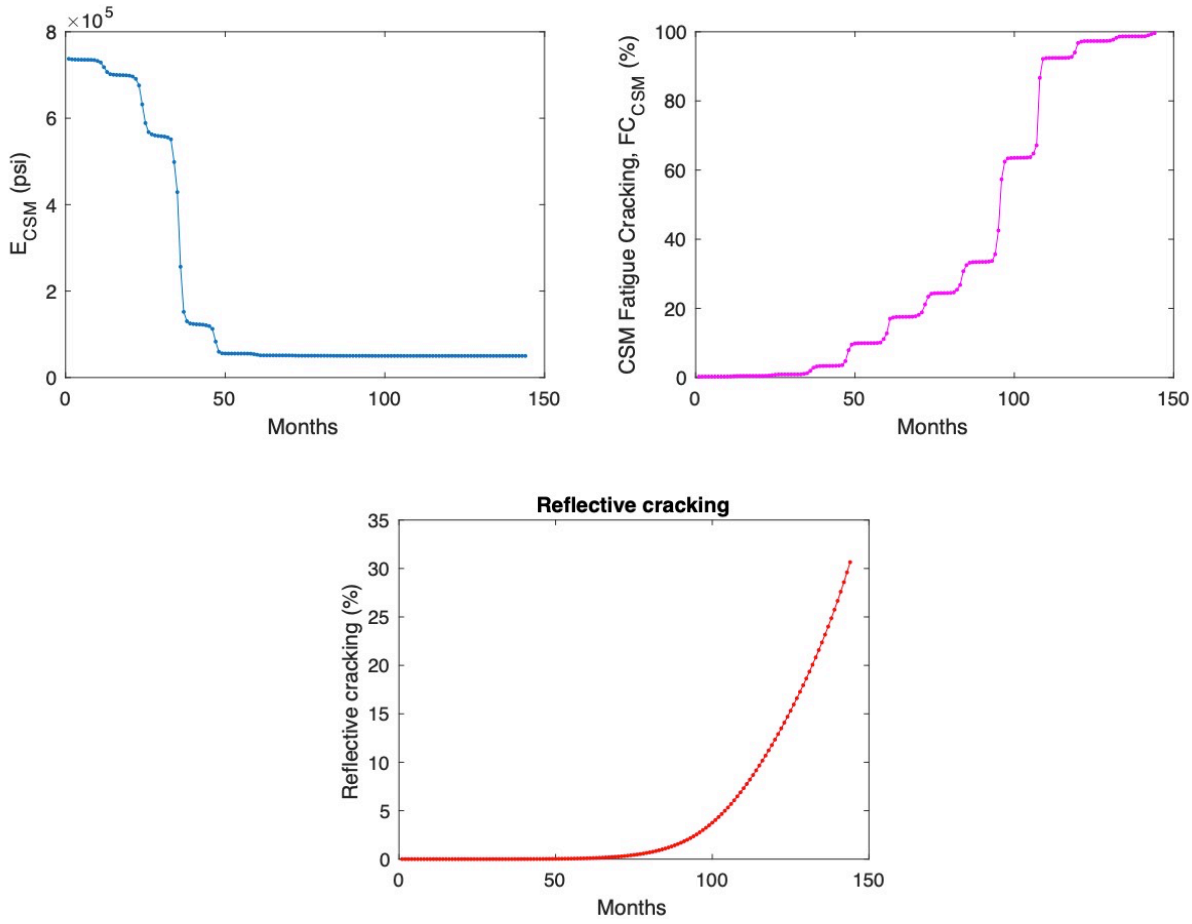

Figure 51. An example intermediate outputs of the CSM model including the (a) reduction in CSM modulus with time, (b) growth of cracked area in CSM with time and (c) progression of reflective cracking.

5.2 International Roughness Index (IRI)

The IRI for flexible pavements with CSM is calculated using the same formula as that of AC-GB pavement type, except that the total load-related cracking includes the reflective cracking due to the CSM layer:

$$IRI = IRI_o + C_1(RD) + C_2(FC_{total}) + C_3(TC) + C_4(SF) \quad [147]$$

where;

IRI	=	International roughness index, in/mile.
IRI_0	=	Initial IRI, in/mile
RD	=	Total rut depth, in = $\Delta_{p(HMA)} + \Delta_{p(unbound)} + \Delta_{p(subgrade)}$
FC_{total}	=	Total load-related cracking, %
TC	=	Thermal cracking, ft/mile
SF	=	Site factor

C_i = Calibration coefficients. The default values of these coefficients are: C_1=40, C_2= 0.4, C_3=0.008 and C_4=0.015.

Total load-related cracking (FC_{total}) in the IRI formulation above is computed using the formula below, which assumes 12 ft wide design lane (to convert FC_{td} from ft/mile to percentage):

$$FC_{total} = FC_{bu} + FC_{td}\left(\frac{ft}{mile}\right)\frac{1ft\ (assumed\ TD\ cracking\ width)}{\frac{5280ft}{mile} * 12ft(lane\ width)} * 100 + TRA(t) \quad [148]$$

where;

$TRA(t)$ = Total reflected crack area, %.
FC_{bu} = Bottom-up fatigue cracking, %.
FC_{td} = Top-down fatigue cracking,%.

Site factor is defined using the following set of equations:

$$SF = \left(Frost + Swell\right) \times Age^{1.5} \quad [149]$$

$$Frost = Ln\left[\left(Rain + 1\right) \times \left(FI + 1\right) \times P_4\right] \quad [150]$$

$$Swell = Ln\left[\left(Rain + 1\right) \times \left(FI + 1\right) \times P_{200}\right] \quad [151]$$

where;

SF = Site factor
Age = Pavement age (years)
FI = Freezing index, °F-days.
Rain = Mean annual rainfall (in.)
P_4 = Percent material passing No. 4 sieve for the subgrade soil
P_{200} = Percent passing No. 200 sieve for the subgrade soil.

6. MODELING AC-EAC-GB and AC-EAC-CSM: ASPHALT CONCRETE OVER EXISTING ASPHALT CONCRETE

Asphalt overlays over existing asphalt overlays are modeled somewhat similar to the AC-CSM pavement type. The main difference is how the reflective cracking is computed. The following is the list of the distresses computed for this pavement type:

1. AC reflective cracking due to the damage in the existing asphalt concrete (EAC)
2. AC top-down fatigue cracking (ft/mile)
3. AC bottom-up fatigue cracking (%)
4. AC thermal cracking (ft/mile)
5. Rutting – AC, base, subbase, subgrade (in)
6. International Roughness Index (IRI) (in/mile)

The steps of the calculation of AC top-down fatigue cracking, bottom-up fatigue cracking, thermal cracking (ft/mile), and rutting of the AC, base and subgrade layers are identical to those of the AC-GB pavement type described earlier. Therefore, it will not be repeated here for brevity.

The general steps of the algorithm are as follows:

1. Development of the |E*| master curves for the AC layer(s)
2. Sublayering of the structure
3. Calculating equivalent frequencies and load correction factors using the MEPDG procedure
4. Running the climatic model and obtaining temperature at the center of each sublayer
5. Running the Global Aging System (GAS) model
6. Calculation of the elastic moduli in five quintiles in a given month using the temperature at each quintile, frequency and the |E*| master curve coefficients.
7. Defining the critical strain locations for each type of distress
8. Running the thermal cracking model
9. Running the MatLEA structural response model at each quintile of each month, then:
    a. Compute the top-down cracking increment
    b. Compute the bottom-up cracking increment
    c. Compute the AC rutting increment
    d. Compute the EAC layer damage and cracking increment
    e. Compute the base/subbase rutting (same model) increment
    f. Compute the subgrade rutting increment.
    g. Summation of the distresses computed during 5 quintiles of each month to compute the cumulative monthly distresses.
10. Compute IRI values for each month

6.1 Calculation of Damage and Reflective Cracking Due to Existing Asphalt Concrete

The existing asphalt concrete (EAC) layer modeled in a very similar to the traditional AC layer. The main difference is that since the EAC layer is a ‘damaged’ layer, where in-situ dynamic

modulus master curve is somewhat difficult to estimate. Similar to AC, the following sigmoid formulation is used to represent the |E*| master curve for the EAC layer:

$$log\left(|E^*|_{\text{undamaged}}\right) = c_1 + \frac{c_2}{1 + e^{c_3 + c_4 log((t_r)}} \quad [152]$$

where;

$|E^*|_{\text{undamaged}}$ = Dynamic modulus of EAC layer in undamaged state.
t_r = Time of loading at the reference temperature.
c_1 = Minimum value of E^*.
$c_1 + c_2$ = Maximum value of E^*.
c_3, c_4 = Parameters describing the shape of the sigmoidal function.

The equation above represents the |E*| master curve of the EAC layer in its undamaged state. Effect of damage on the |E*| master curve is modeled through the following relationship:

$$|E^*|_{\text{damaged}} = 10^{c_1} + \frac{|E^*|_{\text{undamaged}} - 10^{c_1}}{1 + e^{-0.3 + 5log(D_{bu}^{EAC}(t))}} \quad [153]$$

where;

$|E^*|_{\text{damaged}}$ = Dynamic modulus of the EAC layer in a damaged state (before overlay construction)
$D_{bu}^{EAC}(t)$ = Total bottom-up damage within EAC layer in month t.

The calculation procedure of damage within EAC layer in month t (i.e., $D_{bu}^{EAC}(t)$) is identical that of the bottom-up damage calculation procedure described earlier for the AC-GB pavement type. The only difference is that the evaluation point for the maximum tensile strain is the bottom of the EAC layer. As damage grows within the EAC layer, at the end of each month, $D_{bu}^{EAC}(t)$ is updated and used in the equation above to compute a new $|E^*|_{\text{damaged}}$, which is subsequently used in the MatLEA strain calculations in the upcoming month.

In order to calculate the reflective cracking, cracked area within the EAC layer is needed (just like the model for CSM), which is computed using the following formula:

$$CA_{EAC}(t) = \frac{100}{1 + e^{6 - 6D_{bu}^{EAC}(t)}} \quad [154]$$

where;

$D_{bu}^{EAC}(t)$ = Cumulative bottom-up damage within EAC layer in month t.
$CA_{EAC}(t)$ = Cracked area in EAC layer.

Then total reflected crack is computed using the following (convolution-like) equation:

$$TRA(t) = \sum_{\tau=1}^{t-1} RC(t-\tau) * \left(CA_{EAC}(\tau+1) - CA_{EAC}(\tau)\right) \quad [155]$$

where;

$TRA(t)$ = Total reflected crack area, %.
$CA_{EAC}(t)$ = Cracked area in EAC layer, as decimal (not %)
$RC(t)$ = Percent cracking relected for age t

Percent cracking reflected for age t ($RC(t)$) can be computed using the following empirical formula (Part 3, Chapter 6 of (ARA Inc. ERES Consultants Division, 2004));

$$RC(t) = \frac{100}{1 + e^{a+bt}} \quad [156]$$

where;

$RC(t)$	=	Percent cracking rfelected for age t
t	=	Time (in years)
a, b	=	Constants; $a = 3.5 + 0.75 * \mathrm{h_{AC}}$ and $b = -0.688584 - 3.37302 * \mathrm{h_{AC}^{-0.915469}}$ where $\mathrm{h_{AC}}$ = total height of the AC layers above EAC layer.

6.2 International Roughness Index (IRI)

The IRI formulations for AC-EAC pavement type identical to those of the AC-CSM pavement type, therefore, they are not repeated here for brevity.

7. REFERENCES

ARA Inc. ERES Consultants Division. (2004). *Guide for Mechanistic-Empirical Designof New and Rehabilitated Pavement Structures*.

Ayres Jr, M., & Witczak, M. W. (1998). AYMA: mechanistic probabilistic system to evaluate flexible pavement performance. *Transportation Research Record*, *1629*(1), 137–148.

Buch, N., Haider, S. W., Brown, J., Chatti, K., & Engineering, M. S. University. Dept. of C. and E. (2009). *Characterization of truck traffic in Michigan for the new mechanistic empirical pavement design guide.* Michigan. Dept. of Transportation. Construction and Technology Division. https://rosap.ntl.bts.gov/view/dot/18335

Burmister, D. M. (1945). The general theory of stresses and displacements in layered soil systems. II. *Journal of Applied Physics*, *16*(3), 126–127. https://doi.org/10.1063/1.1707562

Dempsey, B. J. (1969). *A heat-transfer model for evaluation frost action and temperature related effects in multilayered pavement systems*.

Dempsey, B. J., & Thompson, M. R. (1970). A HEAT TRANSFER MODEL FOR EVALUATING FROST ACTION AND TEMPERATURE-RELATED EFFECTS IN MULTILAYERED PAVEMENT SYSTEMS. *Highway Research Record*, *342*. https://trid.trb.org/view/102331

Diefenderfer, B., & Al-Qadi, IL, S. R. (2003). Development and validation of a model to predict pavement temperature profile. *TRB 2003 Annual Meeting*. http://citeseerx.ist.psu.edu/viewdoc/download?doi=10.1.1.476.6560&rep=rep1&type=pdf

Forman, B. A., & Margulis, S. A. (2010). Assimilation of multiresolution radiation products into a downwelling surface radiation model: 1. Prior ensemble implementation. *Journal of Geophysical Research Atmospheres*, *115*(22). https://doi.org/10.1029/2010JD013920

Haider, S. W., Brink, W. C., & Buch, N. (2016). Local calibration of flexible pavement performance models in Michigan. *Canadian Journal of Civil Engineering*, *43*(11), 986–997. https://doi.org/10.1139/cjce-2015-0556

Haider, S. W., Buch, N., Brink, W., Chatti, K., & Baladi, G. (2014). *Preparation for Implementation of the Mechanistic-Empirical Pavement Design Guide in Michigan Part 3: Local Calibration and Validation of Performance Models*. https://trid.trb.org/view/1343694

Islam, M. R., & Tarefder, R. A. (2015). Coefficients of thermal contraction and expansion of asphalt concrete in the laboratory. *Journal of Materials in Civil Engineering*, *27*(11). https://doi.org/10.1061/(ASCE)MT.1943-5533.0001277

Jamrah, A., & Kutay, M. E. (2015). Investigation of different methods for obtaining asphalt mixture creep compliance for use in pavement mechanistic-empirical design software. In *Transportation Research Record* (Vol. 2524). https://doi.org/10.3141/2524-10

Jamrah, A., Kutay, M. E., & Ozturk, H. (2014). Characterization of Asphalt Materials Common to Michigan in Support of the Implementation of the Mechanistic-Empirical Pavement Design Guide. *TRB 93rd Annual Meeting Compendium of Papers*.

Kaloush, K. E., & Witczak, M. W. (2000). Development of a permanent to elastic strain ratio model for asphalt mixtures. *Development of the 2002 Guide for the Design of New and Rehabilitated Pavement Structures. NCHRP*, 1–37.

Khazanovich, L., & Wang, Q. (Chuck). (2007). MnLayer: High-Performance Layered Elastic Analysis Program. *Transportation Research Record: Journal of the Transportation Research Board*, *2037*(1), 63–75. https://doi.org/10.3141/2037-06

Kutay, M Emin, & Jamrah, A. (2013). *Preparation for Implementation of the Mechanistic-Empirical Pavement Design Guide in Michigan: Part 1-HMA Mixture Characterization*. https://trid.trb.org/view/1247913

Kutay, M.E., & Lanotte, M. (2018). Viscoelastic continuum damage (VECD) models for cracking problems in asphalt mixtures. *International Journal of Pavement Engineering*, *19*(3). https://doi.org/10.1080/10298436.2017.1279492

Larson, G., & Dempsey, B. (1997). *Enhanced integrated climatic model Version 2.0*. https://www.ideals.illinois.edu/handle/2142/95718

Leahy, R. B. (1989). *Permanent deformation characteristics of asphalt concrete*.

Lytton, R L, Pufahl, D. E., Michalak, C. H., Liang, H. S., & Dempsey, B. J. (1993). *An integrated model of the climatic effects on pavements*. *FHWA-RD-90-033*.

Lytton, Robert L, Luo, X., Ling, M., Chen, Y., Hu, S., & Gu, F. (2018). *A Mechanistic--Empirical Model for Top--Down Cracking of Asphalt Pavements Layers*.

Marchetti, M., Muzet, V., Pitre, R., Datcu, S., Ibos, L., & Livet, J. (2004). *Emissivity measurements of road materials*.

Minhoto, M., Pais, J., 2006, P. P.-A. R., & 2006, undefined. (n.d.). Asphalt pavement temperature prediction. *Bibliotecadigital.Ipb.Pt*. Retrieved May 16, 2018, from http://bibliotecadigital.ipb.pt/handle/10198/1992

Mirza, M. W., & Witczak, M. W. (1995). Development of a global aging system for short and long term aging of asphalt cements (with discussion). *Journal of the Association of Asphalt Paving Technologists*, *64*.

Park, S. W., & Schapery, R. A. (1999). Methods of interconversion between linear viscoelastic material functions. Part I—a numerical method based on Prony series. *International Journal of Solids and Structures*, *36*(11), 1653–1675. https://doi.org/10.1016/S0020-7683(98)00055-9

Sugita, M., & Brutsaert, W. (1993). Cloud effect in the estimation of instantaneous downward longwave radiation. *Water Resources Research*, *29*(3), 599–605. https://doi.org/10.1029/92WR02352

Tseng, K.-H., & Lytton, R. L. (1989). Prediction of permanent deformation in flexible pavement materials. In *Implication of aggregates in the design, construction, and performance of flexible pavements*. ASTM International.

Wang, G., & Roque, R. (2011). Impact of wide-based tires on the near-surface pavement stress states based on three-dimensional tire-pavement interaction model. *Road Materials and Pavement Design*, *12*(3), 639–662. https://doi.org/10.1080/14680629.2011.9695264

Wang, G., Roque, R., & Morian, D. (2012). Effects of Surface Rutting on Near-Surface Pavement Responses Based on a Two-Dimensional Axle-Tire-Pavement Interaction Finite-Element Model. *Journal of Materials in Civil Engineering*, *24*(11), 1388–1395. https://doi.org/10.1061/(ASCE)MT.1943-5533.0000526

8. APPENDIX G. MatLEA solution based on Burmister Layered Elastic Formulations

8.1 Description of the MatLEA Solution

The MatLEA formulations and computational steps are almost identical to those of the MnLayer software (Khazanovich & Wang, 2007). The concept is based on the Burmister's multi layered elastic theory (Burmister, 1945). The main differences between the MnLayer software and MatLEA are:

- A, B, C, D parameters are computed via 3D matrix inversion (making the program faster)
- The integration over the 'm' (the inverse Henkel transform variable) is done via bulk matrix operations.

In MatLEA solution, the boundaries between the layer interfaces are used to compute the main parameters called A, B, C and D shown in the figures below. Problem geometry, dimensions and material property inputs are illustrated in Figure G. 2.

Figure G. 3, Figure G. 4, Figure G. 5 and Figure G. 6 show the vertical displacement, horizontal displacement, vertical stress and shear stress formulations. For each of these formulations, boundary conditions at the interfaces were considered to come up with equations for A, B, C and D of each layer (See Figure G. 9, Figure G. 10, Figure G. 11 and Figure G. 12). Then a grand matrix created for solution of A, B, C and D based on the surface load (see Figure G. 13). The grand matrix in Figure G. 13 is in the form of a linear system of equations defined as **[M]{X}=[Y]** (matrix operations). The matrix **X** can be solved via least square method as follows:

$$\boldsymbol{X} = (\boldsymbol{M}^{\boldsymbol{T}}\boldsymbol{M})^{-1}(\boldsymbol{MY})$$

Figure G. 1 Least squares solution formulation

Once A, B, C and D values in matrix **X** are obtained for each layer, equations shown in Figure G. 3, Figure G. 4, Figure G. 5, Figure G. 6, Figure G. 7 and Figure G. 8 are used to compute vertical displacement, horizontal displacement, vertical stress, shear stress, radial stress and tangential stress, respectively.

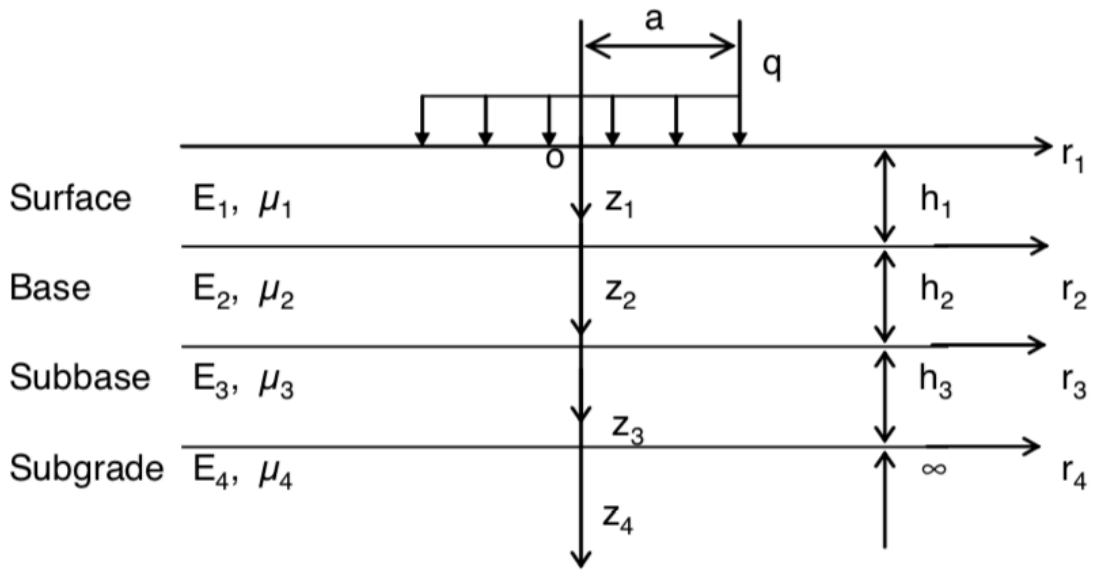

Figure G. 2 Problem geometry, dimensions and material properties

$$w = \int_0^\infty w_i J_o(mr) m dm$$

$$w_i = \frac{1+\mu_i}{E_i}(-A_i m e^{mz} + B_i m e^{-mz} + C_i(2-4\mu_i - mz)e^{mz} + D_i(2-4\mu_i + mz)e^{-mz})$$

$$w_i = \frac{1+\mu_i}{E_i}\begin{bmatrix} -me^{mz} & me^{-mz} & (2-4\mu_i - mz)e^{mz} & (2-4\mu_i + mz)e^{-mz} \end{bmatrix}\begin{bmatrix} A_i \\ B_i \\ C_i \\ D_i \end{bmatrix}$$

Figure G. 3 Vertical displacement formulations

$$u = \int_0^\infty u_i J_1(mr) m dm$$

$$u_i = \frac{1+\mu_i}{E_i}(A_i m e^{mz} + B_i m e^{-mz} + C_i(1+mz)e^{mz} - D_i(1-mz)e^{-mz})$$

$$u_i = \frac{1+\mu_i}{E_i}\begin{bmatrix} me^{mz} & me^{-mz} & (1+mz)e^{mz} & (-1+mz)e^{-mz} \end{bmatrix}\begin{bmatrix} A_i \\ B_i \\ C_i \\ D_i \end{bmatrix}$$

Figure G. 4 Horizontal displacement formulations

$$\sigma_z = -\int_0^\infty \sigma_{zi} J_o(mr) m^2 dm$$

$$\sigma_{zi} = (A_i m e^{mz} + B_i m e^{-mz} - C_i(1-2\mu_i - mz)e^{mz} + D_i(1-2\mu_i + mz)e^{-mz})$$

$$\sigma_{zi} = \begin{bmatrix} me^{mz} & me^{-mz} & (-1+2\mu_i + mz)e^{mz} & (1-2\mu_i + mz)e^{-mz} \end{bmatrix}\begin{bmatrix} A_i \\ B_i \\ C_i \\ D_i \end{bmatrix}$$

Figure G. 5 Vertical stress formulations

$$\tau_{rz} = \int_0^\infty \tau_{rzi} J_1(mr) m^2 dm$$

$$\tau_{rzi} = (A_i m e^{mz} - B_i m e^{-mz} + C_i(2\mu_i + mz)e^{mz} + D_i(2\mu_i - mz)e^{-mz})$$

$$\tau_{rzi} = \begin{bmatrix} me^{mz} & -me^{-mz} & (2\mu_i + mz)e^{mz} & (2\mu_i - mz)e^{-mz} \end{bmatrix}\begin{bmatrix} A_i \\ B_i \\ C_i \\ D_i \end{bmatrix}$$

Figure G. 6 Shear stress formulations

$$\sigma_{ri} = \int_0^\infty \begin{pmatrix} A_i(m)me^{mz} + B_i(m)me^{-mz} \\ + C_i(m)(1+2\mu_i+mz)e^{mz} \\ - D_i(m)(1+2\mu_i-mz)e^{-mz} \end{pmatrix} J_0(mr)m^2 dm$$
$$- \frac{1}{r}\int_0^\infty \begin{pmatrix} A_i(m)me^{mz} + B_i(m)me^{-mz} \\ + C_i(m)(1+mz)e^{mz} \\ - D_i(m)(1-mz)e^{-mz} \end{pmatrix} J_1(mr)mdm$$

Figure G. 7 Radial stress formulations

$$\sigma_{\theta i} = \int_0^\infty \left(2C_i(m)\mu_i e^{mz} - 2D_i(m)\mu_i e^{-mz}\right) J_0(mr)m^2 dm$$
$$+ \frac{1}{r}\int_0^\infty \begin{pmatrix} A_i(m)me^{mz} + B_i(m)me^{-mz} \\ + C_i(m)(1+mz)e^{mz} \\ - D_i(m)(1-mz)e^{-mz} \end{pmatrix} J_1(mr)mdm$$

Figure G. 8 Tangential stress formulations

For $z = h_i$, layer i: $w_{i(z=h_i)} =$

$$\frac{1+\mu_i}{E_i}\begin{bmatrix}-me^{mh_i} & me^{-mh_i} & (2-4\mu_i-mh_i)e^{mh_i} & (2-4\mu_i+mh_i)e^{-mh_i}\end{bmatrix}\begin{bmatrix}A_i\\B_i\\C_i\\D_i\end{bmatrix}$$

For $z = 0$, layer i+1: $w_{i+1(z=0)} = \frac{1+\mu_{i+1}}{E_{i+1}}\begin{bmatrix}-m & m & (2-4\mu_{i+1}) & (2-4\mu_{i+1})\end{bmatrix}\begin{bmatrix}A_{i+1}\\B_{i+1}\\C_{i+1}\\D_{i+1}\end{bmatrix}$

At the interface between i and i+1; $w_{i(z=h_i)} - w_{i+1(z=0)} = 0$

$$\frac{1+\mu_i}{E_i}\begin{bmatrix}-me^{mh_i} & me^{-mh_i} & (2-4\mu_i-mh_i)e^{mh_i} & (2-4\mu_i+mh_i)e^{-mh_i}\end{bmatrix}\begin{bmatrix}A_i\\B_i\\C_i\\D_i\end{bmatrix} - \frac{1+\mu_{i+1}}{E_{i+1}}\begin{bmatrix}-m & m & (2-4\mu_{i+1}) & (2-4\mu_{i+1})\end{bmatrix}\begin{bmatrix}A_{i+1}\\B_{i+1}\\C_{i+1}\\D_{i+1}\end{bmatrix} = 0$$

$$\begin{bmatrix}-me^{mh_i} & me^{-mh_i} & (2-4\mu_i-mh_i)e^{mh_i} & (2-4\mu_i+mh_i)e^{-mh_i}\end{bmatrix}\begin{bmatrix}A_i\\B_i\\C_i\\D_i\end{bmatrix} - \alpha_i\begin{bmatrix}-m & m & (2-4\mu_{i+1}) & (2-4\mu_{i+1})\end{bmatrix}\begin{bmatrix}A_{i+1}\\B_{i+1}\\C_{i+1}\\D_{i+1}\end{bmatrix} = 0$$

where

$$\alpha_i = \frac{E_i(1+\mu_{i+1})}{E_{i+1}(1+\mu_i)}$$

Then:

$$\begin{bmatrix}-me^{mh_i} & me^{-mh_i} & (2-4\mu_i-mh_i)e^{mh_i} & (2-4\mu_i+mh_i)e^{-mh_i} & \alpha_i m & -\alpha_i m & -\alpha_i(2-4\mu_{i+1}) & -\alpha_i(2-4\mu_{i+1})\end{bmatrix}\begin{bmatrix}A_i\\B_i\\C_i\\D_i\\A_{i+1}\\B_{i+1}\\C_{i+1}\\D_{i+1}\end{bmatrix} = 0$$

or

$$\begin{bmatrix}me^{mh_i} & -me^{-mh_i} & (-2+4\mu_i+mh_i)e^{mh_i} & (-2+4\mu_i-mh_i)e^{-mh_i} & -\alpha_i m & \alpha_i m & \alpha_i(2-4\mu_{i+1}) & \alpha_i(2-4\mu_{i+1})\end{bmatrix}\begin{bmatrix}A_i\\B_i\\C_i\\D_i\\A_{i+1}\\B_{i+1}\\C_{i+1}\\D_{i+1}\end{bmatrix} = 0$$

Figure G. 9 Boundary condition at the layer interfaces, based on displacement

For $z = h_i$, layer i: $$\sigma_{zi} = [me^{mh_i} \quad me^{-mh_i} \quad (-1 + 2\mu_i + mh_i)e^{mh_i} \quad (1 - 2\mu_i + mh_i)e^{-mh_i}] \begin{bmatrix} A_i \\ B_i \\ C_i \\ D_i \end{bmatrix}$$

For $z = 0$, layer i+1: $$\sigma_{z(i+1)} = [m \quad m \quad (-1 + 2\mu_{i+1}) \quad (1 - 2\mu_{i+1})] \begin{bmatrix} A_{i+1} \\ B_{i+1} \\ C_{i+1} \\ D_{i+1} \end{bmatrix}$$

At the interface between i and i+1; $\sigma_{i(z=h_i)} - \sigma_{i+1(z=0)} = 0$

$$[me^{mh_i} \quad me^{-mh_i} \quad (-1 + 2\mu_i + mh_i)e^{mh_i} \quad (1 - 2\mu_i + mh_i)e^{-mh_i}] \begin{bmatrix} A_i \\ B_i \\ C_i \\ D_i \end{bmatrix} - [m \quad m \quad (-1 + 2\mu_{i+1}) \quad (1 - 2\mu_{i+1})] \begin{bmatrix} A_{i+1} \\ B_{i+1} \\ C_{i+1} \\ D_{i+1} \end{bmatrix} = 0$$

Then:

$$[me^{mh_i} \quad me^{-mh_i} \quad (-1 + 2\mu_i + mh_i)e^{mh_i} \quad (1 - 2\mu_i + mh_i)e^{-mh_i} \quad -m \quad -m \quad (1 - 2\mu_{i+1}) \quad (-1 + 2\mu_{i+1})] \begin{bmatrix} A_i \\ B_i \\ C_i \\ D_i \\ A_{i+1} \\ B_{i+1} \\ C_{i+1} \\ D_{i+1} \end{bmatrix} = 0$$

Figure G. 10 Boundary condition at the layer interfaces, based on vertical stress

For $z = h_i$, layer i: $u_{i(z=h_i)} = \frac{1+\mu_i}{E_i}[me^{mh_i} \quad me^{-mh_i} \quad (1+mh_i)e^{mh_i} \quad (-1+mh_i)e^{-mh_i}] \begin{bmatrix} A_i \\ B_i \\ C_i \\ D_i \end{bmatrix}$

For $z = 0$, layer i+1: $u_{i+1(z=0)} = \frac{1+\mu_{i+1}}{E_{i+1}}[m \quad m \quad 1 \quad -1] \begin{bmatrix} A_{i+1} \\ B_{i+1} \\ C_{i+1} \\ D_{i+1} \end{bmatrix}$

At the interface between i and i+1; $u_{i(z=h_i)} - u_{i+1(z=0)} = 0$

$$\frac{1+\mu_i}{E_i}[me^{mh_i} \quad me^{-mh_i} \quad (1+mh_i)e^{mh_i} \quad (-1+mh_i)e^{-mh_i}] \begin{bmatrix} A_i \\ B_i \\ C_i \\ D_i \end{bmatrix} - \frac{1+\mu_{i+1}}{E_{i+1}}[m \quad m \quad 1 \quad -1] \begin{bmatrix} A_{i+1} \\ B_{i+1} \\ C_{i+1} \\ D_{i+1} \end{bmatrix} = 0$$

$$[me^{mh_i} \quad me^{-mh_i} \quad (1+mh_i)e^{mh_i} \quad (-1+mh_i)e^{-mh_i}] \begin{bmatrix} A_i \\ B_i \\ C_i \\ D_i \end{bmatrix} - \alpha_i[m \quad m \quad 1 \quad -1] \begin{bmatrix} A_{i+1} \\ B_{i+1} \\ C_{i+1} \\ D_{i+1} \end{bmatrix} = 0$$

where

$$\alpha_i = \frac{E_i(1+\mu_{i+1})}{E_{i+1}(1+\mu_i)}$$

Then:

$$[me^{mh_i} \quad me^{-mh_i} \quad (1+mh_i)e^{mh_i} \quad (-1+mh_i)e^{-mh_i} \quad -\alpha_i m \quad -\alpha_i m \quad -\alpha_i \quad \alpha_i] \begin{bmatrix} A_i \\ B_i \\ C_i \\ D_i \\ A_{i+1} \\ B_{i+1} \\ C_{i+1} \\ D_{i+1} \end{bmatrix} = 0$$

Figure G. 11 Boundary condition at the layer interfaces, based on horizontal displacement

For $z = h_i$, layer i: $\tau_{rzi} = [me^{mh_i} \quad -me^{-mh_i} \quad (2\mu_i + mh_i)e^{mh_i} \quad (2\mu_i - mh_i)e^{-mh_i}] \begin{bmatrix} A_i \\ B_i \\ C_i \\ D_i \end{bmatrix}$

For $z = 0$, layer i+1: $\tau_{rz(i+1)} = [m \quad -m \quad 2\mu_{i+1} \quad 2\mu_{i+1}] \begin{bmatrix} A_{i+1} \\ B_{i+1} \\ C_{i+1} \\ D_{i+1} \end{bmatrix}$

At the interface between i and i+1; $\tau_{rzi(z=h_i)} - \tau_{rz(i+1)(z=0)} = 0$

$$[me^{mh_i} \quad -me^{-mh_i} \quad (2\mu_i + mh_i)e^{mh_i} \quad (2\mu_i - mh_i)e^{-mh_i}] \begin{bmatrix} A_i \\ B_i \\ C_i \\ D_i \end{bmatrix} - [m \quad -m \quad 2\mu_{i+1} \quad 2\mu_{i+1}] \begin{bmatrix} A_{i+1} \\ B_{i+1} \\ C_{i+1} \\ D_{i+1} \end{bmatrix} = 0$$

Then:

$$[me^{mh_i} \quad -me^{-mh_i} \quad (2\mu_i + mh_i)e^{mh_i} \quad (2\mu_i - mh_i)e^{-mh_i} \quad -m \quad m \quad -2\mu_{i+1} \quad -2\mu_{i+1}] \begin{bmatrix} A_i \\ B_i \\ C_i \\ D_i \\ A_{i+1} \\ B_{i+1} \\ C_{i+1} \\ D_{i+1} \end{bmatrix} = 0$$

Figure G. 12 Boundary condition at the layer interfaces, based on shear stress

$$M_{ij} = \begin{bmatrix}
m & m & -1+2\mu_1 & 1-2\mu_1 & 0 & 0 & 0 & 0 & .. & 0 & 0 \\
m & -m & 2\mu_1 & 2\mu_1 & 0 & 0 & 0 & 0 & .. & 0 & 0 \\
me^{mh_i} & me^{-mh_i} & (-1+2\mu_i+mh_i)e^{mh_i} & (1-2\mu_i+mh_i)e^{-mh_i} & -m & -m & (1-2\mu_{i+1}) & (-1+2\mu_{i+1}) & .. & 0 & 0 \\
me^{mh_i} & -me^{-mh_i} & (-2+4\mu_i+mh_i)e^{mh_i} & (-2+4\mu_i-mh_i)e^{-mh_i} & -\alpha_i m & \alpha_i m & \alpha_i(2-4\mu_{i+1}) & \alpha_i(2-4\mu_{i+1}) & .. & 0 & 0 \\
me^{mh_i} & -me^{-mh_i} & (2\mu_i+mh_i)e^{mh_i} & (2\mu_i-mh_i)e^{-mh_i} & -m & m & -2\mu_{i+1} & -2\mu_{i+1} & .. & 0 & 0 \\
me^{mh_i} & me^{-mh_i} & (1+mh_i)e^{mh_i} & (-1+mh_i)e^{-mh_i} & -\alpha_i m & -\alpha_i m & -\alpha_i & \alpha_i & .. & 0 & 0 \\
: & : & : & : & : & : & : & : & .:. & : & : \\
0 & 0 & 0 & 0 & .. & me^{mh_{n-1}} & me^{-mh_{n-1}} & (-1+2\mu_{n-1}+mh_{n-1})e^{mh_{n-1}} & (1-2\mu_{n-1}+mh_{n-1})e^{-mh_{n-1}} & -m & (-1+2\mu_n) \\
0 & 0 & 0 & 0 & .. & me^{mh_{n-1}} & -me^{-mh_{n-1}} & (-2+4\mu_{n-1}+mh_{n-1})e^{mh_{n-1}} & (-2+4\mu_{n-1}-mh_{n-1})e^{-mh_{n-1}} & \alpha_{n-1}m & \alpha_{n-1}(2-4\mu_n) \\
0 & 0 & 0 & 0 & .. & me^{mh_{n-1}} & -me^{-mh_{n-1}} & (2\mu_{n-1}+mh_{n-1})e^{mh_{n-1}} & (2\mu_{n-1}-mh_{n-1})e^{-mh_{n-1}} & m & -2\mu_n \\
0 & 0 & 0 & 0 & .. & me^{mh_{n-1}} & me^{-mh_{n-1}} & (1+mh_{n-1})e^{mh_{n-1}} & (-1+mh_{n-1})e^{-mh_{n-1}} & -\alpha_{n-1}m & \alpha_n
\end{bmatrix}$$

$$X = \begin{bmatrix} A_i \\ B_i \\ C_i \\ D_i \\ A_{i+1} \\ B_{i+1} \\ C_{i+1} \\ D_{i+1} \\ : \\ A_{n-1} \\ B_{n-1} \\ C_{n-1} \\ D_{n-1} \\ B_n \\ D_n \end{bmatrix} \qquad Y = \begin{bmatrix} \frac{qaJ_1(ma)}{m^2} \\ 0 \\ 0 \\ 0 \\ 0 \\ 0 \\ 0 \\ 0 \\ : \\ 0 \\ 0 \\ 0 \\ 0 \\ 0 \\ 0 \end{bmatrix}$$

Solve for X in MX=Y

Figure G. 13 Grand M matrix created for solution of A, B, C and D for each layer.

9. APPENDIX H. Comparison of MatLEA with CHEVLAY2 and JULEA.

Several example comparisons between the MatLEA solution and CHEVLAY2 and JULEA are shown in figures below.

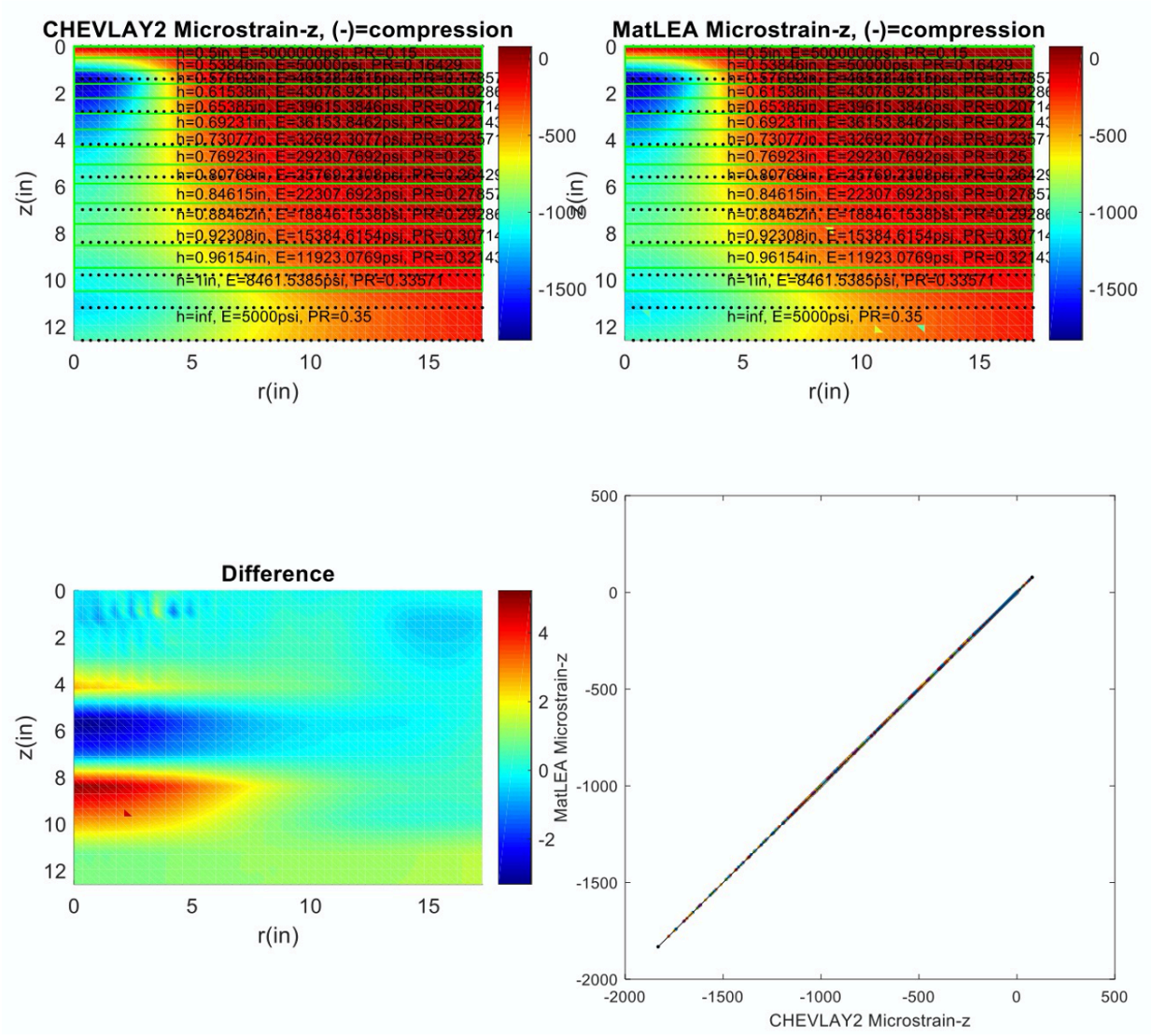

Figure H. 14 MatLEA vs CHEVLAY2 Microstrain-z

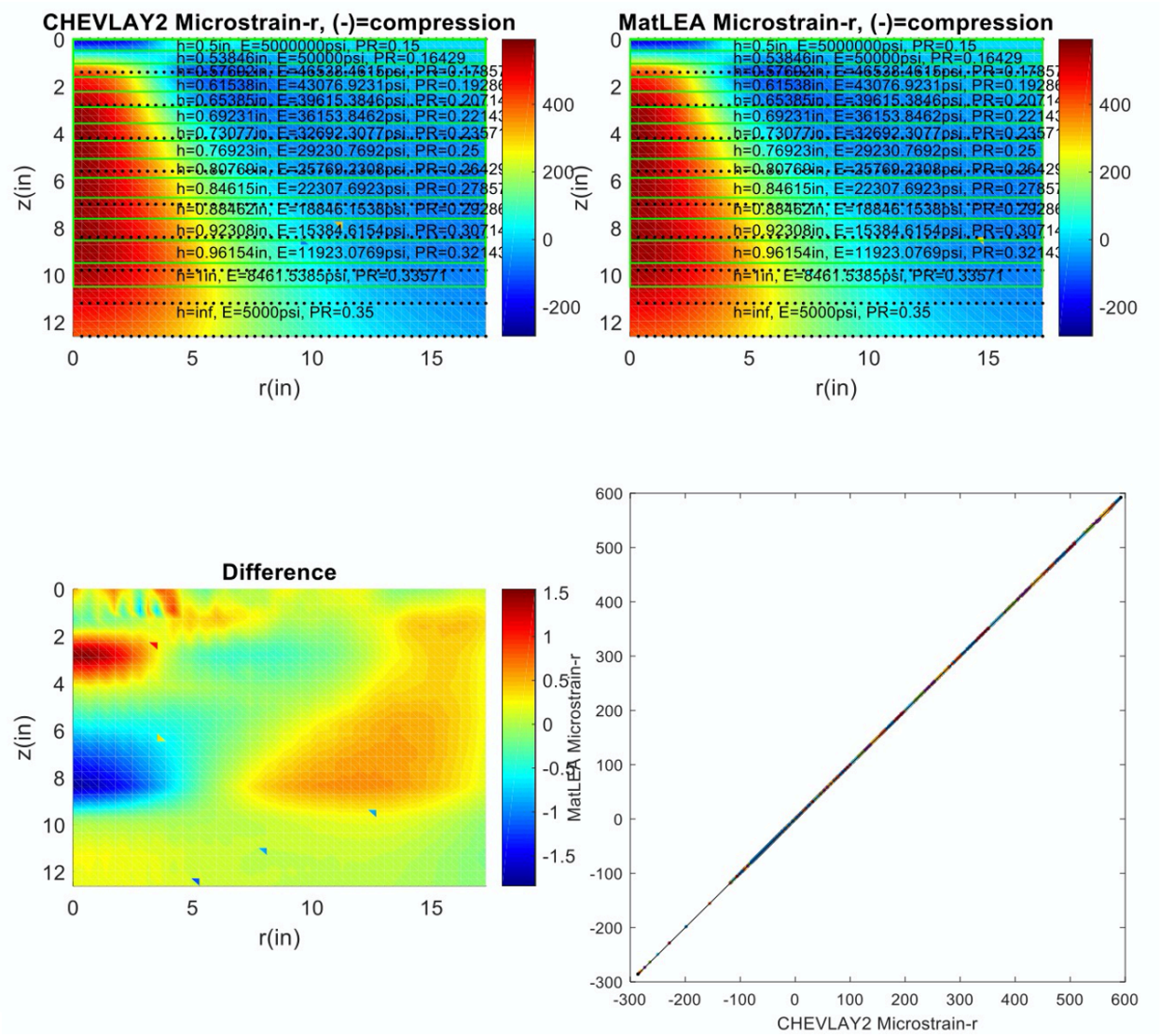

Figure H. 15 MatLEA vs CHEVLAY2 Microstrain-r

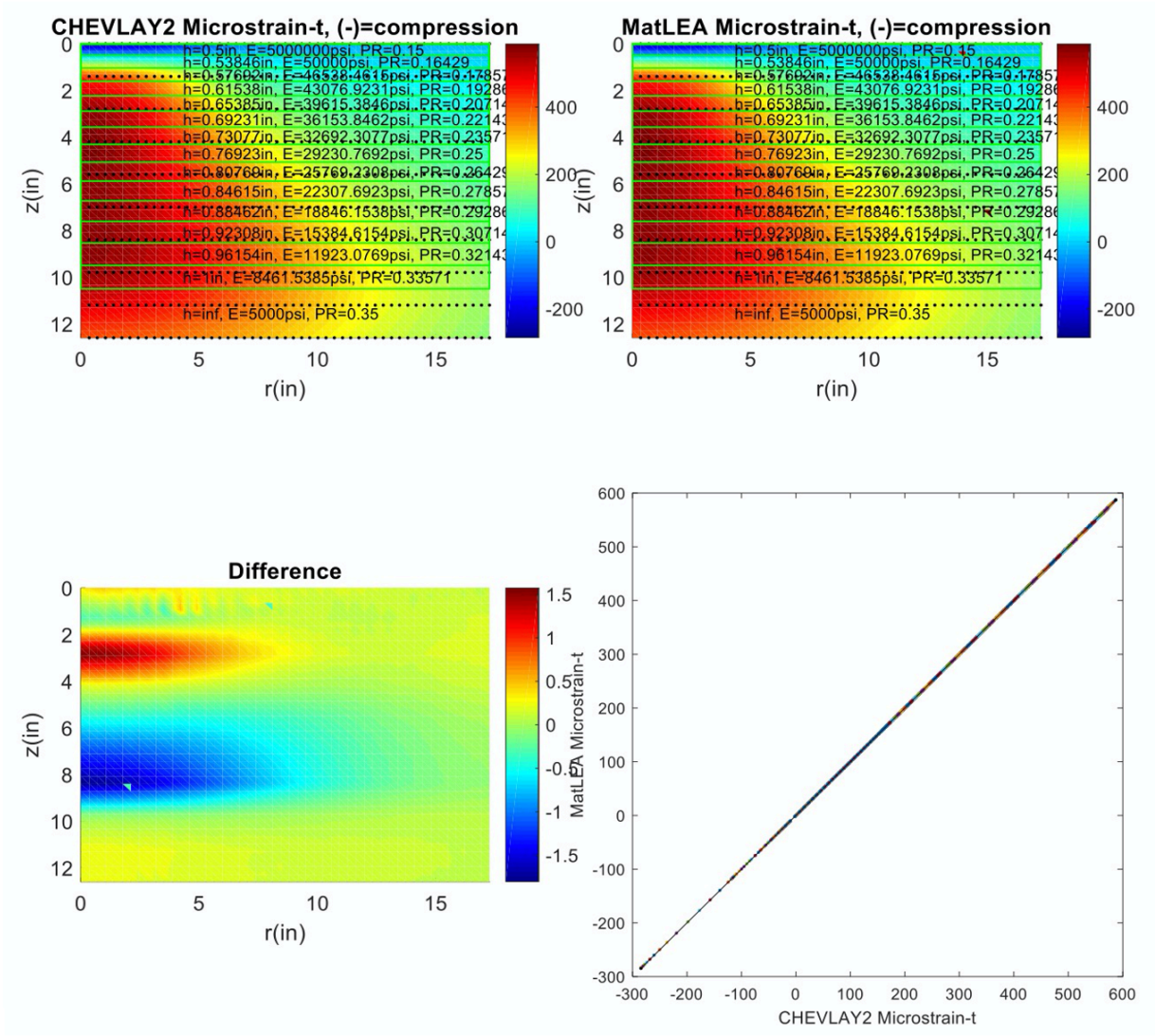

Figure H. 16 MatLEA vs CHEVLAY2 Microstrain-t

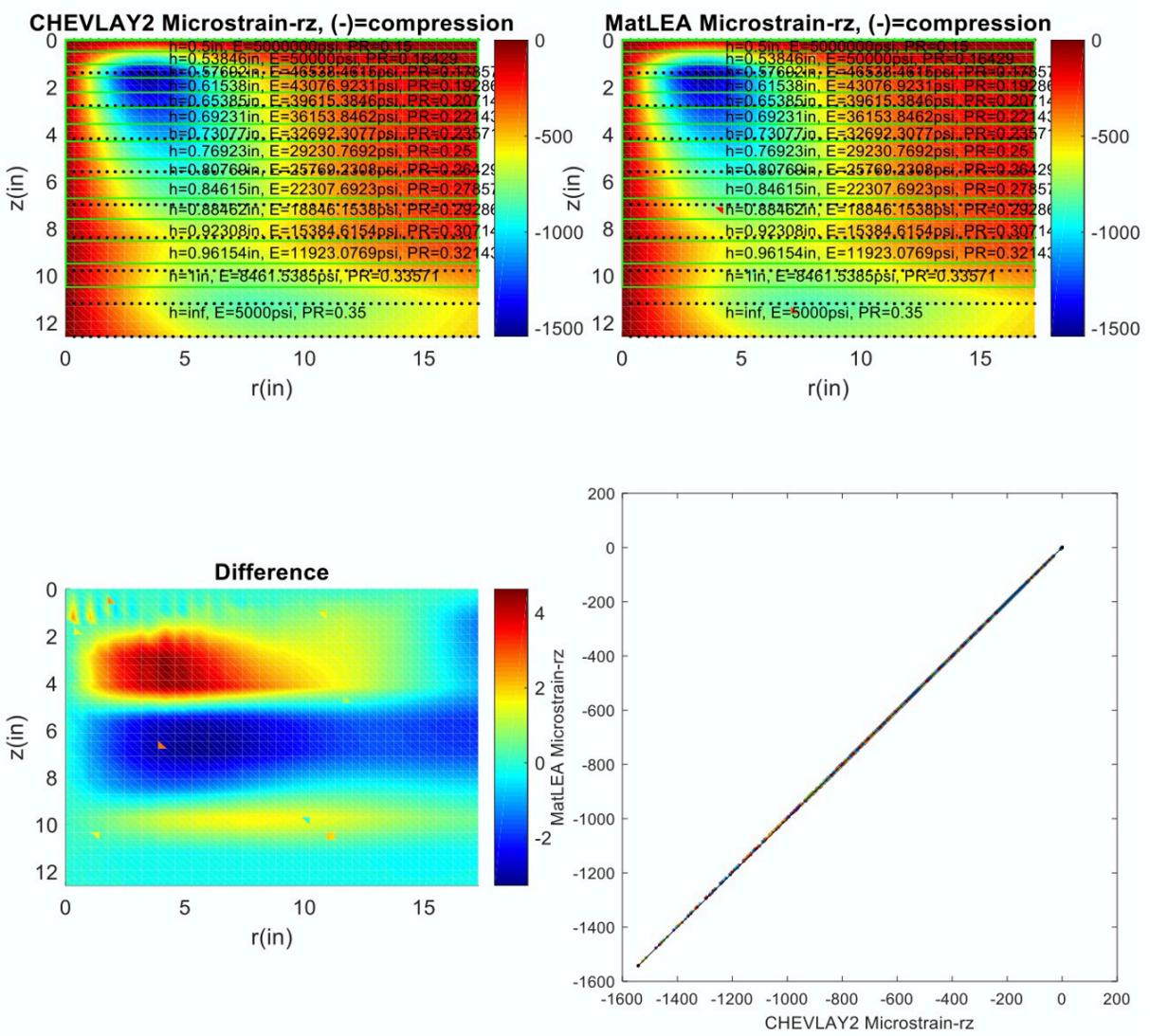

Figure H. 17 MatLEA vs CHEVLAY2 Microstrain-rz

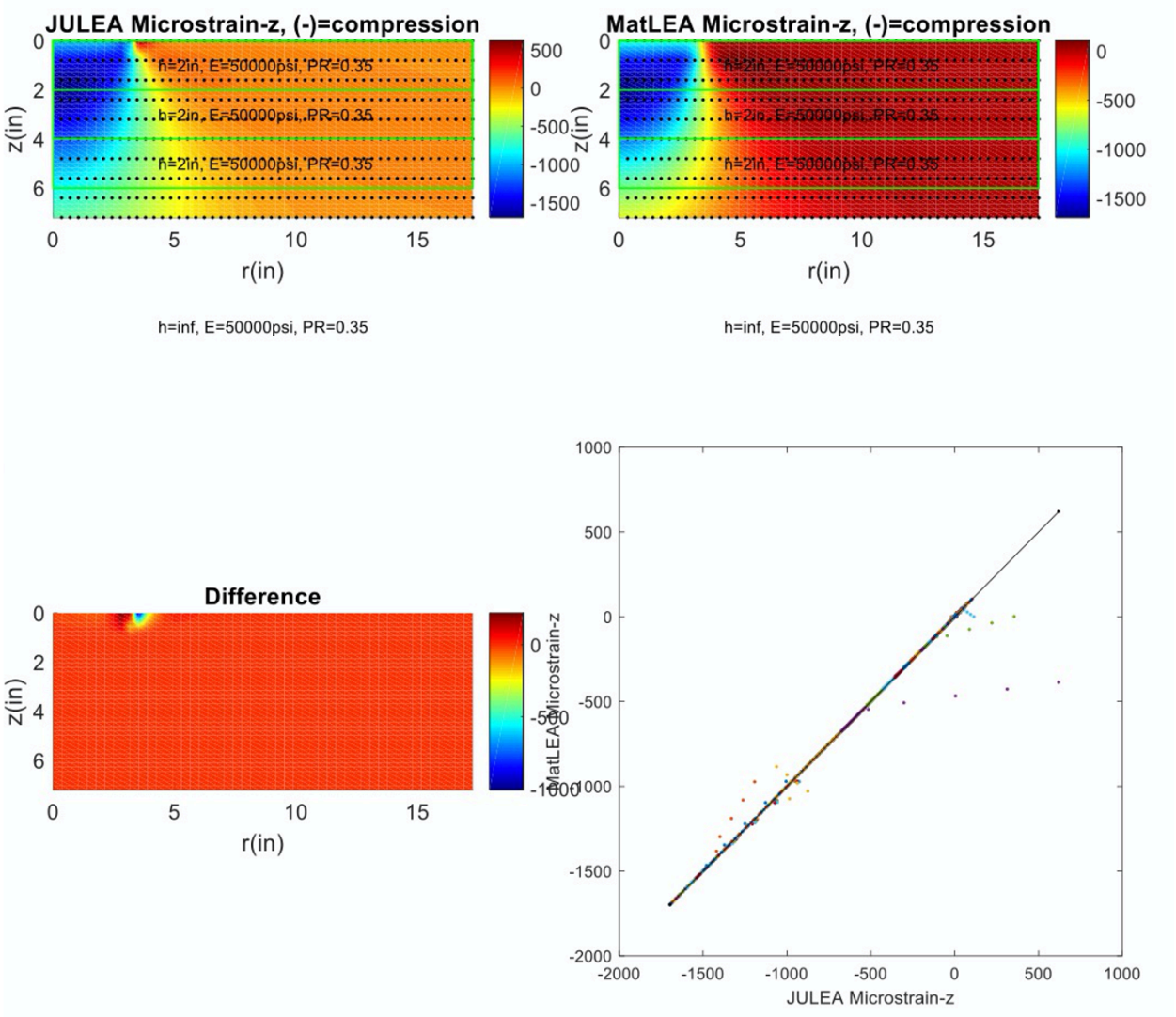

Figure H. 18 MatLEA vs JULEA Microstrain-z

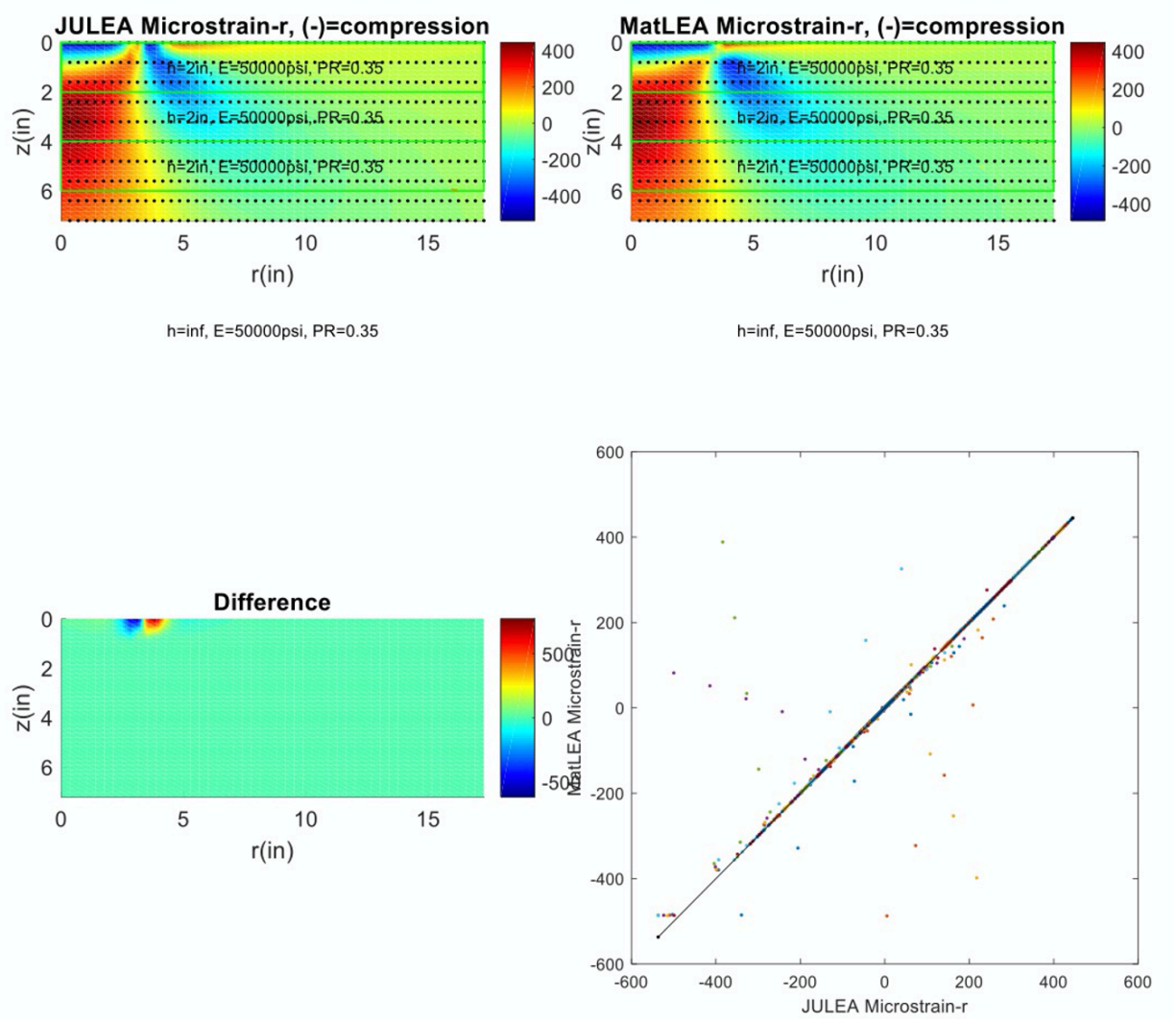

Figure H. 19 MatLEA vs JULEA Microstrain-r

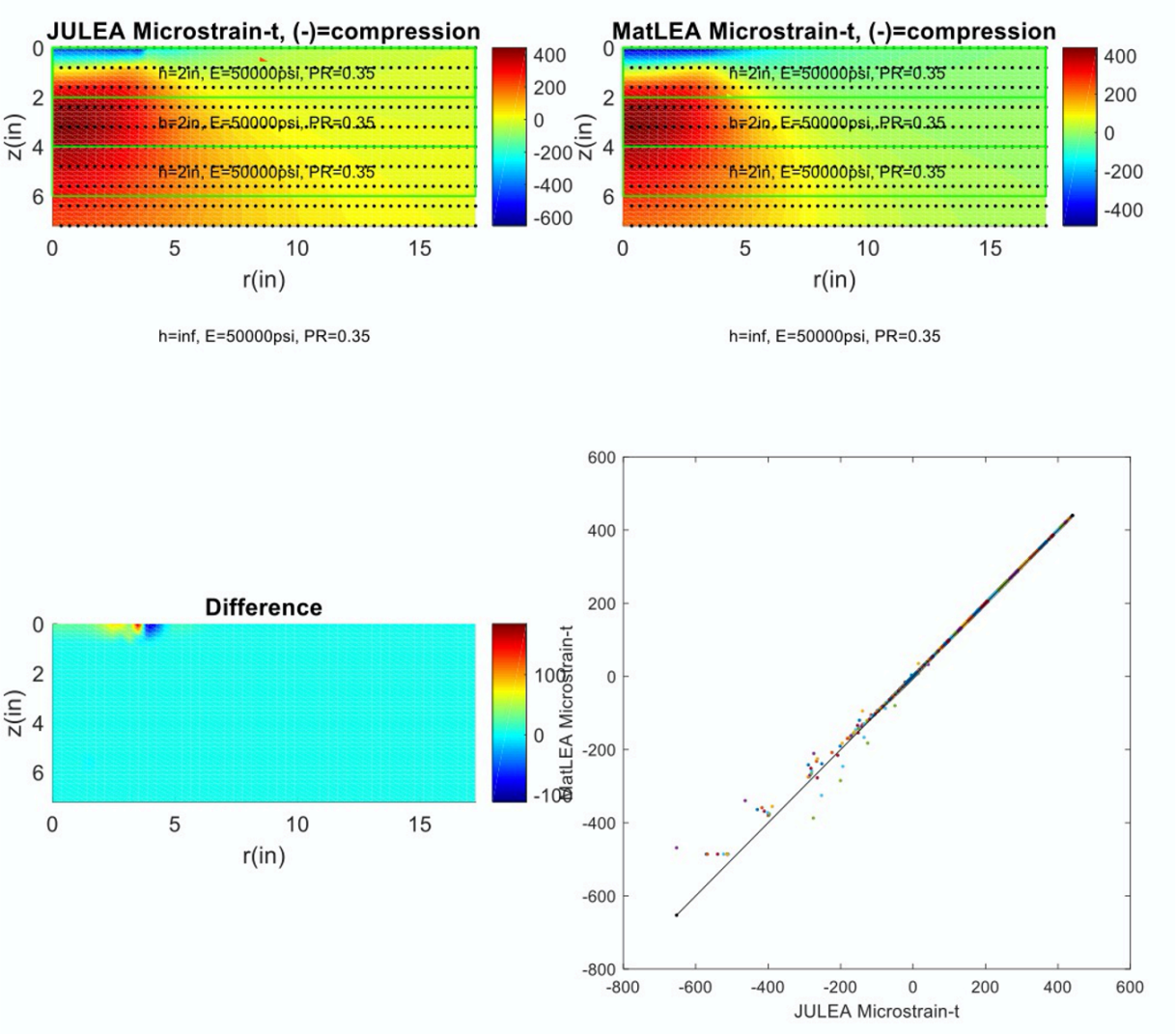

Figure H. 20 MatLEA vs JULEA Microstrain-t

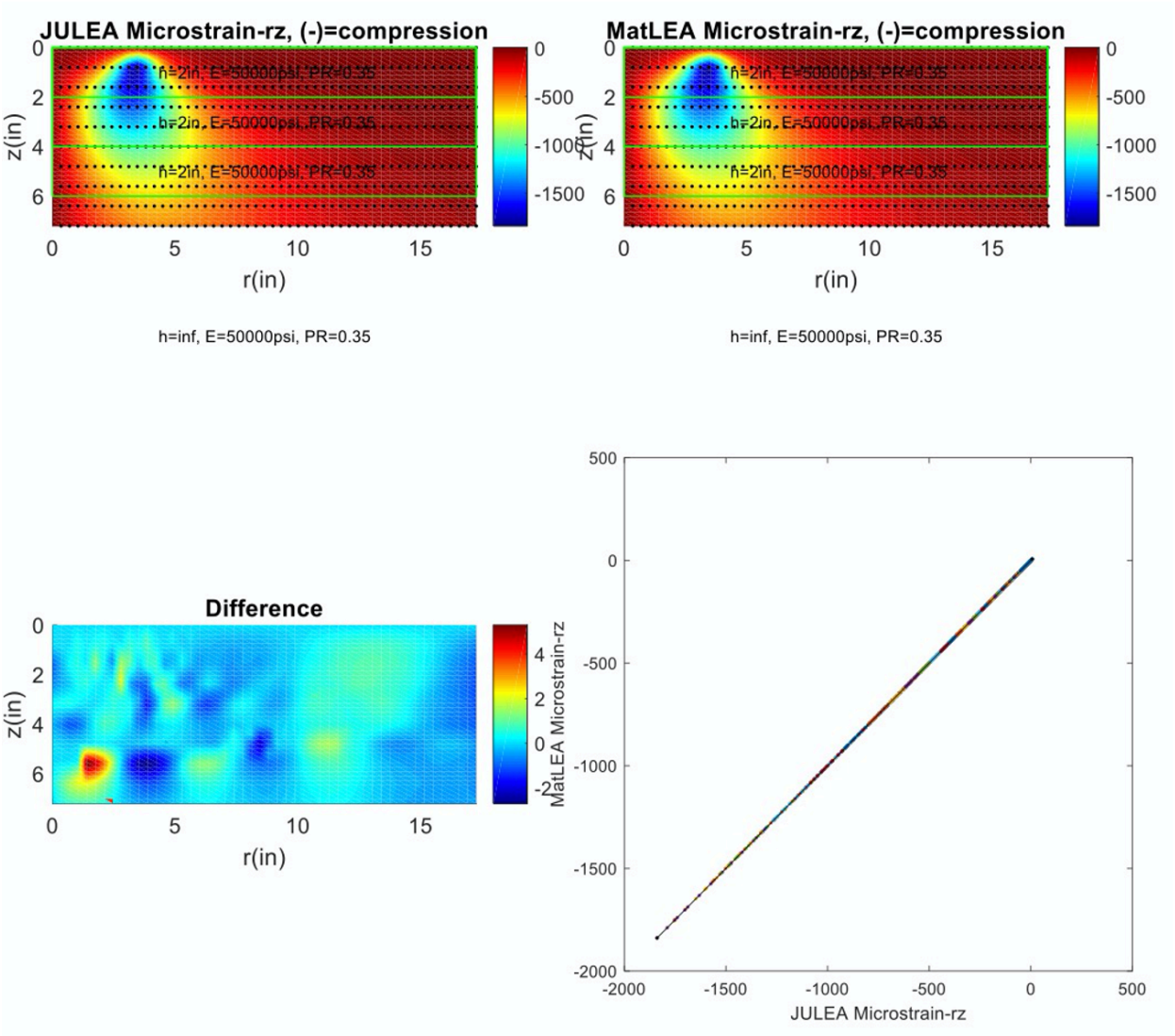

Figure H. 21 MatLEA vs JULEA Microstrain-rz